ABSTRACT

BOGERT, PHILIP B. Transient Waves from Acoustic Emission Sources in Isotropic Plates Using a Higher Order Extensional and Bending Theory. (Under the direction of Fuh-Gwo Yuan).

This dissertation presents a derivation for the transient wave response of an infinite isotropic plate to a general acoustic emission (AE) point source discontinuity loading, based on third-order plate theory. The calculation of the wave response is facilitated by employing the concept of a seismic moment tensor (or derived "equivalent" body-forces) to describe the loading from highly localized displacement discontinuities on a fracture surface. Further, the body forces from 3-D elasticity are converted to plate loadings for use in the plate theory wave equations of motion. The transient wave response can be detected as AE signals using piezoelectric sensors. In particular, time-dependent surface strains can be readily obtained experimentally. Therefore the results emphasize the calculation of the surface strains for potential comparison with future experiments. The calculated transient response, which represents waves propagating from a general AE point source in the plate, is expressed in an explicit integral form. It is shown that the transient response, which is given by double inverse Fourier transforms, can be simplified into a finite series involving inverse Hankel transforms which only require one-dimensional inversions for an isotropic plate. Thus numerical evaluation of the transient wave is more robust and accurate than that generated using two-dimensional inverse transforms and also, asymptotic solutions can be readily obtained. Nine types of AE sources representing different micro-damage mechanisms and their corresponding plate loads are discussed. Numerical results for four types of AE point sources with a Heaviside time history loading are presented.

The long-term goal of the development, having established a relationship between disturbance and response, is to monitor responses in a structure and be able to determine the source, i.e. damage, type and location by solving the inverse problem in real time. What is new and different from previous work upon which this is building is that the extensional formulation is evaluated for general AE loading, and a higher order bending theory is developed and evaluated. Additionally, the polar conversion reduction to a single variable spatial integration is implemented for both theories.

Transient Waves from Acoustic Emission Sources in Isotropic Plates Using a Higher Order Extensional and Bending Theory

by
Philip B. Bogert

A dissertation submitted to the Graduate Faculty of
North Carolina State University
in partial fulfillment of the
requirements for the degree of
Doctor of Philosophy

Aerospace Engineering

Raleigh, North Carolina

2010

APPROVED BY:

_____	_____
Fuh-Gwo Yuan Committee Chair	Eric Klang
_____	_____
Kara Peters	Yong Zhu

BIOGRAPHY

Mr. Bogert is an aerospace engineer in the Structural Mechanics and Concepts Branch at the NASA Langley Research Center (LaRC). He has nearly 20 years of experience with NASA developing, designing and analyzing structures for the aerospace industry and managing aerospace research programs. He chaired the Loads and Dynamics, Microgravity and Orbital Debris Penetration Working Groups in his role as Loads and Dynamics Manager for the Space Station Program in the early 1990s. In the mid 1990s he was the Headquarters Manager of the Advanced Subsonic Technology Program's Advanced Composites Technology and Aging Aircraft Elements. In the late 1990s he managed the High Speed Research Program's Composite Fuselage Element. He is currently the Associate Principal Investigator for the Lightweight Durable Airframes portion of the Supersonics Element of NASA's Fundamental Aeronautics Program.

Before working at NASA, Mr. Bogert worked for 15 years in private industry. He managed a structural dynamics division for an engineering company where, in addition to management duties, he performed underwater explosion qualification analysis for all recent classes of US Navy submarine propulsion plants. Mr. Bogert started his career in the Nuclear Power industry where he performed seismic analysis for nuclear power plant structures and later managed a structural analysis and pipe rupture mitigation group.

Before commencing his current research at the North Carolina State University, Mr. Bogert earned a B.S. degree in Civil Engineering from Lafayette College, a M.S degree in Structures from Columbia University and a M.S. degree in Solid Mechanics from the George

Washington University. He has been married for 32 years and has three children and three grandchildren. In his non working time he enjoys, church, golf, running, bird watching and hunting with family and friends.

ACKNOWLEDGMENTS

I would like my express gratitude and appreciation to my advisor and friend, Dr. Fuh-Gwo Yuan for his technical guidance and great patience throughout this long process which included many interruptions due to my work commitments at NASA. I would not have completed this effort without his constant encouragement, guidance and understanding over the years. I am also very grateful to Dr. Shaorui Yang who patiently answered my many and detailed technical questions throughout this time drawing on his broad and deep knowledge of mathematics and solid mechanics. I am grateful to my other committee members, Dr. Eric Klang, Dr. Kara Peters and Dr. Yong Zhu whose time commitment and encouragement were never in doubt, and also to Dr. Bob Nagel who kept me on track procedurally when I most needed it.

I am greatly indebted to Dr. Olaf Weckner of the Boeing Company who unselfishly helped me navigate through the learning curve of the MATHEMATICA code in addition to supplying keen technical insights into the physics of the problem often giving up evening and weekend time in his support.

I am also quite grateful to several individuals who made a big impression during my time with NASA, for their support but, unfortunately, are not here to witness the completion of this journey. The first was the late Dr. James H. Starnes, Jr. who encouraged me to embark on this quest late in my career, along with my first Advisor, the late Dr. Harold Liebowitz from the George Washington University. Secondly I am grateful to my former Branch Head, Dr. Damodar Ambur who supported me and created an environment where I

could fulfill the requirements of university residency with much time away from Langley. My former and current Branch Heads, Mr. Kevin Rivers, Dr. Stephen Scotti and Mr. David Brewer, encouraged me greatly and shielded me as much as possible from additional work commitments so that I could focus on completing my research, especially towards the end. I am very grateful to my Program Lead, Mr. Peter Coen, who supported my research time even when it meant being less dedicated to my day to day program tasks, and also to my co-worker and friend Mr. William T. Freeman who filled the gaps in my missing efforts in those day to day tasks.

Finally, and perhaps most of all, I want to thank my wife, Mary Ellen, for her tremendous patience and support and for giving up much time when we otherwise could have been together, so that I could complete long hours or study and frequent travel from Hampton Roads to Raleigh. With her love I think I could do just about anything.

TABLE OF CONTENTS

LIST OF FIGURES

CHAPTER 1.0

INTRODUCTION

1.1 Preliminaries

Acoustic emission (AE), a passive monitoring technique, involves instrumenting the chosen structures and 'listening' for characteristic signals from the structures under stress (Bray and McBride, 1992 [6]). Physically, acoustic emission is the term used to describe elastic waves emitted by rapid release of strain energy from sudden localized changes within a structure under stress. The sudden local microstructural changes from, for example, the formation of damage, plasticity, or phase transformations, are often referred to as localized sources. Such localized sources act as a center of radiation over a small or finite area for the duration of bursts of elastic waves in the 100 kHz to several MHz range that propagate throughout the structure. Unlike most of the various non-destructive evaluation (NDE) techniques, the AE monitoring technique detects, locates, and then identifies the damage under stress the moment the damage is created. In contrast, ultrasonic testing detects and characterizes damage after it has been created.

Provided that the elastic waves are of sufficient magnitude to be detected by sensors as AE signals, they can be used to estimate localized changes in assessing the health of the structure. The potential of the AE monitoring technique as a method for remotely detecting and locating damage in a wide range of loaded structures has been long recognized, with initial work developed in the early 1960s (e.g., Hamstad, 2000 [22,23]). One of the distinct advantages of the technique for future structural health monitoring systems, compared to

other NDE techniques for aerospace structures, is the continual *in-situ* monitoring capability during the entire load history in flight.

As elastic waves are emitted from micro-damage formations, and propagate through the structure, the waveform shape transmitted by AE contains information about the location and nature of the source and the host material itself; therefore, accurate sensing of the transmitted transient wave response is necessary to fully evaluate AE waveforms. High-fidelity sensors yield undistorted waveforms that allow distinction between the arrival times of different wave modes as well as subtle distinctions about the source kinematics. In composite structures, localized sources may include various micro-damage mechanisms such as fiber breakage, matrix cracking, and delamination due to foreign object impact, fatigue loading, or even manufacturing defects. In this paper, the terms, micro-damage and AE source are used interchangeably.

1.2 Relevant Literature

In recent decades two main approaches were developed to characterize the AE signals (Aki and Richards [4]):

(1) *Signal-based approach* which characterizes a waveform by simple event counting and statistical correlations between damage mechanisms and experimental data and using these for future event description;

(2) *Waveform-based approach* which aims at reconstructing the damage location and damage mechanisms using transient wave theory.

Signal based Approaches - In the conventional signal-based approach, three types of signal analysis have been explored: AE parameter analysis, AE activity analysis, and AE frequency analysis.

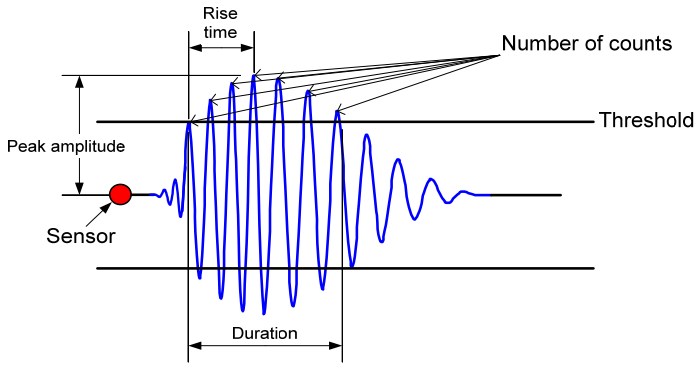

Figure 1.1 Typical AE parameters

AE parameter analysis - Here a number of parameters are extracted from *individual* AE signals. Some of the parameters are defined with reference to Fig. 1, including number of counts, peak amplitude, duration, and rise time. Other parameters can be defined, in terms of energy. Apparently, the number of counts is affected by the threshold setting. These AE parameters for each AE event are usually plotted against test parameters such as load, strain, and temperature. After repeated tests on identical specimens, empirical inferences are made concerning the severity of damage or the discrimination between different damage mechanisms. A number of studies have demonstrated the success of this approach in laboratory settings (Favre and Laizet, 1989, Dzenis and Qian, 2001 [11,12]), but few practical applications of this technique have emerged. Overall, this AE analysis method is capable of providing useful information on damage development in composites. However,

values obtained from conventional parameters are in no way unique to a given source. Derived parameters do not completely describe the signal, and are not generally reproducible with different structures. Further, the discrimination of damage mechanisms is difficult to achieve due to the overlap of AE parameters caused by complex damage and wave propagation processes in composites.

AE activity analysis – This method focuses on measuring the amount of AE signals produced by a specimen or a structure. It primarily results in information about the initiation and the evolution of damage throughout a test or during the service life of a component. A good example is the well known Felicity ratio analysis which is nowadays being used for the monitoring of fiberglass tanks, pressure vessels, and pipes (Fowler *et al*., 1989 and Downs and Hamstad, 1998 [13.21]). This type of analysis has been standardized in a number of CARP and ASME codes and constitutes one of the main fields where AE has found successful application.

AE frequency analysis – This technique uses Fast Fourier Transform (FFT) techniques to examine the frequency spectrum of AE waves. This approach is primarily used for discrimination purposes, based on the assumption that different damage phenomena will produce signals with different frequency contents. A limited number of papers have been published on this subject and it has not yet found any widespread practical application (Ghaffari and Awerbuch, 1991; and de Groot *et al*., 1995 [14,18]). The main deficiency of this analysis is that the wave propagation through the structure exhibits several dispersive wave modes. Due to the characteristics of propagation of these wave modes, there are

certain characteristic frequency ranges that propagate with sufficient magnitude to be sensed by the AE sensors. These frequency ranges vary as a function of structural properties and geometry even when the damage mechanism is identical. Thus, it is not reasonable to directly associate certain AE signal frequency ranges with certain damage mechanisms in a way that is independent of the material and geometry of the structure.

None of these AE signal analysis techniques used in laboratory studies has proven to be capable of consistently dealing with the difficulties encountered in large structure, namely, large amounts of data, the elimination of noise sources, material anisotropy, and the influence of wave propagating effects (attenuation and dispersion). These analyses often gave controversial results because they lack a physical justification (based on the theory of AE) for the signal features used to sort the experimental signals into different source mechanisms. Summarizing these observations one can state that the conventional AE approaches have remained mainly *qualitative* techniques.

Waveform Based Approach - For AE to monitoring be accepted in practical use as a viable technique for assessing the state of structural health, a *quantitative* approach is required (Scruby, 1985[35]). Such an approach is based on the recognition that the waveform (signature) of AE signals is a characteristic of the process which produces it. Hence the AE signals contain information about (a) the AE source, which includes location, magnitude, and damage mechanisms; (b) the structure through which the wave propagates in the form of transient stress waves; and (c) the monitoring system including the sensor (i.e., piezoelectric sensors) either mounted on or embedded in the structure and the associated signal processing electronics. With the ever increasing power of data

acquisition systems and the increased sensitivity of new sensors, recording the entire waveform with high fidelity becomes feasible. This waveform approach characterizes AE signals by employing transient wave theory to predict the signals generated by different types of damage mechanisms. This, in turn, enables experimentally measured acoustic emission data to be interpreted in a physically meaningful manner. A clear understanding of the quantitative relationship between the waves and their sources is essential in developing algorithms for detecting and characterizing the damage.

Mathematically, identification of an AE source is an inverse problem. If the area of the source formation (sudden micro-damage growth) is small compared to the measured dominant wavelength of the AE signal and source-sensor distance, the AE source can effectively be considered as a point source. The localized sources over a finite area, however, can be modeled as the summation (or integration in the limit) of point sources (Chang and Sachse, 1985 [8]), each of which accounts for the evolutionary micro-damage over a discretized sub-area emitted at different times. Therefore, accurately characterizing the point source is a key in understanding the nature of the micro-damage mechanisms.

Micro-damage and seismic rupture share the same source mechanism, yet, at different temporal and length scales. A moment tensor for describing the different types of point sources (Vvedenskaya, 1956; Aki, 1966; Kostrov, 1974 [39,4,26]) and equivalent body-forces for displacement discontinuities on an internal surface (Maruyama, 1963; Burridge and Knopoff, 1964 [27,7]) provide powerful aids in the description of seismic

source theory. Studies of elastic waves generated by seismic sources have been summarized by Aki and Richards (1992) [5].

From the seismic waveforms, identification of the type of source as well as its time history needs to be extracted. The seismic source has been assumed to be mathematically characterized as buried self-equilibrating force dipoles. Each dipole can be represented mathematically by two impulse delta functions acting in opposite directions, with an infinitesimal separation distance either along, or perpendicular to, the impulse direction or, in the limit, by the spatial derivatives of the impulse with respect to the separation-distance parameter. These force dipoles can be combined to form the moment tensor (Aki and Richards, 1992) [5].

Many research efforts have been devoted to theoretically determining the AE source event from the AE waveforms (Michaels *et al*., 1981; Scruby *et al*., 1985; Shah and Labuz, 1995; and Ohtsu *et al*., 1998 [28,35,36,37,31]). Generalized ray theory has been proposed to analyze the transient AE waves in plates (Pao *et al*., 1979 and Chang and Sachse, 1985 [32,8]). The moment tensor (or derived equivalent body-force) approach has been adopted in the AE field to describe the damage processes (Rice, 1980 [34]). When considering the wave propagation from AE sources, analytic or numerical Green's functions that correspond to buried force dipoles in an infinite domain have been formulated as components of the moment tensor. Although the elastic properties of the material do change as damage accumulates, this effect is not considered for characterization purposes. For the case of the growth of a sudden micro-crack, if the dominant wavelengths are much

larger than the size of the micro-crack growth, radiation patterns should not be significantly affected by these inhomogeneities. Note that this assumption is not valid in the case of micro-growth of an existing crack since radiation may be affected by the presence of the existing crack unless the existing crack size is also small enough. In order to recover information about the point source from the AE waveforms, suitable signal deconvolution and decomposition procedures are often used (Michaels et al., 1981 and Chang and Sachse, 1986 [28,8]). Once calculated, the moment tensor is decomposed into different components, each one representing a particular type of damage mechanism. This approach, requiring extensive mathematical calculations, has been applied to different materials for very simple structural geometry.

As many practical structures are of plate-like geometries, a viable approach using the guided waves propagating along the plane of the plate has been examined. The waves are inherently dispersive and multi-modal. Due to the dispersive nature of the guided waves, the waveforms change as they propagate away from the source. Therefore it is necessary to understand the detailed nature of the guided waves in structures in order to extract information from the sensed waveforms. Considering the specific modes of propagation, the determination of the guided AE response signals can improve the source location accuracy and enable the discrimination of damage mechanisms. This approach is now known as modal acoustic emission (MAE).

Gorman (1991 [17]) first demonstrated how the extensional and flexural modes could be recognized in AE signals by performing pencil lead-breaks on both aluminum and

unidirectional composites. Further work has concentrated on source orientation (Gorman and Ziola, 1990 [16]), matrix crack detection (Gorman and Ziola, 1991 [15]), and source location and attenuation (Hamstad and Downs, 1995 and Prosser, 1996 [21,33]).

A number of inherent advantages of the MAE approach were identified in the literature: (1) easier recognition and discrimination of true AE damage signals; (2) better noise elimination; and (3) more accurate source location. However, a large part of the published results have only dealt with simulated AE sources such as pencil lead break or ball impact to validate the approach. These sources represent a monopole surface loading rather than the typical AE buried self-equilibrating dipole source. Since of all the studies have focused on the first two fundamental bending and extensional modes, A_0 and S_0 respectively, most of these advantages have thus far remained largely on the conceptual level (Hamstad, 2000 [22]). Guo *et al*. (1996 [20]) presented plate loads based on first-order plate theory and modeled acoustic emission from different damage mechanisms in composite laminates. Wave propagation from matrix cracking and fiber fracture in laminated beams was modeled by Aberg and Gudmundson (2000 [1]) employing higher-order beam theory. Numerical simulation of experiments on cracked specimens was conducted by Aizawa *et al*. (1987 [3]). Hamstad *et al*. (2001 [23,43]) simulated AE signals from dipole sources in an aluminum plate with a 3-D finite element code.

1.3 Research Objectives

In the current work at NCSU transient waves emitted from AE sources, such as the formation of micro-damage in isotropic plates, are investigated. Using plate theory to predict extensional and flexural motions in thin plates, equivalent plate loads for different AE sources are first derived. Depending on the orientations of the micro-cracks (horizontal, vertical, and inclined) and the displacement discontinuities across the fracture surfaces represented by one normal and two shear components, a total of nine types of transient wave disturbance sources and their responses are presented. Employing the joint integral transform, that is, a double Fourier transform on the spatial variables and a Laplace transform on time, the transient wave response for the different sources in isotropic plates is formulated in compact form in terms of an inverse Fourier transform (double integration). Further, it can be shown that the transient response to the various point sources can be reduced to inverse 1-D Hankel transforms (single integral) for isotropic plates. Asymptotic solutions obtained from the 1-D transform can be easily derived. Nine types of AE sources representing different micro-damage orientations and their corresponding plate loads are discussed. Numerical results for four of the nine AE point sources with Heaviside loading time histories are presented and compared with predictions from the first order theories. The work builds upon previous work as follows.

- First Order extensional and bending AE theory (Bogert, Yuan, Yang 2009 [44])
  - Considered true AE self-equilibrating dipole loading with first order displacement field
  - Semi-analytical solution for PC (not FEA) with reduced order integration via Bessel functions

- Higher (second) Order Extensional Theory (Yuan, Yang, 2005 [40]) for surface loading with axisymmetric solution only

In the current work:

- Extend the higher order extensional theory to include AE loading (moment tensor of self equilibrating dipoles)
- Extend semi-analytical reduced integration Bessel function transient solution concept to the third order theory
- Develop general semi-analytical Cartesian transient solution for the extensional theory
- Develop higher (third) order bending theory and compatible AE loading
- Extend semi-analytical reduced integration Bessel function transient solution concept to the third order theory
- Develop AE transient general semi-analytical Cartesian solution for bending

1.4 Organization

In order to retain the flow of the presentation and to focus on parts of the development that are new, very detailed steps are generally not shown in the body of the dissertation. Typical operations and manipulations that must be performed on 11 equations, 5 extensional and 6 flexural, are shown for one or two equations in a series of Appendices so as not to bog down the flow of the derivations in Chapters 2 through 7.

CHAPTER 2.0

EQUIVALENT BODY-FORCES FOR DISPLACEMENT DISCONTINUITIES

2.1 Moment Density Tensor

Consider the micro-damage process which involves generation of a displacement discontinuity on an internal surface of an elastic body. From the 3-D elastodynamic representation theorem for an internal crack surface Σ with displacement discontinuities (crack opening and/or slip), the displacement field, generated by the displacement discontinuities commonly used in seismology, can be expressed as (Aki and Richards [5]))

$$u_n(\mathbf{x},t) = \int_\Sigma m_{pq} * \frac{\partial G_{np}}{\partial \xi_q} d\Sigma, \quad (n, p = 1, 2, 3) \tag{2.1}$$

where $(\mathbf{x},t) = (x_1, x_2, x_3, t)$ is the general position and time at which the displacement u_n is to be evaluated, the symbol * denotes the time convolution integral, $G_{np}(\mathbf{x},t;\boldsymbol{\xi},\tau)$ is the Green's function, which represents the nth component of displacement at $(\mathbf{x},t)$ due to a unit impulse applied at $\mathbf{x} = \boldsymbol{\xi}$, $t = \tau$ in the p-direction, $\boldsymbol{\xi}$ is the general position on Σ. G_{np} and its derivatives are continuous across Σ, and m_{pq} is the moment density tensor, namely, the symmetric second-order tensor, depicted in Fig. 2.3, defined by

$$m_{pq} = c_{pqij} \Delta u_i(\boldsymbol{\xi},\tau) n_j \tag{2.2}$$

where $\mathbf{n}$ is the unit outward normal vector to the crack surface, c_{pqij} are elastic constants, and Δu_i represents the discontinuity of the i^{th} displacement component (Note that here and throughout the paper a bolded quantity represents a vector or a matrix).

2.2 Equivalent Body Force

Another approach is to introduce equivalent body-forces (Aki and Richards, 1992 [5]). Using the Dirac delta function $\delta(\boldsymbol{\eta}-\boldsymbol{\xi})$ in describing the displacement discontinuities on Σ within the elastic body with volume V, where $\boldsymbol{\eta}$ varies throughout V and $\boldsymbol{\xi}$ is located on the discontinuity surface Σ, using a property of the Green's functions, and introducing the equivalent body-force $\boldsymbol{f}$ for a displacement discontinuity on Σ, the contribution of the discontinuity to the displacement at $(\mathbf{x},t)$, in Eq. (2.1), can be written in the form

$$u_n(\mathbf{x},t) = \int_{-\infty}^{t} d\tau \int_V f_p(\boldsymbol{\eta},\tau) G_{np}(\mathbf{x},t-\tau;\boldsymbol{\eta},0) dV(\boldsymbol{\eta}) \tag{2.3}$$

where f_p are the equivalent body-forces for the displacement discontinuities given by

$$f_p(\eta,\tau) = -\int_\Sigma \Delta u_i(\boldsymbol{\xi},\tau) n_j c_{ijpq} \frac{\partial}{\partial \eta_q} \delta(\boldsymbol{\eta}-\boldsymbol{\xi}) d\Sigma = -\int_\Sigma m_{pq} \frac{\partial}{\partial \eta_q} \delta(\boldsymbol{\eta}-\boldsymbol{\xi}) d\Sigma \tag{2.4}$$

Eq. (2.3) has a precise form of a common body-force contribution. Clearly, this formulation requires Green's functions and derivatives of delta functions, rather than the spatial derivatives of Green's functions which are often not readily available. Since fracture within the volume V is an internal process, the total momentum and total angular momentum must be conserved. It follows that the total force due to $\boldsymbol{f}$, and the total moment of $\boldsymbol{f}$ about any fixed point, must be zero. These requirements can be easily verified.

The above results are developed for a fracture surface of finite extent, but in practice data is often good only at periods for which the whole of Σ is effectively a point source.

For these waves, the contributions from different surface elements dΣ are all approximately in phase, and the whole surface Σ can be considered as a system of dipoles (derivatives of the delta function) located at a point. Clearly, the point source means that a/r, a/λ <<1, where $r = |\mathbf{x}|$, the source-sensor distance, λ is the dominant wavelength of the AE signal and a is typical radius of the source region, assuming the origin of the coordinates is in the source region. For an effective point source, Eq. (2.1) can be approximately reduced to

$$u_n(\mathbf{x},t) \cong M_{pq} * \frac{\partial G_{np}}{\partial \xi_q}$$

where:

$$M_{pq} = \int_{\Sigma} m_{pq} d\Sigma \cong m_{pq}\Delta\Sigma = c_{pqij}\Delta u_i(\xi,\tau) n_j \Delta\Sigma \qquad (2.5)$$

$\Delta\Sigma$ is area of the point source region, M_{ij} is the moment tensor of the source (symmetric second-order tensor). In this case, the equivalent body-force $\boldsymbol{f}$ to a point source at $\boldsymbol{\xi}$ with moment tensor M_{pq} is given, by using the form of Eq. (2.4),

$$f_p(\mathbf{x},t) = -M_{pq}(t)\frac{\partial}{\partial x_q}\delta(\mathbf{x}-\boldsymbol{\xi}) \qquad (2.6a)$$

For p=1,2,3 on left side

q=1,2,3 on right side in defining the forces f_1, f_2 and f_3 which are the same as those defined in the Mindlin theory [45].

For the extra loading generated from the higher order theory,

p=4,5,6 on the left side and the corresponding right side subscripts are p = 1,2,3 respectively where the 6,3 pair is only needed for bending.

q=1,2,3 for the higher order terms on the right side just as in the lower order theory. In other words the moment tensor stays 3x3.

Expanding Eq. (2.6a) yields:

$$
\begin{aligned}
f_1 &= -M_{11}\frac{\partial}{\partial x_1}\delta(\mathbf{x}-\boldsymbol{\xi}) - M_{12}\frac{\partial}{\partial x_2}\delta(\mathbf{x}-\boldsymbol{\xi}) - M_{13}\frac{\partial}{\partial x_3}\delta(\mathbf{x}-\boldsymbol{\xi}) \\
f_2 &= -M_{21}\frac{\partial}{\partial x_1}\delta(\mathbf{x}-\boldsymbol{\xi}) - M_{22}\frac{\partial}{\partial x_2}\delta(\mathbf{x}-\boldsymbol{\xi}) - M_{23}\frac{\partial}{\partial x_3}\delta(\mathbf{x}-\boldsymbol{\xi}) \\
f_3 &= -M_{31}\frac{\partial}{\partial x_1}\delta(\mathbf{x}-\boldsymbol{\xi}) - M_{32}\frac{\partial}{\partial x_2}\delta(\mathbf{x}-\boldsymbol{\xi}) - M_{33}\frac{\partial}{\partial x_3}\delta(\mathbf{x}-\boldsymbol{\xi}) \\
f_4 &= -M_{11}\frac{\partial}{\partial x_1}\delta(\mathbf{x}-\boldsymbol{\xi}) - M_{12}\frac{\partial}{\partial x_2}\delta(\mathbf{x}-\boldsymbol{\xi}) - M_{13}\frac{\partial}{\partial x_3}\delta(\mathbf{x}-\boldsymbol{\xi}) \\
f_5 &= -M_{21}\frac{\partial}{\partial x_1}\delta(\mathbf{x}-\boldsymbol{\xi}) - M_{22}\frac{\partial}{\partial x_2}\delta(\mathbf{x}-\boldsymbol{\xi}) - M_{23}\frac{\partial}{\partial x_3}\delta(\mathbf{x}-\boldsymbol{\xi}) \\
f_6 &= -M_{31}\frac{\partial}{\partial x_1}\delta(\mathbf{x}-\boldsymbol{\xi}) - M_{32}\frac{\partial}{\partial x_2}\delta(\mathbf{x}-\boldsymbol{\xi}) - M_{33}\frac{\partial}{\partial z}\delta(\mathbf{x}-\boldsymbol{\xi})
\end{aligned}
\tag{2.6b}
$$

Though the last three equations look just like the first 3 on the right side, as will be seen subsequently in Section 3.2, the f_4, f_5 and f_6 forces will be defined from higher order integrals and this will change the integration of the right side terms, hence, giving rise to higher order forces that are different than f_1 and f_2 . Note that the 6th equation is only required for bending. The first five equations apply for both bending and extension.

With $M_{pq} = c_{pqij}\Delta u_i\, n_j\, \Delta\Sigma$.

Eq. (2.6b) indicates that each component of the moment tensor is associated with spatial derivatives of the delta function and that each component f_p of the body force includes three dipoles. There are a total of nine dipoles that form the equivalent body-force

f for a generally oriented displacement discontinuity. The moment tensor components M_{ij} are shown in Fig. 2.1 and the corresponding dipoles are illustrated in Fig. 2.2.

$$\mathbf{M} = \begin{bmatrix} M_{11} & M_{12} & M_{13} \\ M_{21} & M_{22} & M_{23} \\ M_{31} & M_{32} & M_{33} \end{bmatrix}$$

Figure 2.1 Moment Tensor Components M_{ij}

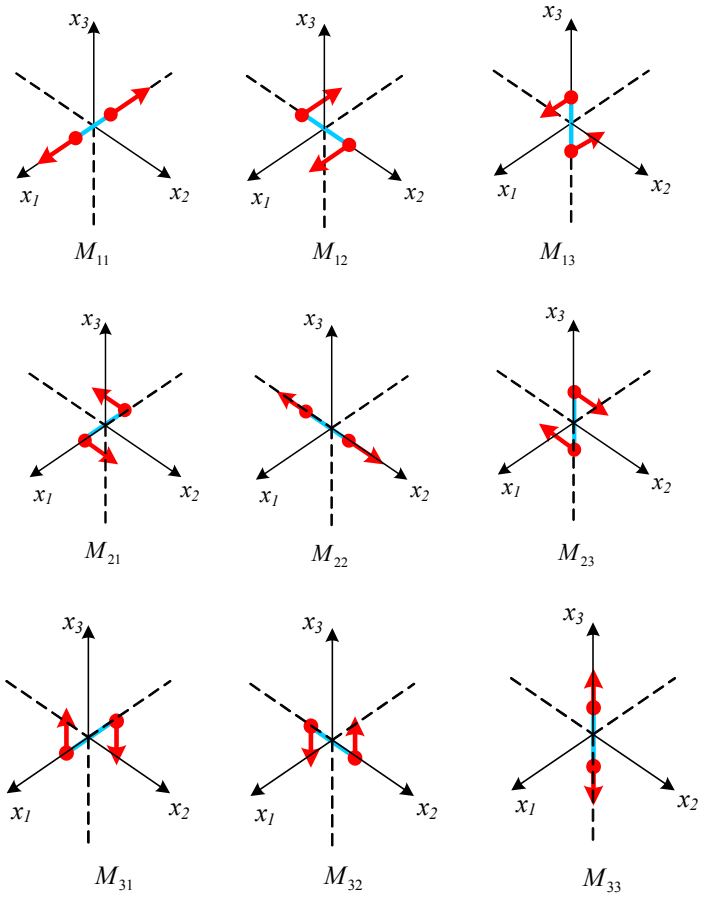

Figure 2.2 Moment tensor component corresponding dipoles

A point source displacement discontinuity in an elastic plate, which can be characterized by its moment tensor M_{ij} (the derived 3-D elasticity equivalent body-forces) as shown in Fig. 3.1, can be transformed into the corresponding plate loads based on plate theory. With the equivalent plate loads the equations of motion can be solved by employing integral transforms. Using the equivalent plate loads and the plate theory, instead of the equivalent body-forces and 3-D elasticity, analysis of AE wave propagation in plates will be greatly simplified.

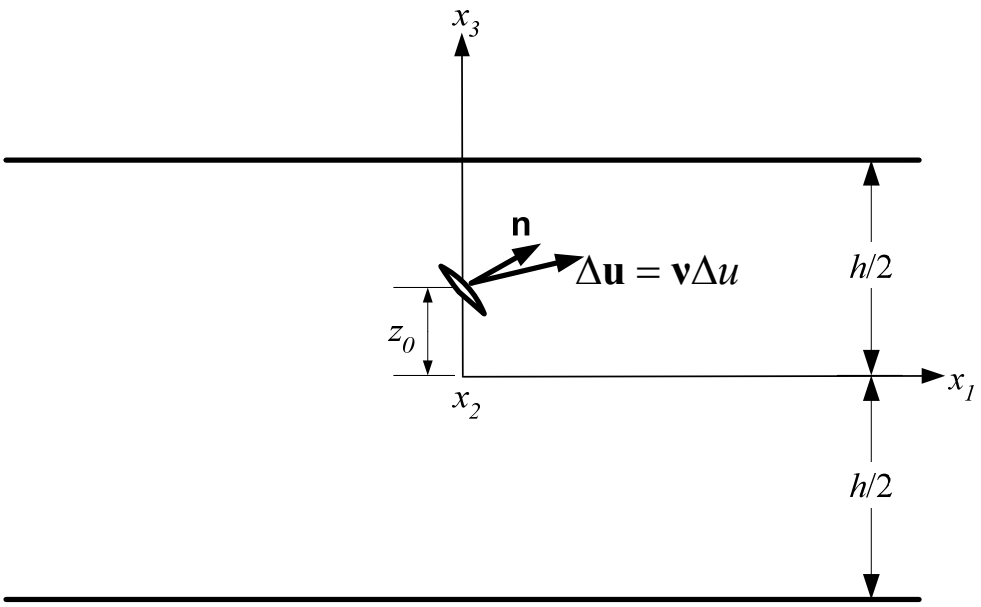

Figure 2.3 A point source with moment tensor M_{ij} and inclined surface at (0, 0, z_0) in plate

In Fig. 2.3 above, $\Delta\mathbf{u} = \boldsymbol{\nu}\Delta u$ is the displacement discontinuity, $\boldsymbol{\nu}$ is a unit vector, **n** is the outward normal to the crack surface. A displacement discontinuity $\Delta\mathbf{u}$ in the direction of any given unit vector $\boldsymbol{\nu}$ may be written as (Rice, 1980[34])

$$\Delta \mathbf{u} = \nu \, \Delta u(\xi, \tau) \tag{2.7}$$

where Δu is the magnitude of the discontinuity. Hence, a general displacement discontinuity can be resolved into an opening displacement and two tangential slip displacements. With Eq. (2.7), the moment tensor in Eq. (2.5) can be expressed as

$$M_{pq} = c_{pqij} \nu_i \, n_j \Delta u \Delta \Sigma \tag{2.8}$$

In the isotropic case, Eq. (2.8) becomes

$$M_{ij} = [\lambda n_k \nu_k \delta_{ij} + G(n_i \nu_j + n_j \nu_i)] \Delta u \, \Delta \Sigma \tag{2.9}$$

where λ and G (more traditionally μ) are the Lame constants and δ_{ij} is Kronecker's delta. For the point source, Δu can be written as $\Delta u = Af(t)$, here A denotes the amplitude of the discontinuity and $f(t)$ source time function. Thus, the moment tensor may be expressed as

$$M_{ij} = M_{ij}^{0} f(t) \tag{2.10}$$

where the spatial component of the loading $M_{ij}^{0} = c_{ijpq} \nu_p n_q A \Delta \Sigma$ results in constants representing the amplitudes of M_{ij}, for the flat fracture surfaces being considered here.

CHAPTER 3.0

EQUIVALENT PLATE LOADS FOR A POINT SOURCE IN A PLATE

3.1 Plate Equations of Motion

Integral solutions from plate theory for the point sources may be derived if the equivalent body forces can be transformed into the corresponding plate loads. For a point source with displacement discontinuities in a plate, there are nine possible dipoles, each dipole with multiplier M_{ij} (corresponding to the component of the moment tensor) representing a part of the equivalent body-force from 3-D elastodynamics. The equivalent body forces can be replaced by plate loads via plate theory by integrating the forces though the thickness. Thus, the waves in the plate excited by $\boldsymbol{M}$ can be evaluated. The derivation is outlined below, starting with the displacement fields and the equations of motion and finally the incorporation of the equivalent plate loads. For more detail see Appendix A.

The approximate displacement field described by the third-order plate theory can be expressed as

$$\begin{aligned} u_1(\mathbf{x},z,t) &= u(\mathbf{x},t) + z\psi_1(\mathbf{x},t) + z^2\varphi_1(\mathbf{x},t) + z^3\chi_1(\mathbf{x},t) \\ u_2(\mathbf{x},z,t) &= v(\mathbf{x},t) + z\psi_2(\mathbf{x},t) + z^2\varphi_2(\mathbf{x},t) + z^3\chi_2(\mathbf{x},t) \\ u_3(\mathbf{x},z,t) &= w(\mathbf{x},t) + z\psi_3(\mathbf{x},t) + z^2\varphi_3(\mathbf{x},t) \end{aligned} \tag{3.1}$$

where $\mathbf{x} = (x_1, x_2)$ and $(u, v, \psi_3, \phi_1, \phi_2)$, $(\psi_1, \psi_2, w, \chi_1, \chi_2, \varphi_3)$ are the generalized extensional and flexural displacements and are uncoupled in linear strain problems with

isotropic plates.

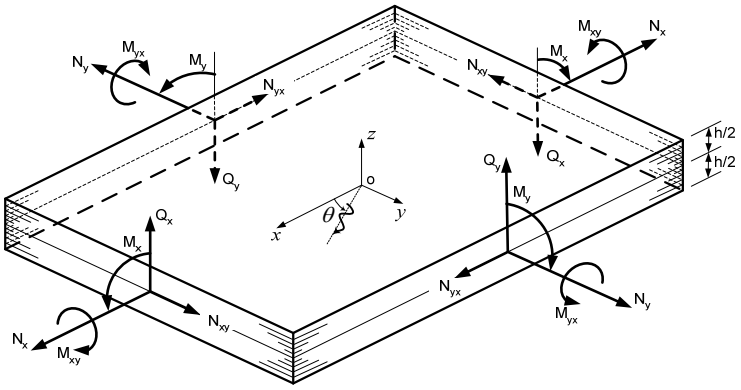

Figure 3.1 Lower order plate forces

The higher order plate forces are not shown on Figure 3.1 and are more of a mathematical construct rather than physical like those from classical theory.

The equations of motion of a plate may be written in terms of the plate resultant forces, by Hamilton's principle or by integration of the elastodynamic equations of motion as shown in Appendix A, Eq. (A.14) - Eq.(A.22) , which results in,

Extensional motion

$$
\begin{aligned}
&N_{11,1} + N_{12,2} + q_1 = I_0\ddot{u} + I_2\ddot{\varphi}_1 \\
&N_{12,1} + N_{22,2} + q_2 = I_0\ddot{v} + I_2\ddot{\varphi}_2 \\
&R_{1,1} + R_{2,2} - N_{33} + m = I_2\ddot{\psi}_3 \\
&S_{11,1} + S_{12,2} - R_1 + \frac{n_1}{2} = \frac{I_2}{2}\ddot{u} + \frac{I_4}{2}\ddot{\varphi}_1 \\
&S_{12,1} + S_{22,2} - R_2 + \frac{n_2}{2} = \frac{I_2}{2}\ddot{v} + \frac{I_4}{2}\ddot{\varphi}_2
\end{aligned}
\tag{3.2}
$$

Flexural motion

$$
\begin{aligned}
&M_{11,1} + M_{12,2} - Q_1 + m_1 = I_2\ddot{\psi}_1 + I_4\ddot{\chi}_1 \\
&M_{12,1} + M_{22,2} - Q_2 + m_2 = I_2\ddot{\psi}_2 + I_4\ddot{\chi}_2 \\
&Q_{x,x} + Q_{y,y} + q = I_0\ddot{w} + I_2\ddot{\varphi}_3 \\
&T_{11,1} + T_{12.2} - 3P_1 + r_1 = I_4\ddot{\psi}_1 + I_6\ddot{\chi}_1 \\
&T_{12,1} + T_{22.2} - 3P_2 + r_2 = I_4\ddot{\psi}_2 + I_6\ddot{\chi}_2 \\
&P_{1,1} + P_{2,2} - 2M_3 + n_z = I_2\ddot{w} + I_4\ddot{\varphi}_3
\end{aligned}
\tag{3.3}
$$

where

$$
I_j = \int_{-h/2}^{h/2} \rho z^j dz \qquad (j = 0, 2, 4, 6) \tag{3.4}
$$

($N_{\alpha\beta}$, $R_{\alpha,}$, $S_{\alpha\beta}$, R_{α}) and ($M_{\alpha\beta}$, $Q_{\alpha,}$ $T_{\alpha\beta}$, $P_{\alpha\beta}$, M_3) are stress resultants which are related to the extensional displacements $(u\ , v\ , \psi_3\ , \phi_1\ , \phi_2)$ and the flexural displacements $(\psi_1,\ \psi_2, w, \chi_1, \chi_2, \varphi_3)$ respectively. Additionally, $(q_1\ , q_2\ , m\ , n_1, n_2)$ and $(m_1, m_2, q, r_1, r_2, n_z)$ are the extensional and flexural plate loads. In the absence of a the localized disturbance inside the plate, they are given by the surface tractions

$$
\begin{Bmatrix} q_\alpha \\ n_\alpha \end{Bmatrix} = [\tau_{\alpha 3}(h/2) - \tau_{\alpha 3}(-h/2)] \begin{Bmatrix} 1 \\ h^2/4 \end{Bmatrix} \qquad \begin{Bmatrix} q \\ n \end{Bmatrix} = [\sigma_{33}(h/2) - \sigma_{33}(-h/2)] \begin{Bmatrix} 1 \\ h^2/4 \end{Bmatrix}
$$

$$
\begin{Bmatrix} m_\alpha \\ r_\alpha \end{Bmatrix} = [\tau_{\alpha 3}(h/2) + \tau_{\alpha 3}(-h/2)] \begin{Bmatrix} h/2 \\ h^3/8 \end{Bmatrix} \qquad m = [\sigma_{33}(h/2) + \sigma_{33}(-h/2)]\ h/2 \tag{3.5}
$$

3.2 AE Loading - Replacement of Tractions with Body Forces

If there is a source of disturbance inside the plate (see Figure 2.3), which is the case with an AE dipole loading, the source will contribute to the plate loads through its equivalent body forces. In other words, the plate forces due to surface tractions shown above will be replaced with body forces as shown below.

The equations of motion with body forces from 3-D elasticity, with the comma indicating differentiation, are

$$\sigma_{ij,j} + f_i = \rho \ddot{u}_i \tag{3.6}$$

where f_i are introduced as the equivalent body forces to the point source with moment tensor $M_{ij}(t)$ in the plate. Multiplying the f_i terms in the above stress equations of motion by z^m (m = 0, 1,2,3), consistent with the power of m multiplying the other terms to produce the equations of motion in terms of plate resultants, and then integrating with respect to z (the plate thickness), the terms

$$\int_{-h/2}^{h/2} f_i z^m dz \qquad z^m \text{ (m=0,1,2,3)} \tag{3.7}$$

represent the plate loads due to the internal point source in the equations of motion of the plate if the equivalent body force is used for f_i. The plate loads generated by the point source can be written as:

$$\begin{aligned} &q_1 = \int_{-h/2}^{h/2} f_1 dz, \quad q_2 = \int_{-h/2}^{h/2} f_2 dz, \quad m = \int_{-h/2}^{h/2} f_3 z dz, \\ &n_1 = \int_{-h/2}^{h/2} f_1 \frac{z^2}{2} dz, \quad n_2 = \int_{-h/2}^{h/2} f_2 \frac{z^2}{2} dz \end{aligned} \tag{3.8}$$

for extensional motion and,

$$m_1 = \int_{-h/2}^{h/2} f_1 z dz, \quad m_2 = \int_{-h/2}^{h/2} f_2 z dz, \quad q = \int_{-h/2}^{h/2} f_3 dz \ ,$$
$$r_1 = \int_{-h/2}^{h/2} f_4 z^3 dz, \quad r_2 = \int_{-h/2}^{h/2} f_5 z^3 dz, \quad n_z = \int_{-h/2}^{h/2} f_6 z^2 dz \tag{3.9}$$

for flexural motion, where f_i are given by Eq. (2.6b).

Performing the integration in Eq. (3.8) and (3.9) in conjunction with the first five of Eqs. (2.6b), and for a single point source in an infinite plate, conveniently letting the source be located at (0, 0, z_0) without loss of generality (see Fig. 2.3), so that the z axis is a symmetry axis through the point source, and after using the following equality,

$$\int_{-h/2}^{h/2} f(z)\delta^{(n)}(z - z_0)dz = (-1)^n f^{(n)}(z_0) \tag{3.10}$$

the plate loads become, for:

Extensional motion (before normalization)

$$\begin{aligned}
q_1 &= -M_{11}\delta'(x_1)\delta(x_2) \quad - M_{12}\delta(x_1)\delta'(x_2) \quad + M_{13}\times 0 \\
q_2 &= -M_{21}\delta'(x_1)\delta(x_2) \quad - M_{22}\delta(x_1)\delta'(x_2) \quad + M_{23}\times 0 \\
m &= -M_{31}z_0\delta'(x_1)\delta(x_2) - M_{32}z_0\delta(x_1)\delta'(x_2) \ + M_{33}\delta(x_1)\delta(x_2) \\
n_1 &= -\frac{M_{11}}{2}\delta'(x_1)\delta(x_2){z_0}^2 - \frac{M_{12}}{2}\delta(x_1)\delta'(x_2){z_0}^2 + M_{13}\delta(x_1)\delta(x_2)z_0 \\
n_2 &= -\frac{M_{21}}{2}\delta'(x_1)\delta(x_2){z_0}^2 - \frac{M_{22}}{2}\delta(x_1)\delta'(x_2){z_0}^2 + M_{23}\delta(x_1)\delta(x_2)z_0
\end{aligned} \tag{3.11}$$

Flexural motion (before normalization)

After performing the integration of all six of Eqs. (2.6b), where the right side of the sixth equation is identical to that of the third equation, to accommodate the extra (sixth)

bending equivalent plate force n_z, in a manner similar to the extensional problem detailed above the, un-normalized bending force equations are:

$$\begin{aligned}
m_1 &= -M_{11} z_0 \delta'(x_1)\delta(x_2) - M_{12} z_0 \delta(x_1)\delta'(x_2) + M_{13}\delta(x_1)\delta(x_2) \\
m_2 &= -M_{21} z_0 \delta'(x_1)\delta(x_2) - M_{22} z_0 \delta(x_1)\delta'(x_2) + M_{23}\delta(x_1)\delta(x_2) \\
q &= -M_{31}\delta'(x_1)\delta(x_2) - M_{32}\delta(x_1)\delta'(x_2) + M_{33}\times 0 \\
r_1 &= -M_{11} z_0^{\,3} \delta'(x_1)\delta(x_2) - M_{12} z_0^{\,3} \delta(x_1)\delta'(x_2) + 3M_{13} z_0^{\,2}\delta(x_1)\delta(x_2) \\
r_2 &= -M_{21} z_0^{\,3} \delta'(x_1)\delta(x_2) - M_{22} z_0^{\,3} \delta(x_1)\delta'(x_2) + 3M_{13} z_0^{\,2}\delta(x_1)\delta(x_2) \\
n_z &= -M_{31} z_0^{\,2} \delta'(x_1)\delta(x_2) - M_{32} z_0^{\,2} \delta(x_1)\delta'(x_2) + 2M_{33} z_0 \delta(x_1)\delta(x_2)
\end{aligned} \tag{3.12}$$

To provide a little more clarity see Appendix B where the first extensional and the last bending equations are derived in more detail.

3.3 Dimensionless Plate Loads

Once the equivalent plate loads for the point source are determined, the plate response to the source can be determined via the plate theory equations of motion via the joint integral transform approach. To calculate the transient response of the plate to the point source, the required equivalent plate loads given by Eq. (3.11) for extension, and Eq. (3.12) for bending, can be conveniently made dimensionless, along with the other variables by normalizing the plate equations of motion. See Appendix A, Eq. (A.25) for a list of normalization constants.

The equations for m, n_1 and n_2 all require normalization. Using the normalization constants defined in Appendix A, and their derivatives as required, the normalized forces can be summarized as:

Extension

$$
\begin{aligned}
q_1 &= -M_{11}\delta'(x_1)\delta(x_2) \quad - M_{12}\delta(x_1)\delta'(x_2) \quad + M_{13}\times 0 \\
q_2 &= -M_{21}\delta'(x_1)\delta(x_2) \quad - M_{22}\delta(x_1)\delta'(x_2) \quad + M_{23}\times 0 \\
m &= -3M_{31}z_0\delta'(x_1)\delta(x_2) - 3M_{32}z_0\delta(x_1)\delta'(x_2) + 3M_{33}\delta(x_1)\delta(x_2) \\
n_1 &= -5M_{11}\delta'(x_1)\delta(x_2)z_0^{\,2} - 5M_{12}\delta(x_1)\delta'(x_2)z_0^{\,2} + 10M_{13}\delta(x_1)\delta(x_2)z_0 \\
n_2 &= -5M_{21}\delta'(x_1)\delta(x_2)z_0^{\,2} - 5M_{22}\delta(x_1)\delta'(x_2)z_0^{\,2} + 10M_{23}\delta(x_1)\delta(x_2)z_0
\end{aligned}
\tag{3.13}
$$

Bending

After performing normalization manipulations similar to those in the extensional problem, the normalized bending equivalent plate forces can be summarized as;

$$
\begin{aligned}
m_1 &= -3M_{11}z_0\delta'(x_1)\delta(x_2) - 3M_{12}z_0\delta(x_1)\delta'(x_2) + 3M_{13}\delta(x_1)\delta(x_2) \\
m_2 &= -3M_{21}z_0\delta'(x_1)\delta(x_2) - 3M_{22}z_0\delta(x_1)\delta'(x_2) + 3M_{23}\delta(x_1)\delta(x_2) \\
q &= -M_{31}\delta'(x_1)\delta(x_2) \quad - M_{32}\delta(x_1)\delta'(x_2) \quad + M_{33}\times 0 \\
r_1 &= -7M_{11}z_0^{\,3}\delta'(x_1)\delta(x_2) - 7M_{12}z_0^{\,3}\delta(x_1)\delta'(x_2) + 21M_{13}z_0^{\,2}\delta(x_1)\delta(x_2) \\
r_2 &= -7M_{21}z_0^{\,3}\delta'(x_1)\delta(x_2) - 7M_{22}z_0^{\,3}\delta(x_1)\delta'(x_2) + 21M_{13}z_0^{\,2}\delta(x_1)\delta(x_2) \\
n_z &= -5M_{31}z_0^{\,2}\delta'(x_1)\delta(x_2) - 5M_{32}z_0^{\,2}\delta(x_1)\delta'(x_2) + 10M_{33}z_0\delta(x_1)\delta(x_2)
\end{aligned}
\tag{3.14}
$$

where all quantities are made dimensionless by using characteristic length $l = h/2$, characteristic time $\tau_0 = \mathrm{l}/c_\mathrm{T}$ ($c_T = \sqrt{G/\rho}$), and by normalizing the moment tensor as $M'_{ij} = M_{ij}/(2Gl^3)$. Note that the primes of the dimensionless moment tensor are dropped in Eq. (3.13) and (3.14) for convenience. An example of the normalization procedure is shown in Appendix C.

3.4 Nine Types of AE Sources and Their Moment Tensor Components

Micro-damage can occur in the form of shear or slip (shear crack), or opening of the crack surfaces (tensile crack), or both (mixed crack). The crack may have different orientations and locations. Nine types of AE point sources are considered, namely, horizontal shear and tensile crack (crack surfaces parallel to middle plane of the plate), vertical shear and tensile crack (crack surfaces are perpendicular to the middle plane), and inclined shear and tensile crack, with each case of the shear crack having two types of shearing directions. For each source, the corresponding plate responses can be evaluated numerically**.**

The shear crack and the tensile crack will be discussed separately. If a fracture surface includes both shear and opening simultaneously (mixed mode crack), the elastic wave emission (AE) from the source can be obtained by using the principle of superposition, as long as linear theory applies.

Without loss of generality in an infinite plate, a point source for an infinite plate located at $(0, 0, z_0)$ can be excited by one of the nine types of micro-damage. For each case the equivalent plate loads, prior to non-dimensionalization, can be obtained from Eq. (3.11) and Eq. (3.12) respectively, where the moment tensor components are defined by Eq. (2.9). The moment tensor components are given below and will be used for numerically simulating the response of the plate to the point source excitations.

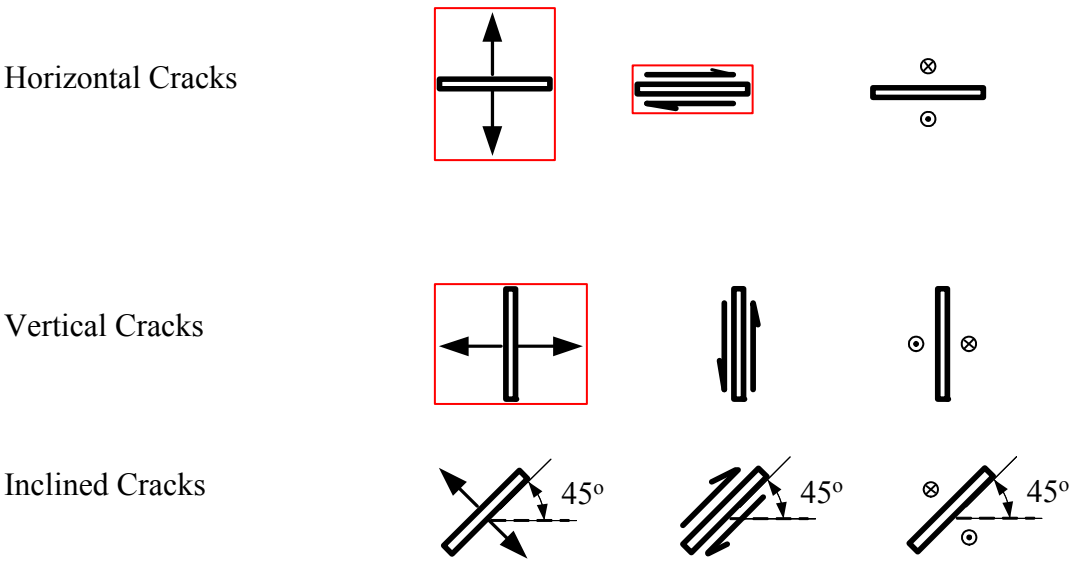

Figure 3.2 AE source orientations

(a) Vertical Tensile crack (crack surface perpendicular to the middle plane)

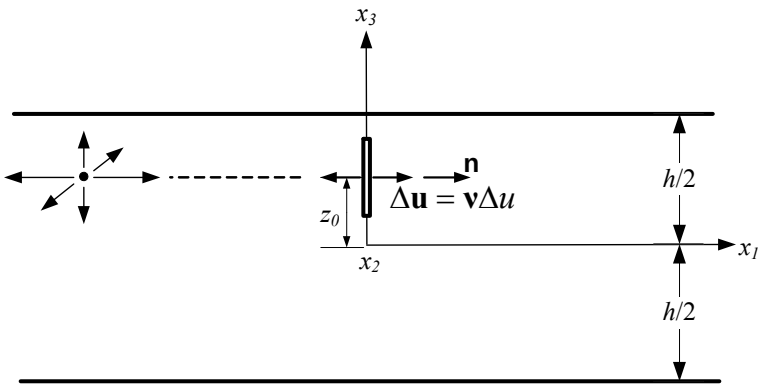

Figure 3.3 Vertical tensile crack

If the crack surface is perpendicular to the x_1 axis, and the displacement discontinuity is in the x_1 direction, $\Delta\mathbf{u} = \Delta u\ [1, 0, 0]^T$,

$$\mathbf{M} = \begin{bmatrix} \lambda + 2\mu & 0 & 0 \\ 0 & \lambda & 0 \\ 0 & 0 & \lambda \end{bmatrix} \Delta u \, \Delta\Sigma$$

To provide more insight, the use of equation 2.9 for calculation the moment tensor is demonstrated for the vertical tensile crack in Appendix D.

(b) Horizontal Tensile Crack

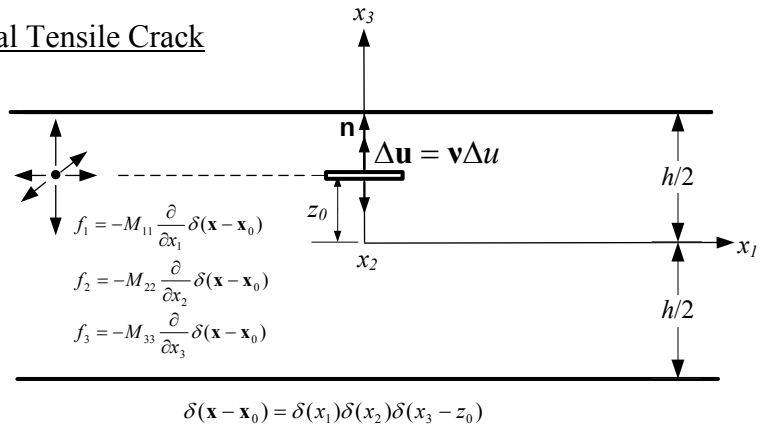

Figure 3.4 Horizontal tensile crack (axi-symmetric w.r.t. x_3-axis)

If the horizontal crack is tension induced with displacement discontinuity is in the z direction, $\Delta\mathbf{u} = \Delta u\,[0, 0, 1]^T$, then **M** becomes;

$$\mathbf{M} = \begin{bmatrix} \lambda & 0 & 0 \\ 0 & \lambda & 0 \\ 0 & 0 & \lambda + 2G \end{bmatrix} \Delta u \, \Delta\Sigma$$

(c) Horizontal Shear Crack

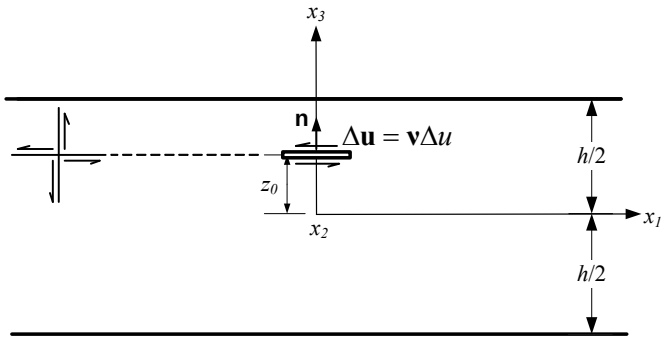

Figure 3.5 Horizontal shear crack

If the horizontal crack ($\boldsymbol{n} = [0, 0, 1]^T$), referencing Fig 3, is shear induced with displacement discontinuity in the x_1 direction, that is, $\Delta\mathbf{u} = \Delta u\ [1,\ 0,\ 0]^T$, the crack is labeled as a **horizontal shear crack I**, and the moment tensor, prior to normalization, defined by Eq. (2.9) is;

$$\mathbf{M} = \begin{bmatrix} 0 & 0 & G \\ 0 & 0 & 0 \\ G & 0 & 0 \end{bmatrix} \Delta u\, \Delta\Sigma$$

If $\Delta\mathbf{u} = \Delta u(0, 1, 0)$, the crack is labeled a **horizontal shear crack II** which gives

$$\mathbf{M} = \begin{bmatrix} 0 & 0 & 0 \\ 0 & 0 & G \\ 0 & G & 0 \end{bmatrix} \Delta u \Delta\Sigma$$

(d) Vertical Shear Crack

If the crack surface is perpendicular to the x_1 axis ($\boldsymbol{n} = [1, 0, 0]^T$). If $\Delta\mathbf{u} = \Delta u[0,\ 0,\ -1]^T$, this crack will be called a **vertical shear crack I** and

$$\mathbf{M}=\begin{bmatrix} 0 & 0 & -G \\ 0 & 0 & 0 \\ -G & 0 & 0 \end{bmatrix}\Delta u\Delta\Sigma$$

In another case, the discontinuity is in the x_2 direction, with $\Delta\mathbf{u} = \Delta u\ [0, 1, 0]^T$, the crack is labeled as **vertical shear crack II**, and

$$\mathbf{M}=\begin{bmatrix} 0 & G & 0 \\ G & 0 & 0 \\ 0 & 0 & 0 \end{bmatrix}\Delta u\,\Delta\Sigma$$

Now consider an inclined micro-crack with normal **n** to the crack surface in the plate (see Fig. 2.3). Let β_0 be angle between the normal **n** and the x_3, or, z-axis, and $\mathbf{n} = [\sin\beta_0, 0, \cos\beta_0]^T$. Then β_0 = 0°, 90° represent the horizontal and vertical cracks respectively. The crack can be tensile if $\Delta\mathbf{u} = \mathbf{n}\,\Delta u$, or a shear crack if $\mathbf{n}\cdot\Delta\mathbf{u} = 0$.

(e) Inclined shear crack

If $\Delta\mathbf{u} = \Delta u[\cos\beta_0,\ 0,\ -\sin\beta_0]^T$, this crack will be called an **inclined shear crack I** in this study, and

$$\mathbf{M}=\begin{bmatrix} G\sin 2\beta_0 & 0 & G\cos 2\beta_0 \\ 0 & 0 & 0 \\ G\cos 2\beta_0 & 0 & -G\sin 2\beta_0 \end{bmatrix}\Delta u\Delta\Sigma$$

If $\Delta\mathbf{u} = \Delta u[0, 1, 0]^T$, the crack is labeled as **inclined shear crack II**, and

$$\mathbf{M} = \begin{bmatrix} 0 & G\sin\beta_0 & 0 \\ G\sin\beta_0 & 0 & G\cos\beta_0 \\ 0 & G\cos\beta_0 & 0 \end{bmatrix} \Delta u \Delta\Sigma$$

(f) Inclined tensile crack

Finally, for an inclined tensile crack

$$\mathbf{M} = \begin{bmatrix} \lambda + 2G\sin^2\beta_0 & 0 & G\sin 2\beta_0 \\ 0 & \lambda & 0 \\ G\sin 2\beta_0 & 0 & \lambda + 2G\cos^2\beta_0 \end{bmatrix} \Delta u \Delta\Sigma$$

CHAPTER 4.0

VECTORIZED EQUATIONS OF MOTION/HOMOGENEOUS INTEGRAL TRANSFORM SOLUTIONS

4.1 Compact Equation of Motion-Extensional Wave

The dimensionless extensional equations of motion in terms of displacements with plate extensional load $\boldsymbol{f}_E(\mathbf{x}, t)$ and zero initial conditions as expressed in the development in Appendix A, in Eqs. (A.27), can be written in matrix notation as

$$\begin{aligned} &\boldsymbol{I}\frac{\partial^2 \boldsymbol{V}}{\partial t^2}+\boldsymbol{T_{11}}\frac{\partial^2 \boldsymbol{V}}{\partial x_1^2}+\boldsymbol{T_{12}}\frac{\partial^2 \boldsymbol{V}}{\partial x_1 \partial x_2}+\boldsymbol{T_{22}}\frac{\partial^2 \boldsymbol{V}}{\partial x_2^2}+\boldsymbol{T_1}\frac{\partial \boldsymbol{V}}{\partial x_1}+\boldsymbol{T_2}\frac{\partial \boldsymbol{V}}{\partial x_2}+\boldsymbol{T_0}\boldsymbol{V}=\mathbf{f}_E, \quad t>0 \\ &\boldsymbol{V}=\frac{\partial \boldsymbol{V}}{\partial t}=\mathbf{0}, \quad at \;\; t=0 \end{aligned} \tag{4.1}$$

Where

$$\boldsymbol{V}=[\mathcal{U}, \mathcal{V}, \Phi_1, \Phi_2, \psi_3]^T$$

$$\mathbf{f}_E=[q_1, q_2, m, n_1, n_2]^T$$

The initial conditions reflect that the plate is unloaded at the time the disturbance occurs. There are no boundary conditions because the plate is assumed to be infinite in the x_1-x_2 plane. This assumption implies that reflections from the boundary are not considered in the formulation. This is a reasonable assumption if the sensors can detect the first wave passage distinctly from later reflections in a large body such as an airplane fuselage.

The Fourier transformation of Eq. (4.1) with respect to the spatial variables x_1 and x_2 yields

$$\frac{\partial^2 \tilde{\boldsymbol{V}}}{\partial t^2} + \mathbf{T}(\mathbf{k})\,\tilde{\boldsymbol{V}} = \tilde{\mathbf{f}}_T\,, \quad t > 0$$
$$\tilde{\boldsymbol{V}} = \frac{\partial \tilde{\boldsymbol{V}}}{\partial t} = \mathbf{0}, \quad at\ t = 0 \tag{4.2}$$

where $\mathbf{x} = (x_1, x_2)$ and the transformed variables $\mathbf{k} = (k_1, k_2)$, and

$$\tilde{\boldsymbol{V}}(\mathbf{k}, t) = \int_{-\infty}^{\infty} \boldsymbol{V}(\mathbf{x}, t) \exp(-i\mathbf{k}\cdot\mathbf{x})\, d\mathbf{x} \tag{4.3}$$
$$\tilde{\mathbf{f}}_{\boldsymbol{T}}(\mathbf{k}, t) = \int_{-\infty}^{\infty} \mathbf{f}_T(\mathbf{x}, t) \exp(-i\mathbf{k}\cdot\mathbf{x})\, d\mathbf{x}$$

and $\boldsymbol{T}_{11}$, $\boldsymbol{T}_{12}$, $\boldsymbol{T}_{22}$, $\boldsymbol{T}_1$, $\boldsymbol{T}_2$, $\boldsymbol{T}_0$ in Eq. (4.1) are *5x5* constant matrices formed simply by isolating the coefficients of each displacement degree of freedom and its derivatives as indicated in Eq. (4.1) above. These can be further combined into a single matrix **T,** after transforming Eq. (4.1) into **k** space**,** to put the equations in their most compact form. The definition of the $\mathbf{T_{ij}}$ terms and the derivation of the **T** matrix are given in Appendix A. See Eq. (A.38).

4.2 Dimensionless Dispersion Relation-Extension

To obtain the dispersion relationship we set all mechanical loads to zero and seek the plane wave elementary solutions to Eq. (4.2) of the form

$$\tilde{\boldsymbol{V}} = \boldsymbol{a} \exp[i(\boldsymbol{k}\cdot\boldsymbol{x} - \omega t)] \tag{4.4}$$

where $V = [u \ , v \ , \psi_3 , \phi_1 , \phi_2]^T$, $\boldsymbol{k} = [k_1, \quad k_2]^{\mathrm{T}}$ is the wave vector, ω is the frequency, and $\boldsymbol{a}$ is a complex-valued vector (or wave amplitude). Substituting Eq. (4.4) into Eq. (4.2), we have the following generalized Eigenvalue problem

$$(\boldsymbol{T} - \omega^2 \boldsymbol{M})\boldsymbol{a} = \boldsymbol{0} \tag{4.5}$$

Setting the determinant of the coefficient matrix in Eq. (4.5) to zero for nontrivial solutions of $\boldsymbol{a}$, $\mathbf{k}$ and ω have to be related by

$$\left|\boldsymbol{T(k)} - \omega^2 \boldsymbol{M}\right| = 0 \tag{4.6}$$

$$\begin{aligned} &\omega_1^{\,2} = k^2 \\ &\omega_2^{\,2} = k^2 + 15\kappa_4^{\,2} \\ &\omega_3^{\,2} \\ &\omega_4^{\,2} \\ &\omega_5^{\,2} \qquad \text{and} \end{aligned} \tag{4.7}$$

$$\begin{aligned} &s_1^2 = -\omega_1^2(\mathbf{k}), \quad s_2^2 = -\omega_2^2(\mathbf{k}), \quad s_3^2 = -\omega_3^2(\mathbf{k}), \\ &s_4^2 = -\omega_4^2(\mathbf{k}), \quad s_5^2 = -\omega_5^2(\mathbf{k}) \end{aligned} \tag{4.8}$$

The explicit analytical expressions for $\boldsymbol{\omega_3^2(k)}$, $\boldsymbol{\omega_4^2(k)}$ and $\boldsymbol{\omega_5^2(k)}$ are much too lengthy to list and were calculated symbolically with the MATHEMATICA code [44]. All 5 modes however can be readily visualized by plotting them as a function of the wave number **k**, after substituting typical values for aluminum for the material constants in **T(k)**. It is usual to plot $\boldsymbol{\omega}_i$ rather than $\boldsymbol{\omega}_i^2$ so MATHEMATICA is used to calculate the square roots of the Eigenvalues. These are plotted in Figure 4.2. $\boldsymbol{\omega_1}$ is a horizontal shear mode propagating transverse to the longitudinal wave and is a straight line with respect to k

passing through the origin with a slope of 1. It is designated $\mathbf{SH_0}$. $\boldsymbol{\omega}_2$ represents the first extensional mode which is designated as the $\mathbf{S_0}$ mode which also starts at the origin of the ω vs. **k** space. The third mode is another horizontal shear mode designated $\mathbf{SH_2}$. The fourth and fifth modes are the higher order extensional modes $\mathbf{S_1}$ and $\mathbf{S_2}$. As will be seen shortly, the contribution of these modes will not be calculated directly as they fall above the cutoff frequency. However they still couple into the problem in the transient solution which requires inversion of the **T** matrix which is 5x5 and affects the calculation of the $\mathbf{S_0}$ response. In fact, it is the inclusion of the $\mathbf{SH_2}$, $\mathbf{S_1}$, and $\mathbf{S_2}$ modes that make the solution different than the one calculated for the first order Mindlin-Kane theory that only includes three degrees of freedom and hence three modes.

The cross-sectional mode shapes for extension, shown in Fig. 4.1, are symmetric, meaning that the response above and below the neutral axis of the plate is such that no transverse deformation or rotation of the cross-section occurs. The mode shapes for flexure, also shown in Fig. 4.1, are antisymmetric, meaning that they give rise to transverse deformation and rotation of the cross-section. Further, the extensional modes $\mathbf{S_0}$ and $\mathbf{S_2}$ are called even symmetric modes as they involve degrees of freedom multiplied by even powers of z in the displacement field. $\mathbf{S_1}$ and $\mathbf{S_3}$ are odd symmetric modes as they involve degrees of freedom multiplied by odd powers of z in the displacement field. The antisymmetric modes can also be odd or even according to the same logic. The flexural modes $\mathbf{A_0}$ and $\mathbf{A_2}$ are even while $\mathbf{A_1}$ and $\mathbf{A_3}$ are odd with deformation patterns as shown in Fig 4.1.

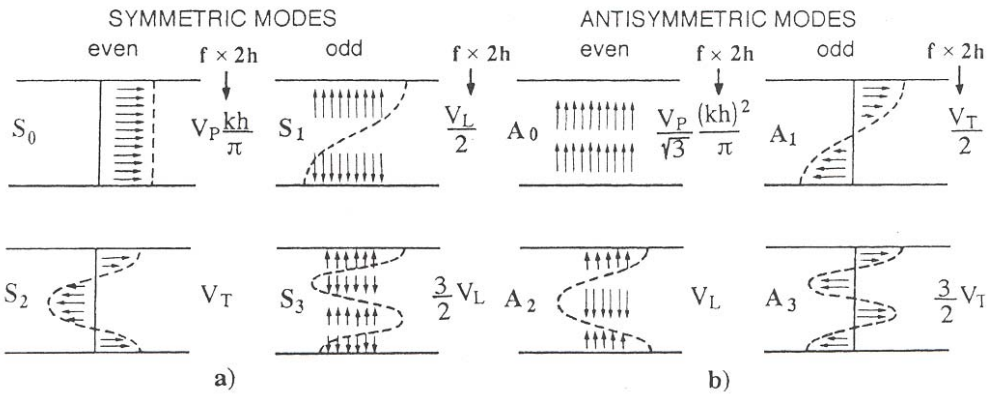

Figure 4.1 Mode shapes for extension bending and transverse shear

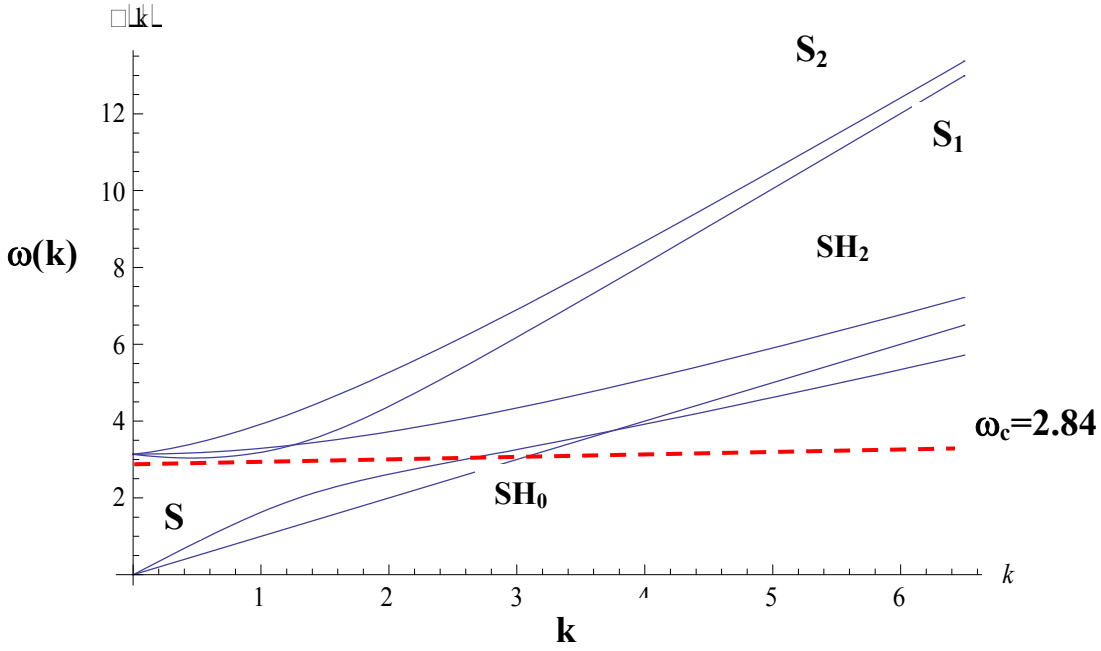

Figure 4.2 Higher order theory extensional dispersion relationships - frequency vs. wave-number

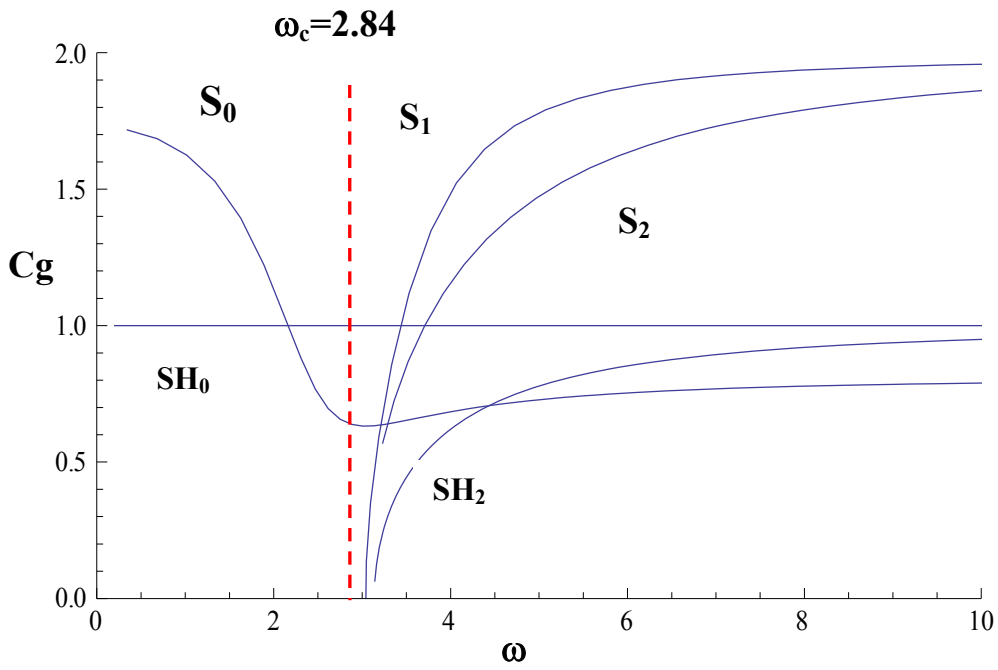

Figure 4.3 Higher order theory extensional theory dispersion group velocity vs. frequency

It is also useful to express the homogeneous solution in terms of the group velocities **C** vs. ω, where $\mathbf{C} = C\mathbf{k}$, $C = \frac{\partial \omega}{\partial k}$. This is shown in Fig. 4.3. In Figs. 4.2 and 4.3 the dimensionless variables, k^*, ω^* and C^*_g, are defined by

$$k_j^* = k\, l, \quad \omega_j^* = \omega \tau_0, \quad C_g^* = C_g / c_T$$

where $l = h/2$, $c_T = \sqrt{G/\rho}$, $\tau_0 = l / c_T$ and k, ω, C_g are the physical wave number, frequency and group velocity with corresponding dimensions, respectively. In the Figures as in the derivation the asterisks are dropped for convenience, which must be remembered when 'un-normalizing' the solution for a real problem with physical material constants and dimensions.

The dispersion relationships from the first order theory (Mindlin Theory) are also shown in Figure 4.6 (Ref. 45). The dispersion relationships for the lower order modes from the elasticity theory are shown in Figure 4.7 [40]. For extensional motion, with both the first and third order theories, due to the normalized cutoff frequency of 2.84 based on the Lamb Wave elasticity theory $\mathbf{S_1}$ minimum, shown as the dashed line in Figure 4.6 (a), and consistent with piezoelectric gage capability around 2MHz, the extensional transient solution will only be calculated for the $\mathbf{S_0}$ mode. The improvement realized in the third order theory comes from the improvement in the $\mathbf{S_0}$ mode dispersion curve. The $\mathbf{S_0}$ mode from the third order theory as observed in Fig. 4.3 agrees much more closely with the elasticity theory result sown in Fig. 4.7 than does the first order mode seen in Fig. 4.6 (b).

4.3 Compact Equation of Motion-Flexural Wave

The dimensionless flexural equations of motion in terms of displacements with plate bending loads $\boldsymbol{f}_B(\mathbf{x}, t)$ and zero initial conditions, as expressed in the development in Appendix A, in Eq. (A.28), can be written in matrix notation as with the extensional problem.

$$\begin{aligned} &\boldsymbol{I}\frac{\partial^2 \boldsymbol{U}}{\partial t^2}+\boldsymbol{A_{11}}\frac{\partial^2 \boldsymbol{U}}{\partial x_1^2}+\boldsymbol{A_{12}}\frac{\partial^2 \boldsymbol{U}}{\partial x_1 \partial x_2}+\boldsymbol{A_{22}}\frac{\partial^2 \boldsymbol{U}}{\partial x_2^2}+\boldsymbol{A_1}\frac{\partial \boldsymbol{U}}{\partial x_1}+\boldsymbol{A_2}\frac{\partial \boldsymbol{U}}{\partial x_2}+\boldsymbol{A_0}\boldsymbol{U}=\mathbf{f}_B, \quad t>0 \\ &\boldsymbol{U}=\frac{\partial \boldsymbol{U}}{\partial t}=\mathbf{0}, \quad at \;\; t=0 \end{aligned} \tag{4.9}$$

Where the flexural degrees of freedom and plate forces are:

$$\mathbf{U}=[\psi_1, \;\; \psi_2, w, \chi_1, \;\; \chi_2, \varphi_3]^T, \;\; \mathbf{f}_B=[m_1, m_2, q, r_1, r_2, n_z]^T,$$

The Fourier transformation of Eq. (4.9) with respect to the spatial variables x_1 and x_2 yields

$$\begin{aligned} &\frac{\partial^2 \tilde{\mathbf{U}}}{\partial t^2} + \tilde{\mathbf{A}}(\mathbf{k})\tilde{\mathbf{U}} = \tilde{\mathbf{f}}_B \,, \quad t > 0 \\ &\tilde{\mathbf{U}} = \frac{\partial}{\partial t}\tilde{\mathbf{U}} = \mathbf{0}, \quad at\ t = 0 \end{aligned} \tag{4.10}$$

where $\mathbf{x} = (x_1, x_2)$ and the transformed variables $\mathbf{k} = (k_1, k_2)$, and

$$\begin{aligned} \tilde{\mathbf{U}}(\mathbf{k},t) &= \int_{-\infty}^{\infty} \mathbf{U}(\mathbf{x},t)\exp(-i\mathbf{k}\cdot\mathbf{x})\,d\mathbf{x} \\ \tilde{\mathbf{f}}_B(\mathbf{k},t) &= \int_{-\infty}^{\infty} \mathbf{f}_B(\mathbf{x},t)\exp(-i\mathbf{k}\cdot\mathbf{x})\,d\mathbf{x} \end{aligned} \tag{4.11}$$

A is formed in a manner similar to its extensional counterpart **T** and is given explicitly in Appendix A, Eq. (A.43).

4.4 Dimensionless Dispersion Relation-Flexure

For the linear equations, Eqs. (4.10) with zero loads, the wave elementary solutions for the flexural wave motion $\mathbf{U} = [\psi_1,\ \psi_2, w\ , \chi_1,\ \chi_2, \varphi_3]^T$ take the basic form:

$$\tilde{\boldsymbol{U}} = \boldsymbol{a}\exp[i(\boldsymbol{k}\cdot\boldsymbol{x} - \omega t)] \tag{4.12}$$

From Eq. (4.12) and (4.10), we have the matrix equation

$$(\boldsymbol{A} - \omega^2\mathbf{I})\boldsymbol{a} = \mathbf{0} \tag{4.13}$$

from which, for non-trival solutions,

$$|\,\boldsymbol{A}(\mathbf{k}) - \omega^2\mathbf{I}\,| = 0 \tag{4.14}$$

Letting $s^2 = -\omega^2$ in the above equation, we have

$$| \boldsymbol{A}(\mathbf{k}) + s^2 \mathbf{I} | = 0 \tag{4.14}$$

where $s_1^2(\mathbf{k}), s_2^2(\mathbf{k}), s_3^2(\mathbf{k}), s_4^2(\mathbf{k}) s_5^2(\mathbf{k}),$ and $s_6^2(\mathbf{k})$ are roots of the equation.

This is the dispersion relation of the plate with **k** being the wave number, and ω the frequency. The roots associated with the bending dispersion relationship are modes, $\boldsymbol{A_0}$, $\boldsymbol{A_1}, \boldsymbol{A_2}, \boldsymbol{A_3}, \boldsymbol{SH_1}$ and $\boldsymbol{SH_3}$ respectively may be expressed in the form

$$\omega_i^2 = \omega_1^2(\mathbf{k}), \quad \omega_2^2(\mathbf{k}), \quad \omega_3^2(\mathbf{k}), \quad \omega_4^2(\mathbf{k}), \quad \omega_5^2(\mathbf{k}), \quad \omega_6^2(\mathbf{k}) \tag{4.16}$$

then

$$\begin{aligned} s_1^2 &= -\omega_1^2(\mathbf{k}), \quad s_2^2 = -\omega_2^2(\mathbf{k}), \quad s_3^2 = -\omega_3^2(\mathbf{k}), \\ s_4^2 &= -\omega_4^2(\mathbf{k}), \quad s_5^2 = -\omega_5^2(\mathbf{k}), \quad s_6^2 = -\omega_6^2(\mathbf{k}) \end{aligned} \tag{4.17}$$

As in the case of extension the actual roots in symbolic form are too lengthy to include explicitly but are plotted below with the material constant $\propto$ based on $\nu = 0.33$. The dispersion relationships from the first order theory (Mindlin Theory) are also shown in Figure 4.6. The dispersion relationships from the 3D elasticity theory, simplified with Lamb Wave theory, are shown in Figure 4.7 [40].

For bending motion, with both first and second order theories, due to a normalized cutoff frequency based on the elasticity theory $\mathbf{S_1}$ minimum value of 2.84, the bending solution will only be calculated for the $\mathbf{A_0}$ and $\mathbf{A_1}$ modes, though the higher order modes couple into the calculation of the lower mode response. By examination of Figs. 4.5, 4.6(b) and 4.7 it can be seen that the $\mathbf{A_0}$ mode result is similar for all three theories. However the second bending mode, $\mathbf{A_1}$ is much more accurately represented by the third

order theory than with the first order theory when comparing with the elasticity theory. The improvement realized in the third order theory comes from the improvement in the $\mathbf{A_1}$ mode dispersion relationship profile.

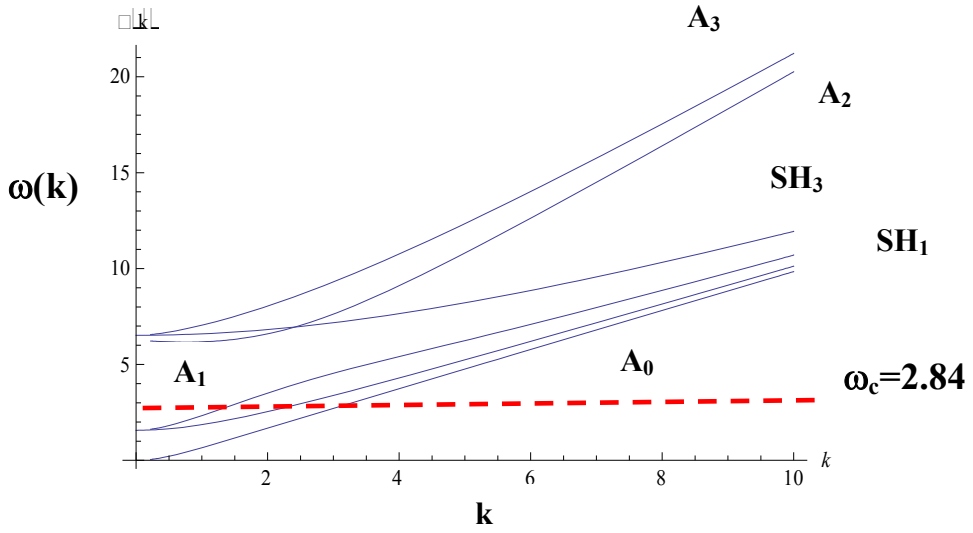

Figure 4.4 Higher order theory bending dispersion relationships frequency vs. wave number

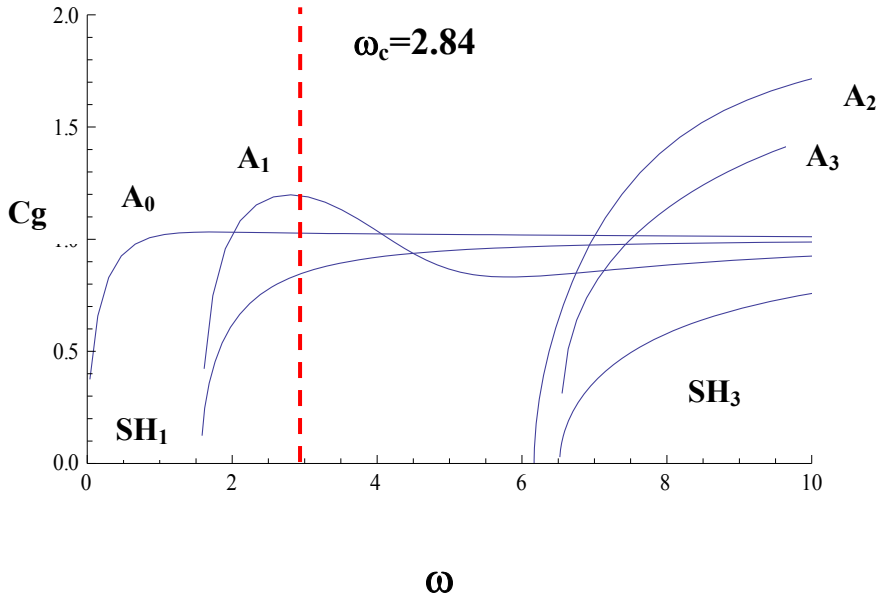

Figure 4.5 Higher order theory bending dispersion relationships group velocity vs. frequency

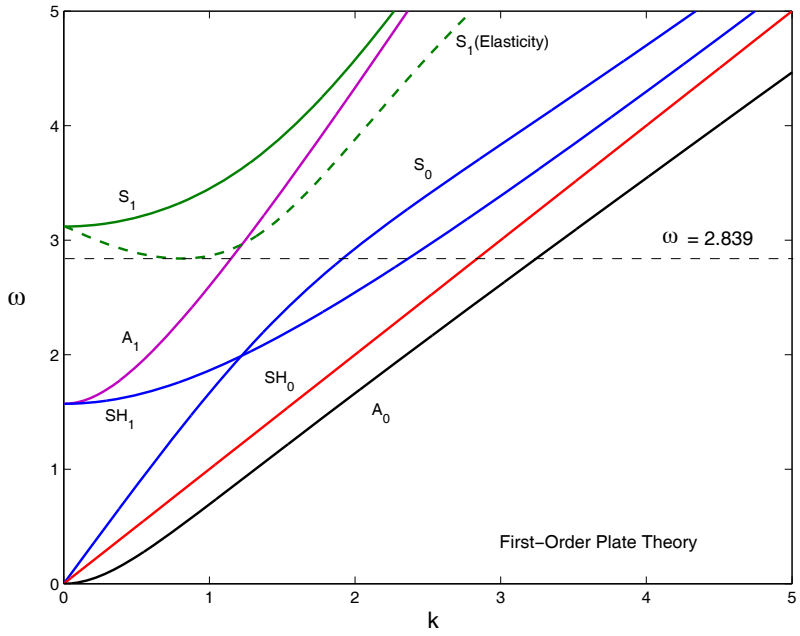

(a)

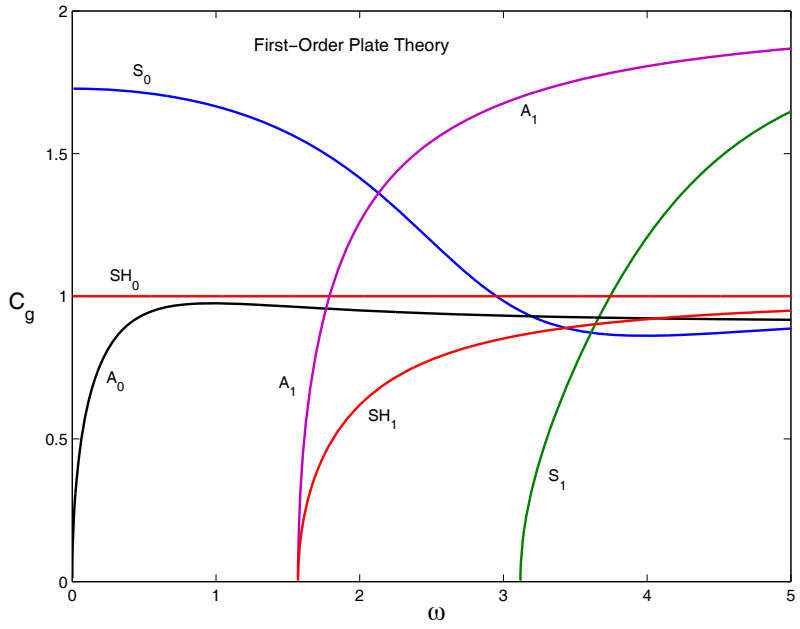

(b)

Figure 4.6 First order theory dispersion relationships (a) - frequency vs. wave number (b) group velocity vs. frequency

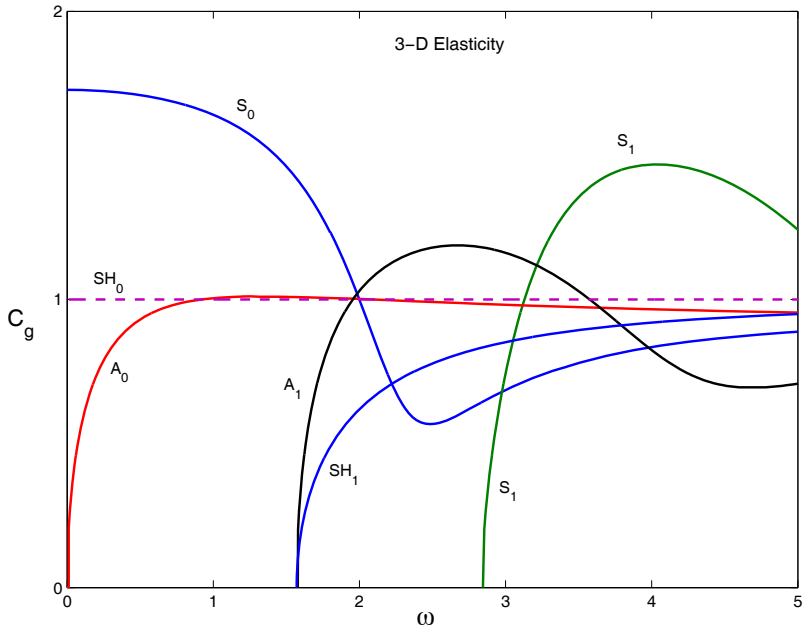

Figure 4.7 Dispersion relation of lower order modes for an isotropic plate with $\nu = 0.33$ from 3-D elasticity

CHAPTER 5.0

NON HOMOGENEOUS INTEGRAL TRANSFORM SOLUTIONS

5.1 Extensional Wave Transformed Solution

Employing the joint integral transforms, first a double Fourier transform on the spatial variables (x_1, x_2) and then a Laplace transform on the time, t, and performing the inverse Laplace transform, explicit expressions for the transient response of the isotropic plate to the point source can be obtained in the integral form of 2-D Fourier transforms. The inverse transform evaluation then yields the solution. For isotropic plates, after some manipulation, the transient solution can be further reduced to a sum of terms which are in the form of inverse Hankel transforms, namely, integrals of products of functions of k and Bessel functions of kr. This 1-D integral solution can be evaluated efficiently and accurately by numerical integration or by asymptotic expansion techniques such as the stationary phase method.

Starting with Eqs. (4.2) and (4.3), repeated below for completeness of the transient solution;

$$\frac{\partial^2 \tilde{\boldsymbol{V}}}{\partial t^2} + \mathbf{T}(\mathbf{k})\,\tilde{\boldsymbol{V}} = \tilde{\mathbf{f}}_E\,, \quad t > 0$$

$$\tilde{\boldsymbol{V}} = \frac{\partial \tilde{\boldsymbol{V}}}{\partial t} = \mathbf{0}, \quad at\ t = 0$$

where $\mathbf{x} = (x_1, x_2)$ and the transformed variables $\mathbf{k} = (k_1, k_2)$, and

$$\widetilde{\boldsymbol{V}}(\mathbf{k},t)=\int_{-\infty}^{\infty}\boldsymbol{V}(\mathbf{x},t)\exp(-i\mathbf{k}\cdot\mathbf{x})\,d\mathbf{x}$$

$$\tilde{\mathbf{f}}_{\boldsymbol{E}}(\mathbf{k},\boldsymbol{t})=\int_{-\infty}^{\infty}\mathbf{f}_{\boldsymbol{E}}(\mathbf{x},\boldsymbol{t})\exp(-\boldsymbol{i}\mathbf{k}\cdot\mathbf{x})\,\boldsymbol{d}\mathbf{x}$$

Where the single material constant

$$\alpha=(2G+\lambda)/G=2(1-\nu)/(1-2\nu)$$

where ν is Poisson's ratio, and λ and G are the Lame constants. **T** is formed by superimposing the coefficient sub matrices $\boldsymbol{T}_{\mathrm{ij}}$ and $\boldsymbol{T}_{\mathrm{i}}$ as shown in Appendix A. For extensional motion then, the application of the Laplace transformation of Eq. (4.2) with respect to t leads to

$$(\mathrm{s}^2\mathbf{I}+\mathbf{T})\bar{\bar{\boldsymbol{V}}}=\bar{\bar{\mathbf{f}}}_{\boldsymbol{E}} \tag{5.1}$$

where

$$\bar{\bar{\boldsymbol{V}}}(\mathbf{k},\mathrm{s})=\int_0^{\infty}\boldsymbol{\tilde{V}}(\mathbf{k},\mathrm{t})\exp(-\mathrm{st})\,\mathrm{dt},\quad \bar{\bar{\mathbf{f}}}_{\boldsymbol{E}}(\mathbf{k},\mathrm{s})=\int_0^{\infty}\tilde{\mathbf{f}}_{\boldsymbol{E}}(\mathbf{k},\mathrm{t})\exp(-\mathrm{st})\,\mathrm{dt} \tag{5.2}$$

The solution of Eq. (5.1) is

$$\begin{aligned}\bar{\bar{\boldsymbol{V}}}&=(\mathbf{T}+s^2\mathbf{I})^{-1}\bar{\bar{\mathbf{f}}}_E\\&=\frac{adj(\mathbf{T}+s^2\mathbf{I})}{\left|\mathbf{T}+s^2\mathbf{I}\right|}\bar{\bar{\mathbf{f}}}_E=\frac{adj(\mathbf{T}+s^2\mathbf{I})}{a_0(s^2-s_1^2)(s^2-s_2^2)(s^2-s_3^2)(s^2-s_4^2)(s^2-s_5^2)}\bar{\bar{\mathbf{f}}}_E\end{aligned}$$

(5.3)

where $s_1^2(\mathbf{k})$, $s_2^2(\mathbf{k})$, $s_3^2(\mathbf{k})$, $s_4^2(\mathbf{k})$ and $s_5^2(\mathbf{k})$ are roots of the equation, developed above,

$$| \mathbf{T}(\mathbf{k}) + s^2 \mathbf{I} |= 0 \tag{5.4}$$

and a_0 is the leading coefficient of the fifth order polynomial that represents the extensional Eigenvalues. Though it is divided out in the homogeneous problem and the Eigenvalue equations are further partitioned into a fourth and a second order polynomial to facilitate the solution, it is still needed for the transient solution. It is carried with D'_m. This term is typically 1 for the lower order theories.

Letting $D(s^2) = | \mathbf{T} + s^2 \mathbf{I} |$, $\mathbf{Q} = [Q^{ij}] = adj(\mathbf{T} + s^2 \mathbf{I})$, Eq. (5.3) can be rewritten as

$$\bar{\bar{\boldsymbol{V}}} = \frac{[\boldsymbol{Q^{ij}}(\boldsymbol{s}^2)]}{\boldsymbol{D}(\boldsymbol{s}^2)} \bar{\bar{\mathbf{f}}}_{\boldsymbol{E}} \tag{5.5}$$

where $Q^{ij}(s^2)$ and $D(s^2)$ are polynomials in s^2 and the degree of D is higher than Q^{ij}.

To carry out the inverse Laplace transform of Eq. (5.5), the method of partial decomposition is used, which yields

$$\frac{Q^{ij}(s^2)}{D(s^2)} = \sum_{m=1}^{5} \frac{Q_m^{ij}}{D'_m} \frac{1}{(s^2 - s_m^2)} \tag{5.6}$$

Where

$$s_m^2 = -\omega_m^2(k)$$
$$Q_m^{ij} = Q^{ij}(s_m^2)$$

$$D'_m = a_0 D'(s_m^2) = \frac{dD}{d(s^2)} \Bigg|_{s^2 = s_m^2} = \prod_{n=1, n \neq m}^{5} (s_m^2 - s_n^2) = \prod_{n=1, n \neq m}^{5} (\omega_n^2 - \omega_m^2) \tag{5.7}$$

With $\prod$ denoting a multiplication of the terms over n rather than a summation.

With Eq. (5.6), Eq. (5.5) becomes

$$\bar{\bar{\tilde{\boldsymbol{V}}}} = \sum_{m=1}^{5} \left[\frac{Q_m^{ij}}{D'_m} \frac{1}{(s^2 - s_m^2)} \right]_{5x5} \bar{\bar{\tilde{\mathbf{f}}}}_E \tag{5.8}$$

Now it is easy to apply the inverse Laplace transform (Debnath, 1995 [9]) to the above equation via the convolution theorem, and

$$\tilde{\boldsymbol{V}} = \sum_{m=1}^{5} \frac{\left[Q_m^{ij} \right]_{5x5}}{D'_m} \frac{\sin(\omega_m t) * \tilde{\mathbf{f}}_E(\mathbf{k}, t)}{\omega_m} \tag{5.9}$$

where * denotes convolution with respect to time,

$$\sin(\omega_{\boldsymbol{m}} \boldsymbol{t}) * \tilde{\mathbf{f}}_{\boldsymbol{E}}(\mathbf{k}.\boldsymbol{t}) = \int_0^{\boldsymbol{t}} \tilde{\mathbf{f}}_{\boldsymbol{E}}(\mathbf{k}, \xi) \sin \omega_{\boldsymbol{m}} (\boldsymbol{t} - \xi) \boldsymbol{d} \xi$$

Finally, applying the inverse Fourier transform to Eq. (5.9), the solution is given by

$$\boldsymbol{V}(\mathbf{x}, t) = [u_0 , v_0 , \psi_3 , \phi_1 , \phi_2]^T = \frac{1}{4\pi^2} \int_{-\infty}^{\infty} \tilde{\mathbf{V}}(t, \mathbf{k}) \exp(i\mathbf{k} \cdot \mathbf{x}) d\mathbf{k} \tag{5.10}$$

$$\begin{aligned} \tilde{\mathbf{V}}(\mathbf{k}, t) &= \sum_{m=1}^{5} \frac{[Q_m^{ij}]_{5x5}}{D'_m} \frac{\sin(\omega_m t) * \tilde{\mathbf{f}}_E(\mathbf{k}, t)}{\omega_m} \\ &= \sum_{m=1}^{5} [\mathbf{Q}_m^1 \tilde{q}_1 + \mathbf{Q}_m^2 \tilde{q}_2 + \mathbf{Q}_m^3 \tilde{m} + \mathbf{Q}_m^4 \tilde{n}_1 + \mathbf{Q}_m^5 \tilde{n}_2] * \frac{\sin(\omega_m t)}{D'_m \omega_m} \end{aligned} \tag{5.11}$$

where $\mathbf{Q}_m^i(\mathbf{k})$ is a 5×1 matrix $\qquad \mathbf{Q}_{\mathbf{m}}^{\mathbf{i}} = \begin{Bmatrix} Q_m^{1i} \\ Q_m^{2i} \\ Q_m^{3i} \\ Q_m^{4i} \\ Q_m^{5i} \end{Bmatrix} i = 1,2,3,4,5$ (5.12)

where the ~ denotes the 2-D Fourier transform of the quantities in space (x_1, x_2), $\mathbf{f}_E = [q_1, q_2, m, n_1, n_2]^T$ is the dimensionless plate loading for extensional motion, the symbol * denotes the convolution between the transposed plate loading $\tilde{\mathbf{f}}_E$ and $\sin W_m t$ with respect to time, $\omega = W_m(\mathbf{k})$ is the dispersion relation of the m^{th} extensional wave mode, and all the other symbols, $D'_m(k)$, $W_m(k)$, $Q^{ij}_m(k)$, $\mathbf{Q}^i_m$ have been defined above.

5.2 Extensional Transformed Plate Loads

For the point source at (0, 0, z_0) with moment tensor $M_{ij}(t)$, the Fourier transform of the dimensionless plate loads, Eq. (3.13), must be computed. The result is,

$\tilde{\mathbf{f}}_E = [\tilde{q}_1, \tilde{q}_2, \tilde{m}, \tilde{n}_1, \tilde{n}_2]^T$, where

$$\begin{aligned}
\tilde{q}_1 &= -ik_1 M_{11} \qquad - ik_2 M_{12} \\
\tilde{q}_2 &= -ik_1 M_{21} \qquad - ik_2 M_{22} \\
\tilde{m} &= -i3k_1 M_{31} z_0 - ik_2 3M_{32} z_0 \quad + 3M_{33} \\
\tilde{n}_1 &= -5ik_1 M_{11} z_0^{\,2} - 5ik_2 M_{12} z_0^{\,2} + 10M_{13} z_0 \\
\tilde{n}_2 &= -5ik_1 M_{21} z_0^{\,2} - 5ik_2 M_{22} z_0^{\,2} + 10M_{23} z_0
\end{aligned} \tag{5.13}$$

In the derivation of Eq. (5.13) the property of the Fourier transform

$$\int_{-\infty}^{\infty} \exp(-ikx)\delta^{(n)}(x)dx = (ik)^n \tag{5.16}$$

has been used. Note that $\mathbf{F_i}$ is used later and is simply $\tilde{\mathbf{f}}_E$ with a –i factored out.

To provide more clarity into the transforming of the normalized plate loads the third of Eqs. (3.13) is transformed in Appendix E to produce the third of Eqs. (5.13).

5.3 Flexural Wave Transformed Solution

Proceeding in similar fashion to the extensional problem for bending, starting with Eqs. (4.10) and (4.11), repeated below for completeness of the transient solution;

$$\frac{\partial^2 \tilde{\mathbf{U}}}{\partial t^2} + \mathbf{A}(\mathbf{k})\tilde{\mathbf{U}} = \tilde{\mathbf{f}}_B \,, \quad t > 0$$

$$\tilde{\mathbf{U}} = \frac{\partial}{\partial t}\tilde{\mathbf{U}} = \mathbf{0}, \quad at\ t = 0$$

where $\mathbf{x} = (x_1, x_2)$ and the transformed variables $\mathbf{k} = (k_1, k_2)$, and

$$\tilde{\mathbf{U}}(\mathbf{k}, t) = \int_{-\infty}^{\infty} \mathbf{U}(\mathbf{x}, t) \exp(-i\mathbf{k} \cdot \mathbf{x})\, d\mathbf{x}$$

$$\tilde{\mathbf{f}}_B(\mathbf{k}, t) = \int_{-\infty}^{\infty} \mathbf{f}_B(\mathbf{x}, t) \exp(-i\mathbf{k} \cdot \mathbf{x})\, d\mathbf{x}$$

then application of the Laplace transformation of Eq. (4.10) with respect to t leads to

$$(s^2\mathbf{I} + \boldsymbol{A})\bar{\tilde{\boldsymbol{U}}} = \bar{\tilde{\mathbf{f}}}_B \tag{5.15}$$

where

$$\bar{\tilde{\boldsymbol{U}}}(\mathbf{k}, s) = \int_0^{\infty} \tilde{\boldsymbol{U}}(\mathbf{k}, t) \exp(-st)\, dt, \quad \bar{\tilde{\mathbf{f}}}_B(\mathbf{k}, s) = \int_0^{\infty} \tilde{\mathbf{f}}_B(\mathbf{k}, t) \exp(-st)\, dt \tag{5.16}$$

The solution of Eq. (5.15) is

$$\begin{aligned} \bar{\tilde{\boldsymbol{U}}} &= (\mathbf{A} + s^2\mathbf{I})^{-1} \bar{\tilde{\mathbf{f}}}_B = \frac{adj(\mathbf{A} + s^2\mathbf{I})}{\left|\mathbf{A} + s^2\mathbf{I}\right|} \bar{\tilde{\mathbf{f}}}_B \\ &= \frac{adj(\mathbf{T} + s^2\mathbf{I})}{b_0(s^2 - s_1^2)(s^2 - s_2^2)(s^2 - s_3^2)(s^2 - s_4^2)(s^2 - s_5^2)(s^2 - s_6^2)} \bar{\tilde{\mathbf{f}}}_B \end{aligned} \tag{5.17}$$

where $s_1^2(\mathbf{k}), s_2^2(\mathbf{k}), s_3^2(\mathbf{k}), s_4^2(\mathbf{k}), s_5^2(\mathbf{k})$ *and* $s_6^2(\mathbf{k})$ are roots of the equation, developed above,

and b_0 is the leading coefficient of the sixth order polynomial that represents the flexural Eigenvalues. Though it is divided out in the homogeneous problem and the Eigenvalue equations are further partitioned into a fourth and a second order polynomial to facilitate the solution, it is still needed for the transient solution. As in the extensional case it is carried with D'_m. This term is typically 1 for the lower order theories.

$$| \boldsymbol{A}(\mathbf{k}) + s^2\mathbf{I} | = 0$$

Letting $D(s^2) = | \mathbf{T} + s^2\mathbf{I} |, \mathbf{Q} = [Q^{ij}] = adj(\mathbf{T} + s^2\mathbf{I})$, Eq. (5.17) can be rewritten as

$$\bar{\bar{\tilde{\boldsymbol{U}}}} = \frac{[Q^{ij}(s^2)]}{D(s^2)} \bar{\bar{\tilde{\mathbf{f}}}}_B \tag{5.19}$$

where $Q^{ij}(s^2)$ and $D(s^2)$ are polynomials in s^2 and the degree of D is higher than Q^{ij}.

To carry out the inverse Laplace transform to Eq. (5.19), the method of partial decomposition is used, which yields

$$\frac{Q^{ij}(s^2)}{D(s^2)} = \sum_{m=1}^{6} \frac{Q_m^{ij}}{D'_m} \frac{1}{(s^2 - s_m^2)} \tag{5.20}$$

where $s_m^2 = -\omega_m^2(k)$

$$Q_m^{ij} = Q^{ij}(s_m^2)$$

$$D'_m = b_0 D'(s_m^2) = \frac{dD}{d(s^2)} \bigg|_{s^2 = s_m^2} = \prod_{n=1, n\neq m}^{6} (s_m^2 - s_n^2) = \prod_{n=1, n\neq m}^{6} (\omega_n^2 - \omega_m^2) \tag{5.21}$$

With $\prod$ denoting a multiplication of the terms over n rather than a summation.

With Eq. (5.20), Eq. (5.19) becomes

$$\bar{\tilde{U}} = \sum_{m=1}^{6} \left[\frac{Q_m^{ij}}{D_m'} \frac{1}{(s^2 - s_m^2)} \right]_{6x6} \bar{\tilde{\mathbf{f}}}_B \tag{5.22}$$

Now it is easy to apply the inverse Laplace transform (Debnath, 1995 [9]) to the above equation via the convolution theorem, and

$$\tilde{U} = \sum_{m=1}^{6} \frac{\left[Q_m^{ij} \right]_{6x6}}{D_m'} \frac{\sin(\omega_m t) * \tilde{\mathbf{f}}_B(\mathbf{k}, t)}{\omega_m} \tag{5.23}$$

where * denotes convolution with respect to time,

$$\sin(\omega_m t) * \tilde{\mathbf{f}}_B(\mathbf{k}.t) = \int_0^t \tilde{\mathbf{f}}_B(\mathbf{k}, \xi) \sin \omega_m (t - \xi) d\xi$$

Finally, applying the inverse Fourier transform to Eq. (A.18), the solution is given by

$$\mathbf{U}(\mathbf{x}, t) = [\psi_1, \ \psi_2, w, \chi_1, \ \chi_2, \varphi_3]^T = \frac{1}{4\pi^2} \int_{-\infty}^{\infty} \tilde{\mathbf{U}}(\mathbf{k}, t) \exp(i\mathbf{k} \cdot \mathbf{x}) d\mathbf{k} \tag{5.24}$$

with

$$\begin{aligned} \tilde{\mathbf{U}}(\mathbf{k}, t) &= \sum_{m=1}^{6} \frac{[Q_m^{ij}]_{6x6}}{D_m'} \frac{\sin(\omega_m t) * \tilde{\mathbf{f}}_B(\mathbf{k}, t)}{\omega_m} \\ &= \sum_{m=1}^{6} [\mathbf{Q}_m^1 \tilde{m}_1 + \mathbf{Q}_m^2 \tilde{m}_2 + \mathbf{Q}_m^3 \tilde{q} + \mathbf{Q}_m^4 \tilde{r}_1 + \mathbf{Q}_m^5 \tilde{r}_2 + \mathbf{Q}_m^6 \tilde{n}_z] * \frac{\sin(\omega_m t)}{D_m' \omega_m} \end{aligned} \tag{5.25}$$

where $\mathbf{Q}_m^i(\mathbf{k})$ is the 6×1 matrix,

$$\mathbf{Q}_\mathbf{m}^\mathbf{i} = \begin{Bmatrix} Q_m^{1j} \\ Q_m^{2j} \\ Q_m^{3j} \\ Q_m^{4j} \\ Q_m^{5j} \\ Q_m^{6j} \end{Bmatrix} i = 1, 2, 3, 4, 5, 6 \tag{5.26}$$

5.4 Flexural Transformed Plate Loads

$\mathbf{f}_B = [m_1, m_2, q, r_1, r_2, n_z]^T$ is the dimensionless plate load for flexural motion. In the case of a point source at (0, 0, z_0) with moment tensor $M_{ij}(t)$, the Fourier transform of the dimensionless plate load,

$$\tilde{\mathbf{f}}_B = [\tilde{m}_1, \tilde{m}_2, \tilde{q}, \tilde{r}_1, \tilde{r}_2, \tilde{n}_z]^T \tag{5.27}$$

as expressed in Eqs. (3.14) is:

$$\begin{aligned}
\tilde{m}_1 &= -i3k_1M_{11}z_0 - i3k_2M_{12}z_0 + 3M_{13} \\
\tilde{m}_2 &= -i3k_1M_{21}z_0 - i3k_2M_{22}z_0 + 3M_{23} \\
\tilde{q} &= -ik_1M_{31} - ik_2M_{32} \\
\tilde{r}_1 &= -7ik_1M_{11}z_0^3 - 7ik_2M_{12}z_0^3 + 21M_{13}z_0^2 \\
\tilde{r}_2 &= -7ik_1M_{21}z_0^3 - 7ik_2M_{22}z_0^3 + 21M_{23}z_0^2 \\
\tilde{n}_z &= -5ik_1M_{31}z_0^2 - 5ik_2M_{32}z_0^2 + 10M_{33}z_0
\end{aligned} \tag{5.28}$$

The transformation process is similar to that employed for the extensional plate forces and will not be shown here for brevity. Note that $\mathbf{F_i}$ is used later and is simply $\tilde{\mathbf{f}}_B$ with a $-i$ factored out.

5.5 Transient Solution by Application of Inverse Fourier Transform

Thus, the total transient response of the plate to the point source is expressed in a compact integral form as the sum of Eqs. (5.10) and (5.24). Note that the derivations for the extensional and flexural motions follow the same procedures and that for convenience, Eq. (5.10) and (5.24) are written in the same form except for the loadings. Note however

that the symbols $D'_m(k)$, $\omega_m(k)$, $Q^{ij}_m(k)$, $\mathbf{Q}^i_m$, are associated with different motions, and are defined separately for extension and bending.

Recall that the moment tensor $M_{ij}(t)$ for a point source can be expressed as $M_{ij} = M^0_{ij} f(t)$ (Eq. (2.10)) where M^0_{ij}, the spatial components, are constants for a given source. With Eq. (5.10) and (5.24), the inverse Fourier transform integral solution can also be rewritten in the form

$$\mathbf{V} = \frac{-i}{4\pi^2} \sum_{m=1}^{5} \int_{-\infty}^{\infty} [F_1 \mathbf{Q}^1_m + F_2 \mathbf{Q}^2_m + F_3 \mathbf{Q}^3_m + F_4 \mathbf{Q}^4_m + F_5 \mathbf{Q}^5_m] \frac{H_m}{D'_m} \exp(i\mathbf{k} \cdot \mathbf{x}) d\mathbf{k} \tag{5.29}$$

$$\mathbf{U} = \frac{-i}{4\pi^2} \sum_{m=1}^{6} \int_{-\infty}^{\infty} [F_1 \mathbf{Q^1_m} + F_2 \mathbf{Q^2_m} + F_3 \mathbf{Q^3_m} + F_4 \mathbf{Q^4_m} + F_5 \mathbf{Q^5_m} + F_6 \mathbf{Q^6_m}] \frac{H_m}{D'_m} \exp(i\mathbf{k} \cdot \mathbf{x}) d\mathbf{k} \tag{5.30}$$

With $F_i = -\tilde{f}_E / i$ for extension and $F_i = -\tilde{f}_B / i$ for flexure, which essentially factors the imaginary number i out of the transformed forces and places it as a multiplier on the solution vectors as seen above.

The function $H_m(\mathbf{k}, t)$ is defined by

$$H_m(\mathbf{k}, t) = f(t) * \frac{\sin \omega_m t}{\omega_m} = \omega_m^{-1} \int_0^t f(\tau) \sin \omega_m (t - \tau) d\tau, \quad i = 1, 2, 3 \tag{5.31}$$

From the above solutions, the total surface strains, $\varepsilon_{\alpha\alpha} = (\varepsilon_{11} + \varepsilon_{22})_{z=h/2}$, which are easily measured from the experiments using piezoelectric sensors, can be derived from the strain displacement relationships.

5.6 Strain Formulation

Extensional motion

$$\varepsilon_{\alpha\alpha} = \frac{1}{4\pi^2}\sum_{m=1}^{5}\int_{-\infty}^{\infty}\sum_{i=1}^{5}[(k_1(\boldsymbol{Q_m^{1i}} + z_0{}^2\boldsymbol{Q_m^{3i}}) + k_2(\boldsymbol{Q_m^{2i}} + z_0{}^2\boldsymbol{Q_m^{3i}})]\{\boldsymbol{F_i}\}\frac{H_m}{D'_m}\exp(i\mathbf{k}\cdot\mathbf{x})d\mathbf{k} \qquad (5.32)$$

Flexural motion

$$\varepsilon_{\alpha\alpha} = \frac{1}{4\pi^2}\sum_{m=1}^{6}\int_{-\infty}^{\infty}\sum_{i=1}^{6}[(k_1(\boldsymbol{Q_m^{1i}} + z_0{}^3\boldsymbol{Q_m^{4i}}) + k_2(z_0\boldsymbol{Q_m^{2i}} + z_0{}^3\boldsymbol{Q_m^{5i}})]\{\boldsymbol{F}_i\}\frac{H_m}{D'_m}\exp(i\mathbf{k}\cdot\mathbf{x})d\mathbf{k} \qquad (5.33)$$

Again, the **Q** terms are different for extension and flexure even if they carry the same subscripts and superscripts. A derivation of the strain expressions is detailed in Appendix G

5.7 Cartesian to Polar Transformation – Reduction to 1D Hankel Transforms

The transient solutions, Eq. (5.29), (5.30), (5.32), and (5.33), are given in terms of the two-dimensional inverse Fourier transform, where the integration is a double integral with respect to k_1 and k_2 when the wave number vector **k** is expanded. For isotropic plates the solutions may be expressed as a series involving the integral of products of Bessel functions of *kr* and other functions of a single variable *k* which take the form of inverse Hankel transforms. This reduction from a 2-D to 1-D integral is developed as follows.

In terms of polar coordinates

$$k_1 = k\cos\phi, \quad k_2 = k\sin\phi \qquad (5.34)$$

$$x_1 = r\cos\theta, \quad x_2 = r\sin\theta \tag{5.35}$$

The exponential term becomes

$$\exp(i\mathbf{k}\cdot\mathbf{x}) = \exp[ikr\cos(\phi-\theta)], \quad d\mathbf{k} \equiv dk_1 dk_2 = kdkd\phi$$

Eq. (5.10) and (5.24), along with (5.29) and (5.30), indicate that the Fourier transform of any displacement component, for example, the extensional displacement $\tilde{u}$, can be written as

$$\tilde{u}(\mathbf{k},t) = \sum_{m=1}^{5} -i[F_1\mathbf{Q}_m^1 + F_2\mathbf{Q}_m^2 + F_3\mathbf{Q}_m^3 + F_4\mathbf{Q}_m^4 + F_5\mathbf{Q}_m^5]\frac{H_m}{D_m'} \tag{5.36}$$

Note that $Q_m^{ij}, j = 1, 2, 3, 4, 5$ for $\tilde{u}, \tilde{v}, \tilde{\psi}_3, \tilde{\phi}_1, \tilde{\phi}_2$ respectively, picking the proper row of the $\mathbf{Q_{ij}}$ matrix, according to the matrix notation, Eq. (5.26). Substituting Eq. (5.34) into Eq. (5.36), $\tilde{u}$ can be expressed as a summation

$$\begin{aligned}\tilde{u}(\mathbf{k},t) &= \sum_{m=1}^{5}\sum_{n=0}^{5}[C_{mn}(k)\cos n\varphi + S_{mn}(k)\sin n\varphi]\frac{H_m(k,t)}{D_m'(k)} \\ &= \sum_{m=1}^{5}\sum_{n=0}^{5}[(C_{mn} - iS_{mn})\exp(in\varphi) + (C_{mn} + iS_{mn})\exp(-in\varphi)]\frac{H_m(k,t)}{2D_m'(k)}\end{aligned} \tag{5.37}$$

Where the coefficients $C_{mn}(k)$ and $S_{mn}(k)$ are complex and determined by carrying out the multiplications indicated in Eq. (5.36) and then reducing all powers $\sin^n\phi$ and $\cos^n\phi$ to $\sin(n\phi)$ and $\cos(n\phi)$. These considerable algebraic and trigonometric manipulations lead to Eq. (5.40). Note that in Eq. (5.37) $C_{mn}, S_{mn}, H_m, D_m'$ are independent of ϕ.

These manipulations cannot be done reasonably by hand but were accomplished with the MATHEMATICA code for the third order theory. This process can be carried out

manually, with difficulty, for simpler problems. As an example, for a 2D plane stress problem with only 2 displacement degrees of freedom, u and *v*, which is the subject of Appendix J, the coefficients are calculated in Appendix J.A in order to provide insight into how they are computed here. Appendix J is included to provide insight into the higher order theories using a simpler problem where all quantities can be manually computed. Substituting Eq. (5.37) into the integrand of Eq. (5.29) for extension, and integrating with respect to ϕ first, the integration with respect to k leads to a series of inverse Hankel transforms. For example, the displacement u in extensional motion can be expressed as

$$u(r,\theta,t)=\frac{1}{4\pi^2}\sum_{m=1}^{5}\sum_{n=0}^{5}\left\{\int_0^\infty \frac{C_{mn}-iS_{mn}}{2}\frac{H_m}{D'_m}kdk\int_0^{2\pi}\exp[in\varphi+ikr\cos(\varphi-\theta)]d\varphi \right. \\ \left. +\int_0^\infty \frac{C_{mn}+iS_{mn}}{2}\frac{H_m}{D'_m}kdk\int_0^{2\pi}\exp[-in\varphi+ikr\cos(\varphi-\theta)]d\varphi\right\} \tag{5.38}$$

Making a change of variable $\phi-\theta=\alpha+\pi/2$, and using the integral representation of the Bessel function of order *n,*

$$J_n(kr)=\frac{1}{2\pi}\int_{\alpha_0}^{2\pi+\alpha_0}\exp[i(n\alpha-kr\sin\alpha)]d\alpha$$

and using the definition $J_{-n}(kr)=(-1)^nJ_n(kr)$ (where the upper limit $\alpha_0=-(\theta+\pi/2)$), Eq. (5.38) is reduced to

$$u=\frac{1}{2\pi}\sum_{m=1}^{5}\sum_{n=0}^{5}\int_0^\infty \frac{H_m(k,t)}{D'_m(k)}U_{mn}(k,\theta)J_n(kr)kdk \tag{5.39}$$

where

$$U_{mn}(k,\theta) = \frac{C_{mn}}{2}[e^{in(\theta+\frac{\pi}{2})} + (-1)^n cc] - i\frac{S_{mn}}{2}[e^{in(\theta+\frac{\pi}{2})} - (-1)^n cc]$$
$$= i^n (C_{mn}\cos n\theta + S_{mn}\sin n\theta) \tag{5.40}$$

and *cc* stands for the complex conjugate of the preceding terms.

Therefore, for isotropic plates the transient wave solutions are reduced to a series of the inverse Hankel transforms. Performing similar manipulation on v, and φ_1, φ_2 and ψ_3 the displacements for extensional motion are,

$$\begin{bmatrix} u \\ v \\ \varphi_1 \\ \varphi_2 \\ \psi_2 \end{bmatrix} = \frac{1}{2\pi}\sum_{m=1}^{5}\sum_{n=0}^{n\max}\int_0^\infty \frac{H_m(k,t)}{D'_m(k)} \begin{bmatrix} U_{mn}(k,\theta) \\ V_{mn}(k,\theta) \\ \Phi_{1mn}(k,\theta) \\ \Phi_{2mn}(k,\theta) \\ \Psi_{mn}(k,\theta) \end{bmatrix} J_n(kr)kdk \tag{5.41}$$

where,

$$\begin{bmatrix} U_{mn} \\ V_{mn} \\ \Phi_{1mn} \\ \Phi_{2mn} \\ \Psi_{mn} \end{bmatrix} = \begin{bmatrix} U_{mnc}(k) \\ V_{mnc}(k) \\ \Phi_{1mnc}(k) \\ \Phi_{2mnc}(k) \\ \Psi_{mnc}(k) \end{bmatrix} \cos n\theta + i \begin{bmatrix} U_{mns}(k) \\ V_{mns}(k) \\ \Phi_{1mns}(k) \\ \Phi_{2mns}(k) \\ \Psi_{mns}(k) \end{bmatrix} \sin n\theta \tag{5.42}$$

The response of the surface strains to the point source due to extensional motion can be obtained from Eq. (5.32) by performing similar manipulations or from Eq. (5.41) by applying spatial differentiation to the displacement field. From Eq. (5.32), it follows that

$$\varepsilon_{\alpha\alpha_E} = \frac{1}{2\pi}\sum_{m=1}^{5}\sum_{n=0}^{5}\int_0^{\infty}\frac{H_m(k,t)}{D'_m(k)}E_{mn}(k,\theta)J_n(kr)kdk \tag{5.43}$$

Note that the 5 extensional modes are used and as many non-zero coefficients are used as result from the trigonometric reduction, up to 5. The coefficients contain components, $E_{mn} = E_{mnc}(k)\cos n\theta + E_{mns}(k)\sin n\theta$. These expressions in symbolic form are extremely lengthy for the third order theory and will not be listed here. However, the expressions for E_{mnc} and E_{mns} are given explicitly in Appendix I for the first order theory.

After performing similar laborious calculations employing MATHEMATICA for flexural motion the resulting displacements are,

$$\begin{bmatrix}\psi_2\\ \psi_2\\ w\\ \chi_1\\ \chi_2\\ \varphi_3\end{bmatrix}\frac{1}{2\pi}\sum_{m=1}^{6}\sum_{n=0}^{n\max}\int_0^{\infty}\frac{H_m(k,t)}{D'(k)}\begin{Bmatrix}\alpha_{1mn}(k,\theta)\\ \alpha_{2mn}(k,\theta)\\ \beta_{mn}(k,\theta)\\ \gamma_{1mn}(k,\theta)\\ \gamma_{2mn}(k,\theta)\\ \Phi_{mn}(k,\theta)\end{Bmatrix}J_n(kr)kdk \tag{5.44}$$

$$\begin{Bmatrix}\alpha_{1mn}\\ \alpha_{1mn}\\ \beta_{mn}\\ \gamma_{1mn}\\ \gamma_{1mn}\\ \Phi_{mn}\end{Bmatrix} = \begin{Bmatrix}\alpha_{1mnc}(k)\\ \alpha_{1mnc}(k)\\ \beta_{mnc}(k)\\ \gamma_{1mnc}(k)\\ \gamma_{1mnc}(k)\\ \Phi_{mnc}(k)\end{Bmatrix}\cos n\theta + \begin{Bmatrix}\alpha_{1mns}(k)\\ \alpha_{1mns}(k)\\ \beta_{mns}(k)\\ \gamma_{1mns}(k)\\ \gamma_{1mns}(k)\\ \Phi_{mns}(k)\end{Bmatrix}\sin n\theta \tag{5.45}$$

The surface-strain response can be derived from Eqs. (5.33) or from Eq. (5.44). Using Eq. (5.33) for extension it follows that

$$\varepsilon_{\alpha\alpha_B} = \frac{1}{2\pi}\sum_{m=1}^{6}\sum_{n=0}^{5}\int_0^{\infty}\frac{H_m(k,t)}{D'(k)}E_{mn}(k,\theta)J_n(kr)kdk \tag{5.46}$$

Though this expression is very similar to its extensional counterpart note that 6 modes are included and the appropriate modes for bending are used here. Where $E_{mn} = E_{mnc}(k)\cos n\theta + E_{mns}(k)\sin n\theta$. The expressions for E_{mnc} and E_{mns} are too lengthy to list for the third order theory but are written explicitly for the first order Mindlin theory in Appendix I, which summarizes the key equations for the first order theory. A derivation of Eqs. (5.43) and (5.46) is the subject of Appendix G.

5.8 Outgoing AE waves and Asymptotic Solutions

The integral representation of the displacement field includes non-propagating (evanescent), outgoing propagating and incoming propagating waves. In order to distinguish outgoing and incoming waves it is useful to replace $J_\nu(kr)$ in the integrands by

$$J_\nu(kr) = [H_\nu^{(1)}(kr) + H_\nu^{(2)}(kr)]/2 \tag{5.47}$$

where $H_\nu^{(1)}(x)$ and $H_\nu^{(2)}(x)$ are the complex Hankel functions of the first and second kind of order ν defined as

$$\begin{aligned} H_\nu^{(1)}(x) &= J_\nu(x) + iY_\nu(x) \\ H_\nu^{(2)}(x) &= J_\nu(x) - iY_\nu(x) \end{aligned} \tag{5.48}$$

where $Y_\nu(x)$ is the Bessel function of the second kind of order ν. For large values of kr, the asymptotic approximations to these complex Hankel functions are

$$H_\nu^{(1)}(kr) \sim \sqrt{\frac{2}{\pi k r}} e^{i(kr-\pi/4-\nu\pi/2)}, \quad H_\nu^{(2)}(kr) \sim \sqrt{\frac{2}{\pi k r}} e^{-i(kr-\pi/4-\nu\pi/2)} \tag{5.49}$$

In conjunction with the factor $exp(-i\omega t)$ contained in the loading term $H_m(k,t)$, these functions represent the outgoing and incoming waves respectively. In general, the response function $H_m(k,t)$ in the integrand of the integral solutions, Eqs. (5.41) or (5.43) for extension, and Eqs. (5.44) or (5.46) for bending, contain the terms, sin $\omega_m t$ or cos $\omega_m t$, which, as is shown in Appendix H, are related to t, for example

$$H_m(k,t) = \frac{(1-\cos\omega_m t)}{\omega_m^2} \tag{5.50}$$

for source time function described by Heaviside step function.

Then the integrand can be simplified by use of the following two expressions

$$\begin{aligned} [H_\nu^{(1)}(kr) + H_\nu^{(2)}(kr)]\cos\omega_n t &= \mathrm{Re}\{[H_\nu^{(1)}(kr) + H_\nu^{(2)}(kr)]e^{-i\omega_n t}\} \\ [H_\nu^{(1)}(kr) + H_\nu^{(2)}(kr)]\sin\omega_n t &= \mathrm{Re}\{[H_\nu^{(1)}(kr) + H_\nu^{(2)}(kr)]ie^{-i\omega_n t}\} \end{aligned} \tag{5.51}$$

From the asymptotic approximations for $H_\nu^{(1)}(kr)$ and $H_\nu^{(2)}(kr)$, the term with $H_\nu^{(1)}(kr)$ represents the outgoing waves while the term with $H_\nu^{(2)}(kr)$ represents the incoming waves. If only outgoing waves are desired, the surface strain responses , Eq. (5.43) for extension and (5.46) for bending become, after utilizing Eqs. (5.47), (5.50), and (5.51),

$$\begin{aligned} \varepsilon_{\alpha\alpha} &= \frac{1}{2\pi}\sum_{m=1}^{5}\sum_{n=0}^{5}\int_0^\infty \frac{-\cos\omega_m t}{\omega_m^2 D_m'(k)} E_{mn}(k,\theta) J_n(kr) k dk \\ &= \frac{-1}{4\pi}\sum_{m=1}^{5}\sum_{n=0}^{5} \mathrm{Re}\left[\int_0^\infty \frac{E_{mn}(k,\theta)}{\omega_m^2 D_m'(k)} H_n^{(1)}(kr) e^{-i\omega_m t} k dk\right] \end{aligned} \tag{5.55}$$

where the appropriate coefficients are used for extension and bending respectively and the summation over m includes 6 modes in bending. It is usually not feasible to evaluate the integral solutions exactly. The alternatives are numerical evaluation, or an approximate analytical evaluation.

CHAPTER 6.0

NUMERICAL RESULTS

6.1 Results Overview

An isotropic plate with Poisson's ratio $\nu = 0.33$ was chosen for the numerical studies.

Now consider the transient response. Assume that the sources are located at $(0, 0, z_0)$ with the moment tensor M_{ij}. The time dependence of the moment tensor $M_{ij}(t)$ is assumed to be the Heaviside step function $H(t)$ in the calculation. Note that a ramp function with a "rise time" (Guo *et al.*, 1996 [19, 20]) can also be used to model the time dependence of $M_{ij}(t)$.

For the source with a unit Heaviside step function, the convolution function $H_m(k,t)$ defined in Eq. (5.31) is

$$H_m(k,t) = \frac{(1-\cos\omega_m t)}{\omega_m^2} \tag{6.1}$$

A derivation of the forcing function in Eq. 6.1 is shown in Appendix H.

The transient response to the local sources in isotropic plates has been evaluated by numerical integration. Since the solutions are given in integral form with infinite upper and lower limits, a high-frequency cutoff (or high-wave number cutoff) should be employed in the numerical calculation.

In general, the frequencies of acoustic emissions that occur in structures are often band-limited. Suppose a wavelet of AE signals has its energy confined mostly within $\omega < \omega_{max}$. Therefore, a proper maximum frequency may be chosen for a given problem in the

numerical integration. With a given maximum frequency, a finite number of wave modes (wave numbers) can be determined. Then from the dispersion relation, $\omega = \omega_m(k)$, the corresponding maximum wavenumber (or cut-off wavenumber) for each mode can be determined. Thus the integration can be carried out using an adaptive step size in the wavenumber domain for each wave mode.

A maximum frequency was often used in stationary phase approximations in Fourier inversions. The frequency of the second propagating extensional mode of a composite beam was considered as the maximum frequency (Aberg and Gudmundson, 2000 [1]), and $f_{max} \cong$ 1.5 MHz and 2.0 MHz, were applied to the first extensional and flexural modes in composite plates, respectively (Guo *et al*., 1996 [19]). For isotropic plates, the cut-off frequency for the $\boldsymbol{S_1}$ mode is $\omega_c = \pi\sqrt{0.5(1-\nu)/(1-2\nu)} \cong 3.118$. It is also the minimum propagating frequency for the $\boldsymbol{S_1}$ mode according to the plate theory. However, 3-D elasticity gives the minimum frequency, $(\omega_{s1})_{min} \cong 2.839$, for the corresponding mode (see Fig. 4.7). Thus, $\omega(k) < (\omega_{s1})_{min} = 2.839$ is used for all wave modes in the inverse Hankel transformation calculation. Obviously, in the frequency region $0 < \omega < (\omega_{s1})_{min}$ five modes: $\boldsymbol{S_0}$, $\boldsymbol{SH_0}$, $\boldsymbol{A_0}$, $\boldsymbol{A_1}$ and $\boldsymbol{SH_1}$, coexist and the numerical solution is valid up to this maximum frequency. For example, if an aluminum plate with thickness h =1.6 *mm* is used, then the dimensionless frequencies ω = 2.839 and 3.118 correspond to f = 1.75 and 1.93 MHz respectively. Hence, the solution is valid up to this cutoff frequency in AE waveform analysis. In other numerical studies, similar bounds are used: Guo *et al.*, 1996 [19] (< 2 MHz); Hamstad *et al.*, 2001 [23] (<1 MHz).

For a point source the moment tensor can be can be expressed as

$$\mathbf{M}' = \mathbf{M} / (2Gl^3), \quad \mathbf{M} = \mathrm{M}_0 f(t) \tag{6.2}$$

with

$$M_0 = \begin{cases} f(G)\, A\, \Delta\Sigma, & \textit{for shear crack} \\ f(\lambda, G)\, A\, \Delta\Sigma, & \textit{for tensile crack} \end{cases}$$

As shown in section 3.4 where A is the amplitude of the displacement discontinuity, $\Delta\Sigma$ is the source (crack) area, and $f(t)$ is the source time function without dimension. In general, the values of $\Delta\Sigma$, A and M_0 are unknown. For convenience it is assumed $M_0 / (2Gl^3) = 1$ in the following numerical calculations. Thus, the simulated strain waveform due to a point source provides relative amplitudes of different wave modes. If $M_0 / (2Gl^3) \neq 1$, the wave shape is the same, and the amplitude can be obtained simply by multiplying the numerical result by the factor $M_0 / (2Gl^3)$. The relative values of the moment tensor components M_0 were detailed in section 3.4.

6.2 Results – General

Figures 6.1 through 6.4 and 6.6 through 6.11 give the transient responses of the surface strains ε_{kk} due to four of the nine source types, vertical tension crack I, horizontal tension crack, horizontal shear crack I and inclined shear crack I at $z_0 = h/4$ (dimensionless $z_0 = ½$), that is, one-fourth plate thickness from the top plate surface. Figure 6.5 shows the u_1 displacement at $\theta = 0^{\circ}$ and 45°. The response location distance is at dimensionless distance r=200 from the source for all of the figures. The wave forms for strain from the

third order theory are compared with those from the first order Mindlin theory which is described in [45] and outlined in Appendix I. For the vertical tensile crack I, results are calculated at $\theta=0^{o}$ and 45^{o} to show the angular dependence. The responses are due to a transient step function H(t), the Heavyside impact loading approximation with a constant force requiring no rise time. The numerical results for the nine types of fundamental AE sources, with the time function being a ramp function, are also readily obtainable from the third order plate theory, but are not presented here for brevity.

For each source, the calculated surface strain response, ε_{kk}, that can be easily measured from a piezoelectric sensor in an experiment, is presented. Note that for the horizontal tensile crack source the response is axisymmetric, $\varepsilon_{kk} = \varepsilon_{kk}(r,t)$.

The waveform due to the vertical shear crack I can be obtained simply by changing the sign of the waveform due to the horizontal shear crack I (see the moment tensors for the two sources in Section 3.4). Thus, the waveform due to the vertical shear crack I is not shown but makes up a fifth source type.

The waveform of the surface strains changes with crack orientation. The effects of the orientation on the waveform are also shown in Figs. 6.8 and 6.10 which are for a horizontal shear crack I and a shear crack inclined at 30^{o}. When β_0 is varied, the ratio between the amplitude of extensional and flexural waves will change.

From the figures discussed above, the following phenomena can be observed. The group velocity for the $\mathbf{A_0}$ mode according to the elasticity and the third order theories is $C_g \approx 1.0$ as can be seen in Figs. 4.5 and 4.7. Note that the arrival time is roughly the distance

divided by the average group velocity, in this case, 200/1.0 or dimensionless t=200. Actually the average group velocity is slightly less due to the rise time. This supports the observed arrival time of about 195 observed for the $\mathbf{A_0}$ mode. The group velocity for the $\mathbf{A_1}$ mode according to the elasticity and the third order theories is $C_g \approx 1.18$ as can be seen in Figs. 4.5 and 4.7. Again, noting that the arrival time is roughly the distance divided by the maximum group velocity, or 200/1.18 here, for a dimensionless t=170. This supports the observed arrival of about 150 to 170 observed for the $\mathbf{A_1}$ mode. Hence, the arrival time for the $\boldsymbol{A_1}$ mode is not close to the arrival time for $\boldsymbol{S_0}$ (maximum $C_g \approx 1.73$ for the $\boldsymbol{S_0}$ mode). In the Mindlin theory the group velocities and hence arrival times for the $\boldsymbol{S_0}$ and $\mathbf{A_1}$ modes are close. This is a shortcoming of the first-order plate theory. Although the plate theory uses the exact cut-off frequency for the $\boldsymbol{A_1}$ mode, the wave behavior of this mode is poorly described beyond this frequency when comparing with the corresponding mode from the elasticity theory.

The most striking difference between the wave forms generated by the third order theory and the first order theory, in addition to the variation in arrival times, is the relative dominance of the $\boldsymbol{S_0}$ extensional contribution to the total response. The $\boldsymbol{S_0}$ mode group velocity is quite different than the one generated from the first order theory being larger in magnitude and longer in duration. Such a change is not unexpected in light of the differences in the dispersion curves.

Some particular observations from the individual disturbance source types are as follows.

6.3 Vertical Tensile Crack

Looking at the $\theta = 0^o$ and $\theta = 45^o$ surface strain results, both for the third order theory, Figs. 6.1 and 6.3, and for the first order theory, Figs. 6.2 and 6.4, it is observed that the strain amplitude is greater at $\theta = 45^o$ rather than at $\theta = 0^o$ at dimensionless r=200 form the source. This is for a dipole loading that simulates a discontinuity along the x_1 axes corresponding to $\theta = 0^o$. It is expected that most of the responses would be the greatest along the line of action of the force, as this loading is not axisymmetric. This is the case for the more fundamental responses such as the u_1 displacement which coincides with the x_1 direction. This can be seen clearly in Fig. 6.5, which is a plot of the u displacements at $\theta = 0^o$ and $\theta = 45^o$ for the bending mode $\mathbf{A_1}$. The u_1 displacement here from the flexural formulation involves the degrees of freedom associated with bending from Eq. (A.1), which are the terms multiplying odd powers of z in the total displacement field.

$$u_1(\mathbf{x}, z, t) = z\psi_1(\mathbf{x}, t) + z^3\chi_1(\mathbf{x}, t)$$

The response along the line of action is significantly greater. The reason that this is not the case with the strain ε_{kk} is inherent in the definition of the strain. ε_{kk} represents an arithmetic sum of the component strains ε_{11} and ε_{22}, which is the total strain that would be sensed by a non-directional piezoelectric strain gage typically used in AE applications. The ε_{11} component which is simply du_1/dx_1 is larger for the sensor located along the x1 axis corresponding to $\theta = 0^o$. However, the ε_{22} component which is du_2/dx_2, is virtually zero along the x1 axis because the transverse component u_2 is nearly zero there. This is not the

case at θ=45^o where the transverse displacement u_2 is nearly 60% of the u_1 displacement, giving rise to the second term in the strain definition. Hence this total strain ε_{kk} is larger at θ = 45^o unlike the more fundamental response quantities that coincide with the intuitive result of being larger along the line of action of the force application. Though the solution accounts for transverse shear waves, the x_1 axis can be thought of as a line of symmetry for the transverse horizontal waves which only build up response away from the line of action of the force. Along the line of action of the force behavior is dominated by the longitudinal waves.

6.4 Horizontal Tensile Crack

The horizontal tensile crack, which accounts for a discontinuity in the x_3 direction can be thought of as having a vertical force line of action. This is somewhat like the pebble in the water scenario except for the dipole nature of the loading, but similar in the sense that the resulting response is axi-symmetric. The ε_{kk} responses can be seen in Fig. 6.6 for the third order theory and Fig. 6.7 for the first order theory. The third order response is characterized by a large, late peaking $\mathbf{S_0}$ mode which clearly couples with the dispersing bending response in later time. This varies substantially from the first order response where the extensional mode is less pronounced, shorter in duration and earlier arriving which largely uncouples it form the bending mode response in its contribution to the total response, as seen in Fig. 6.7

6.5 Shear crack I

The waveforms of the individual strains ε_{11} and ε_{22} both have **SH_1** and **SH_3** mode components as expected, since these are not axi-symmetric waves. However, the waveform of the total surface strain $\varepsilon_{kk} = \varepsilon_{11} + \varepsilon_{22}$ has no SH mode component at all. In fact, according to the plate theory, the SH modes make no contribution to the surface strains ε_{kk} in isotropic plates, and this can be readily proven from the expressions for the surface strain response to a general point source.

Unlike the vertical and horizontal tensile crack responses, the horizontal shear crack response is not as heavily influenced by the extensional **S_0** mode. The bending response has a greater magnitude and therefore is more clearly discerned in the total response.

6.6 Inclined Shear Crack I

The inclined shear crack is in the x_1- x_3 plane inclined at an angle of β_0=30° with the x_1 axis as defined in Fig. 2.3 and depicted in Fig. 3.2 with the moment tensor as defined in Section 3.4. This discontinuity exhibits a strong extensional component **S_0** both for the first and third order theories, particularly so in the third order theory where the extensional response dominates the overall response.

6.7 Comparison with Elasticity Theory

The third order theory was compared with an elasticity formulation developed in Ref. 40. The elasticity solution was derived for non-dipole loadings but adaptable to dipole loading, but only for an axi-symmetric loading. Therefore it was compared with the horizontal tensile loading case from the third order theory. The comparison is seen in Fig. 6.12. The agreement is not perfect but the third order theory waveforms are much closer to the elasticity solution than those predicted by the first order theory.

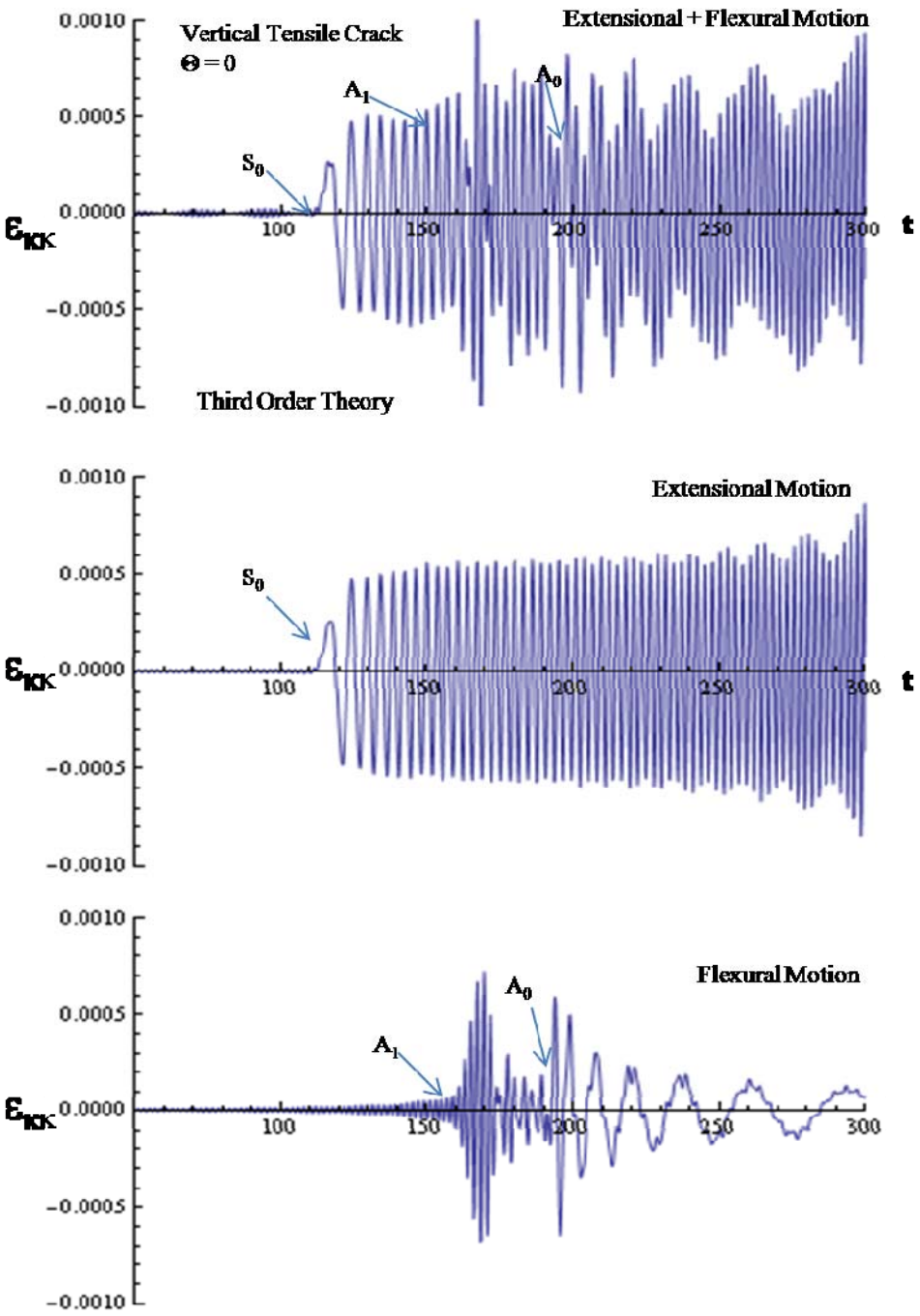

Figure 6.1 Surface strain transient response to source: Vertical Tensile Crack $\theta = 0°$. **Third Order Theory** The arrows indicate the corresponding modes near arrival. r=200, z_0=h/4

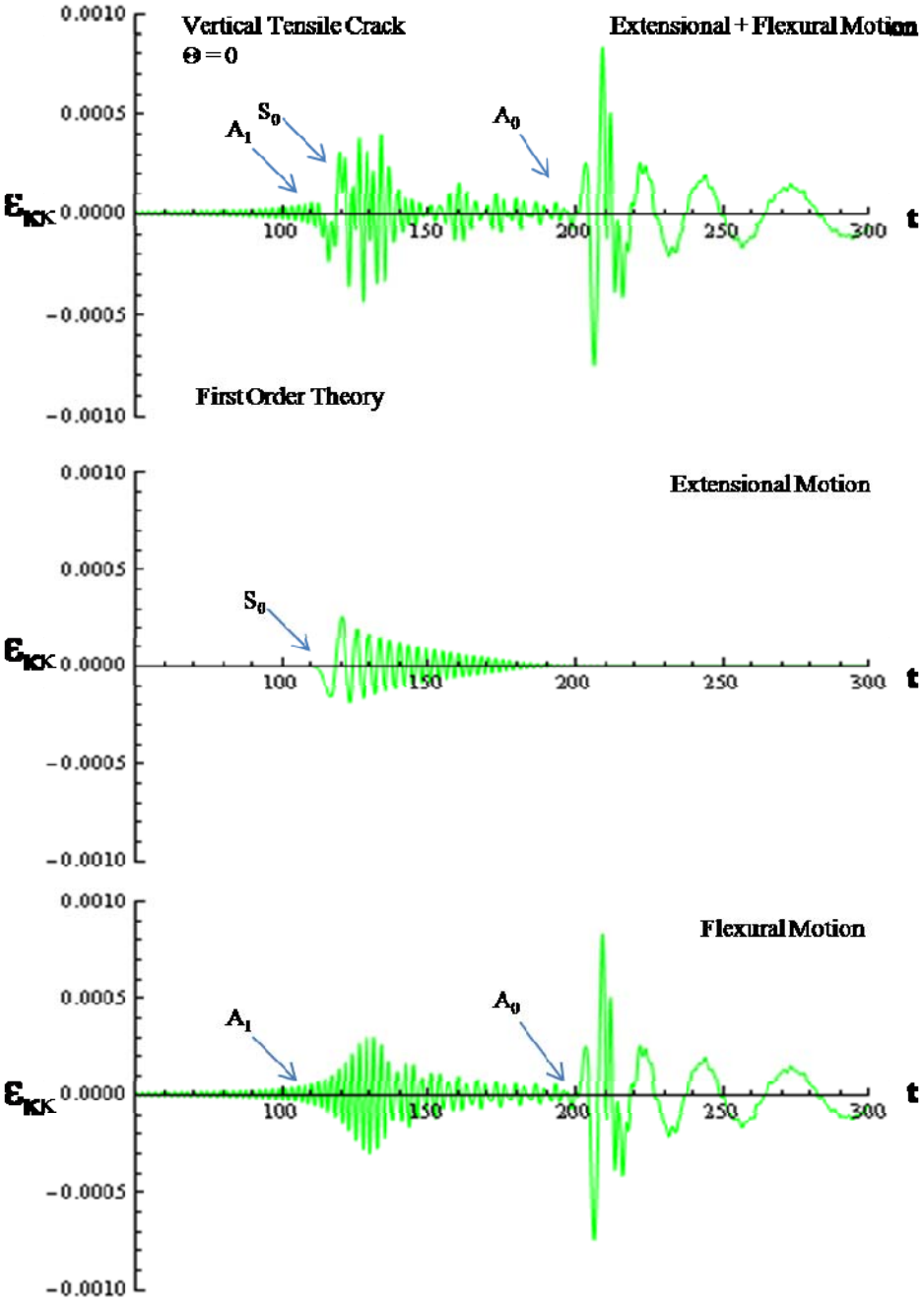

Figure 6.2 Surface strain transient response to source: Vertical Tensile Crack $\theta = 0°$. **First Order Theory.** The arrows indicate the corresponding modes near arrival. r=200, z_0=h/4

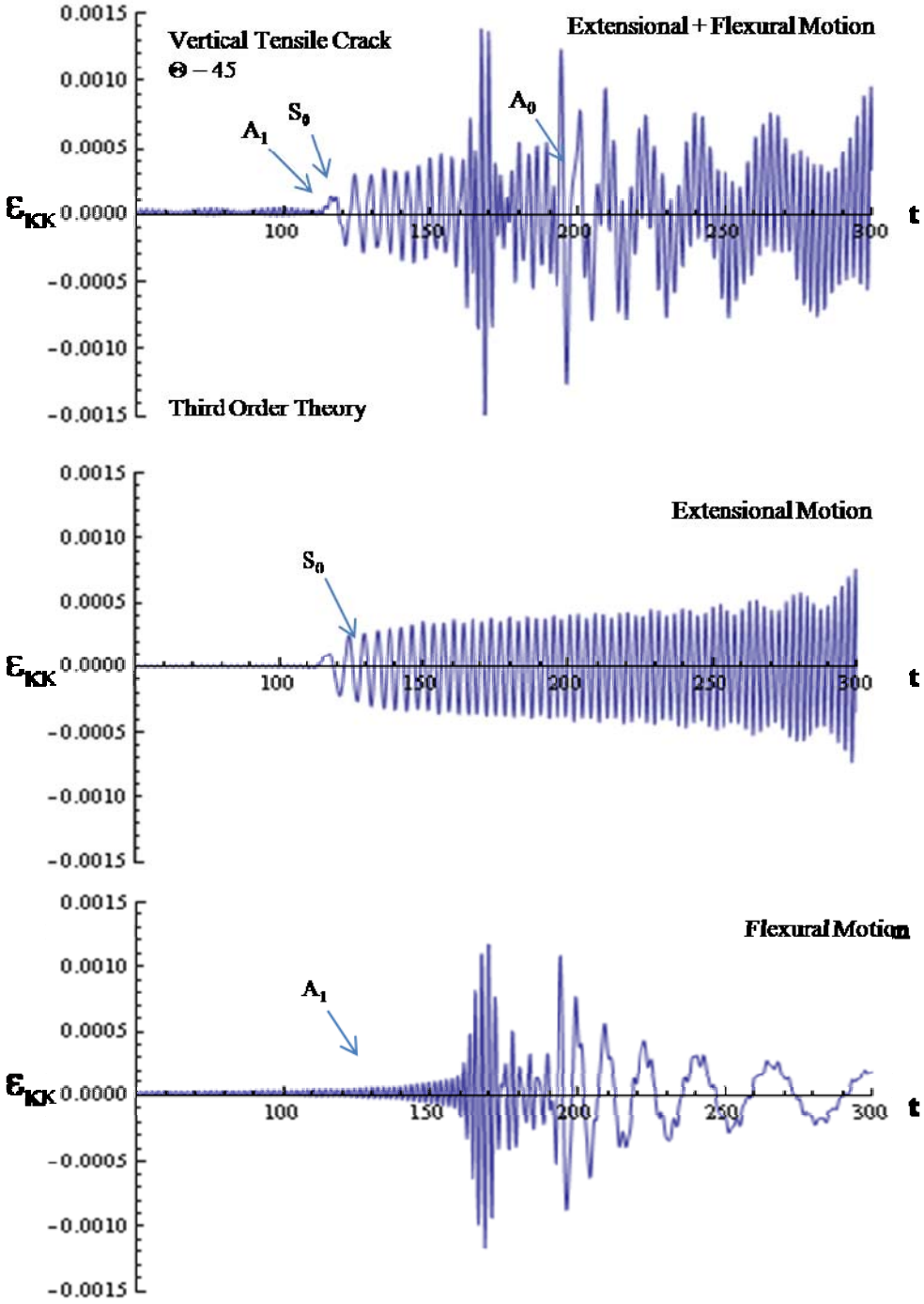

Figure 6.3 Surface strain transient response to source: Vertical Tensile Crack $\theta = 45°$ **Third Order Theory.** The arrows indicate the corresponding mode near arrival r=200, z_0=h/4

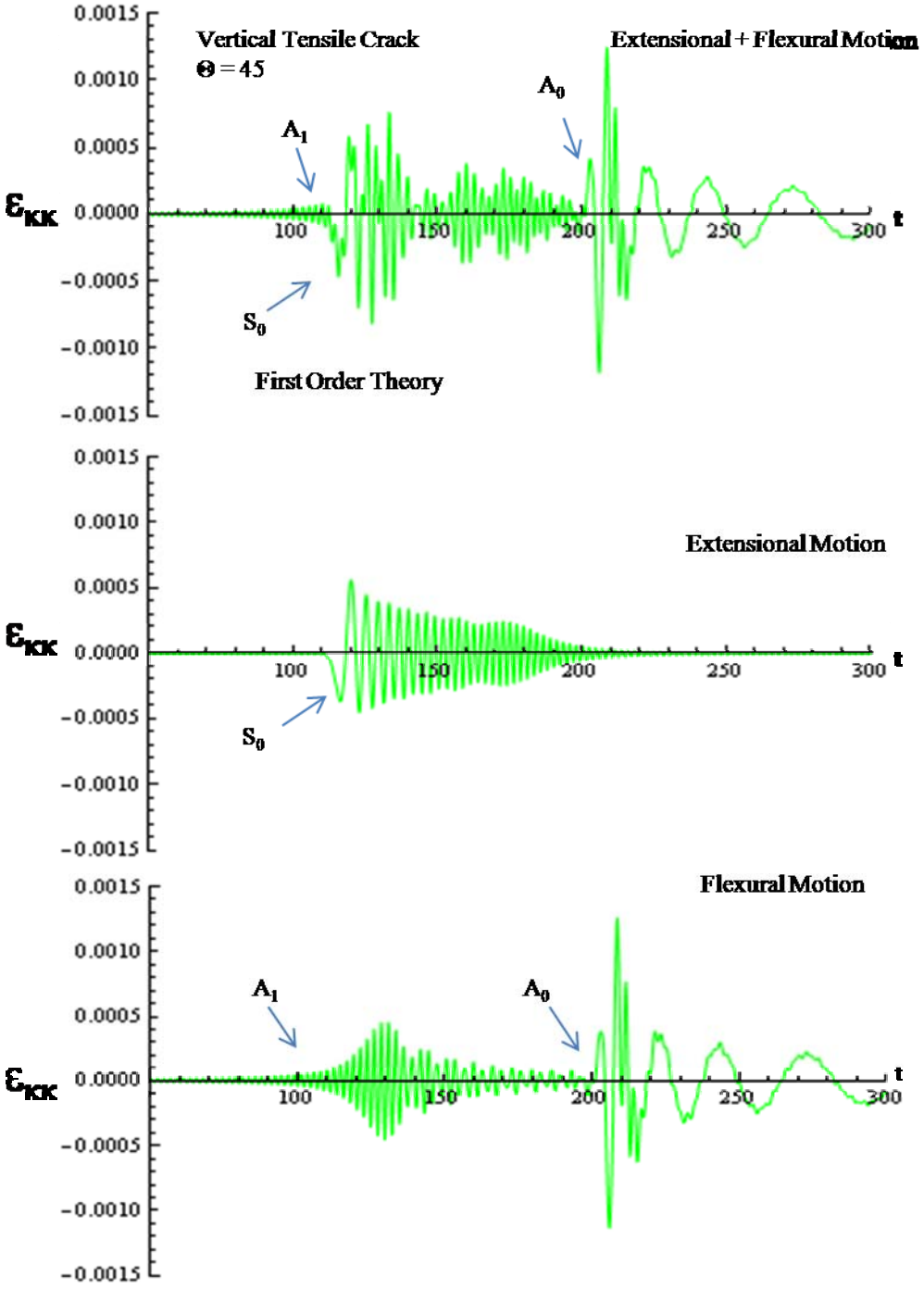

Figure 6.4 Surface strain transient response to source: Vertical Tensile Crack $\theta = 45°$. **First Order Theory.** The arrows indicate the corresponding modes near arrival. r=200, z_0=h/4

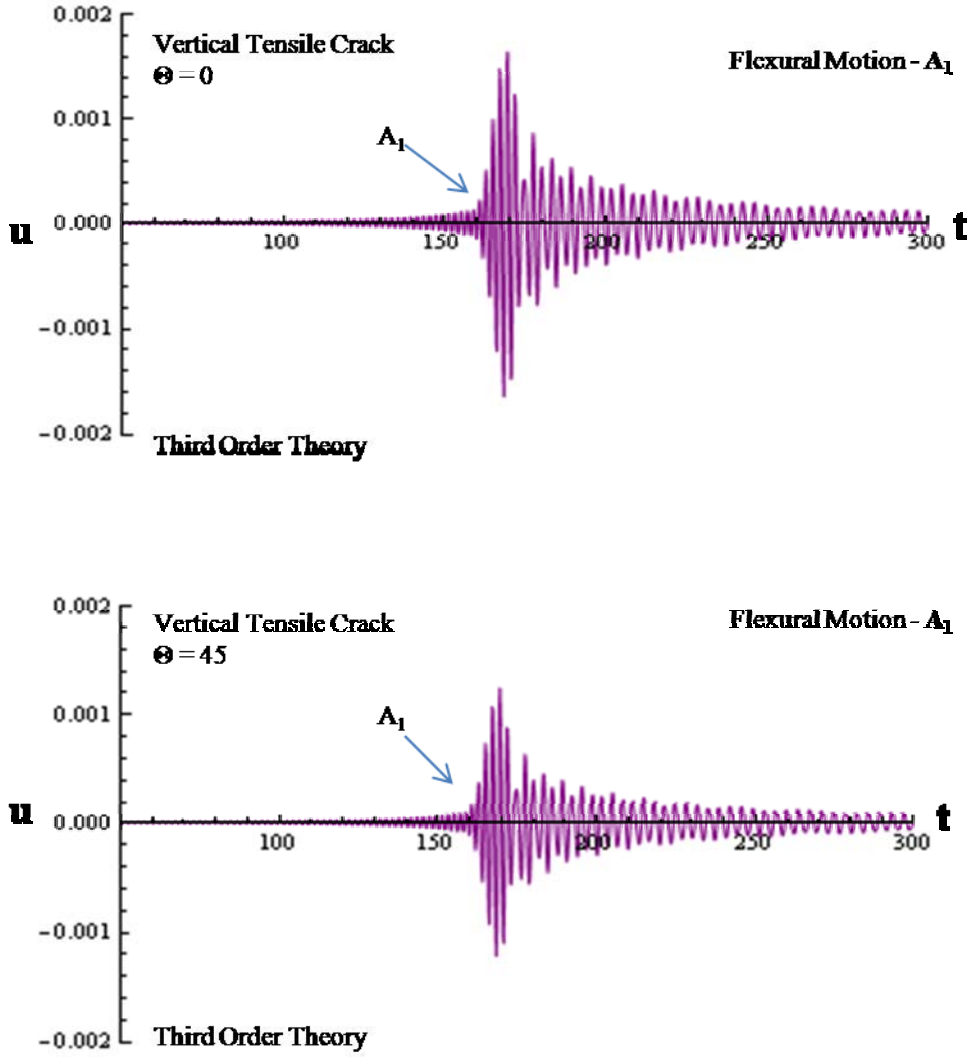

Figure 6.5 Surface displacement transient response to source: Vertical Tensile Crack $\theta = 0°$ and $\theta = 45°$ for $\mathbf{A_1}$ flexural mode. **Third Order Theory.** The arrows indicate the corresponding modes near arrival. r=200, z_0=h/4

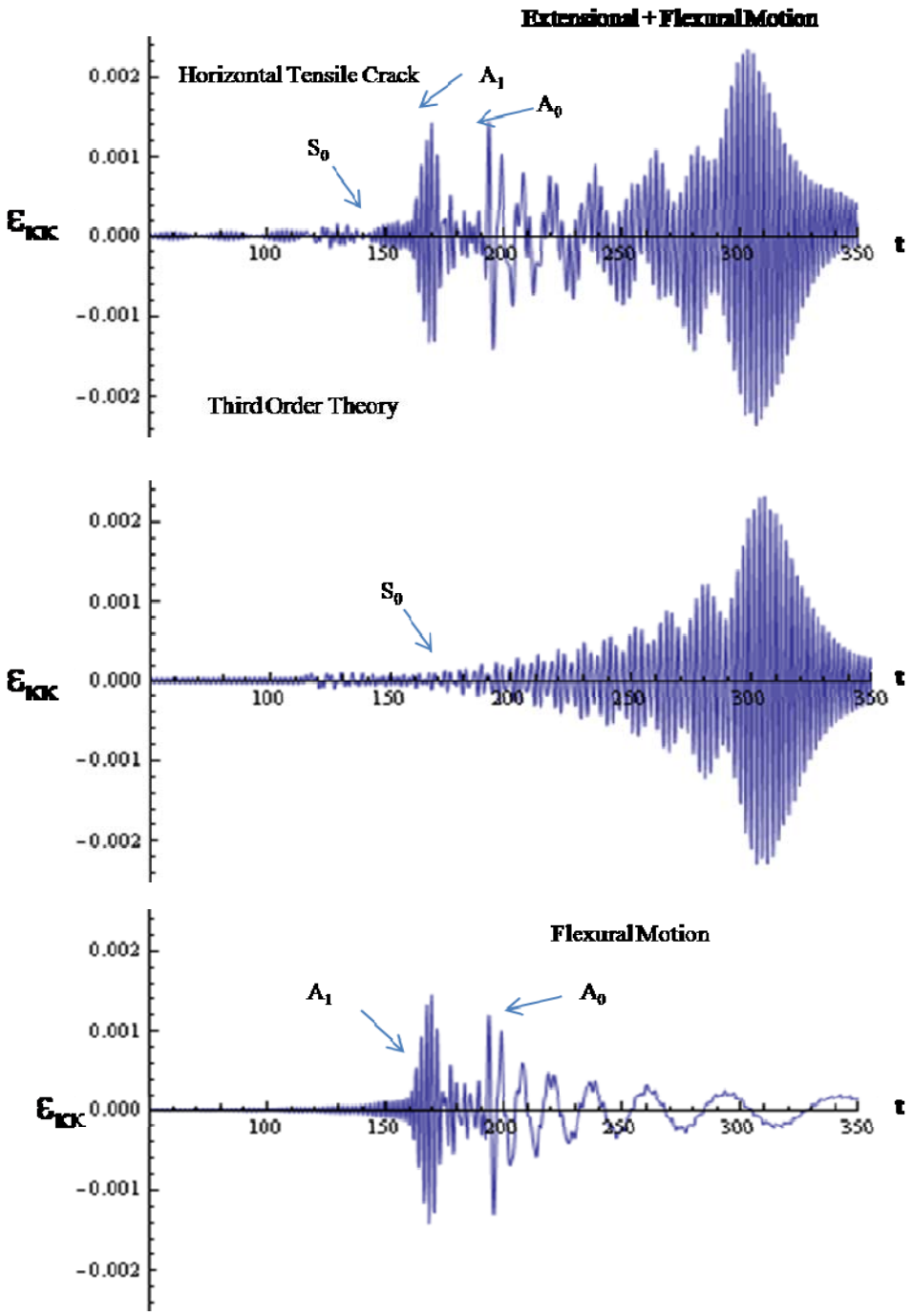

Figure 6.6 Surface strain transient response to source: Horizontal Tensile Crack (axi-symmetric). **Third Order Theory.** The arrows indicate the corresponding modes near arrival. r=200, z_0=h/4

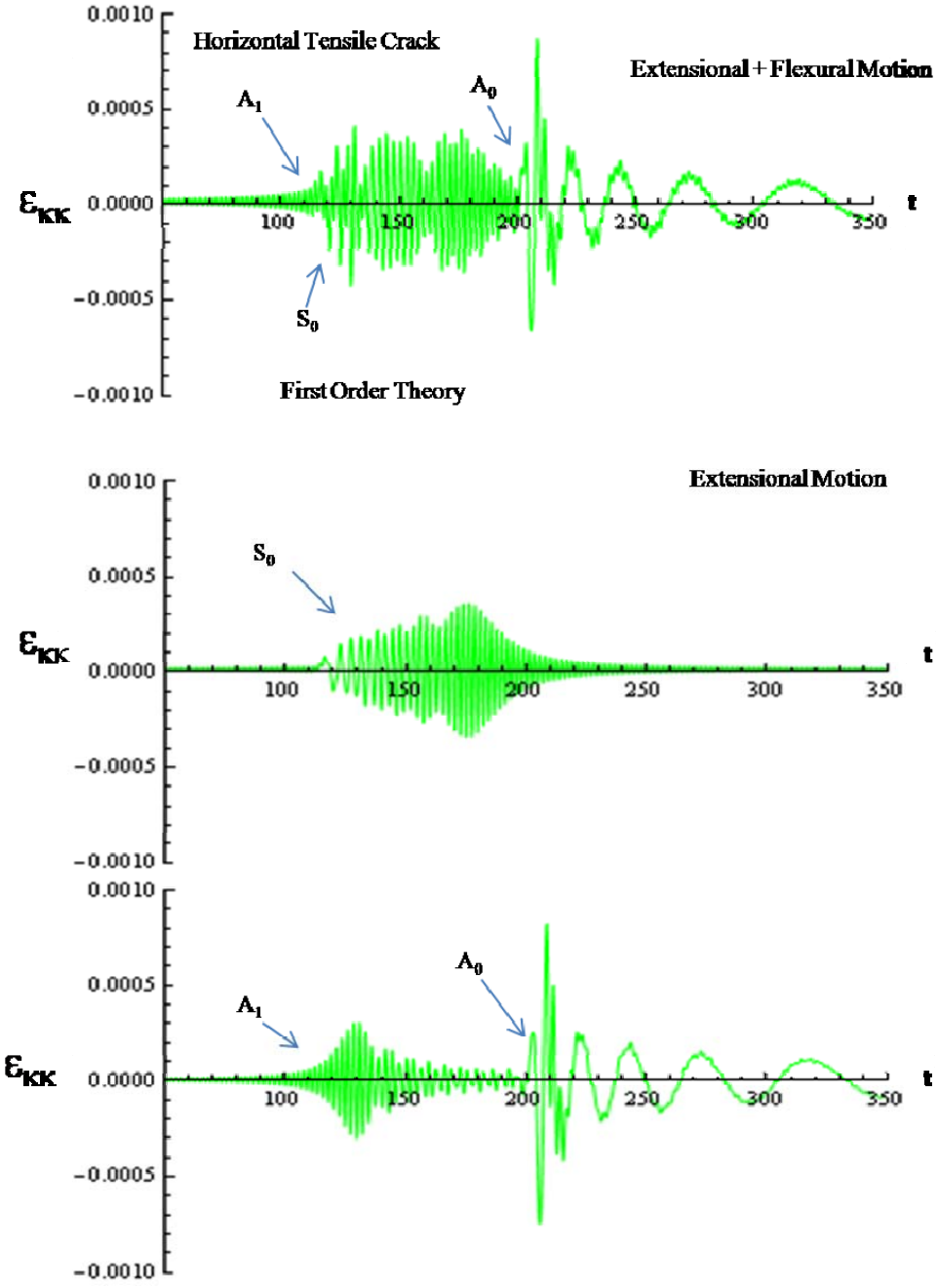

Figure 6.7 Surface strain transient response to source: Horizontal Tensile Crack (axi-symmetric). **First Order Theory.** The arrows indicate the corresponding modes near arrival. r=200, z_0=h/4

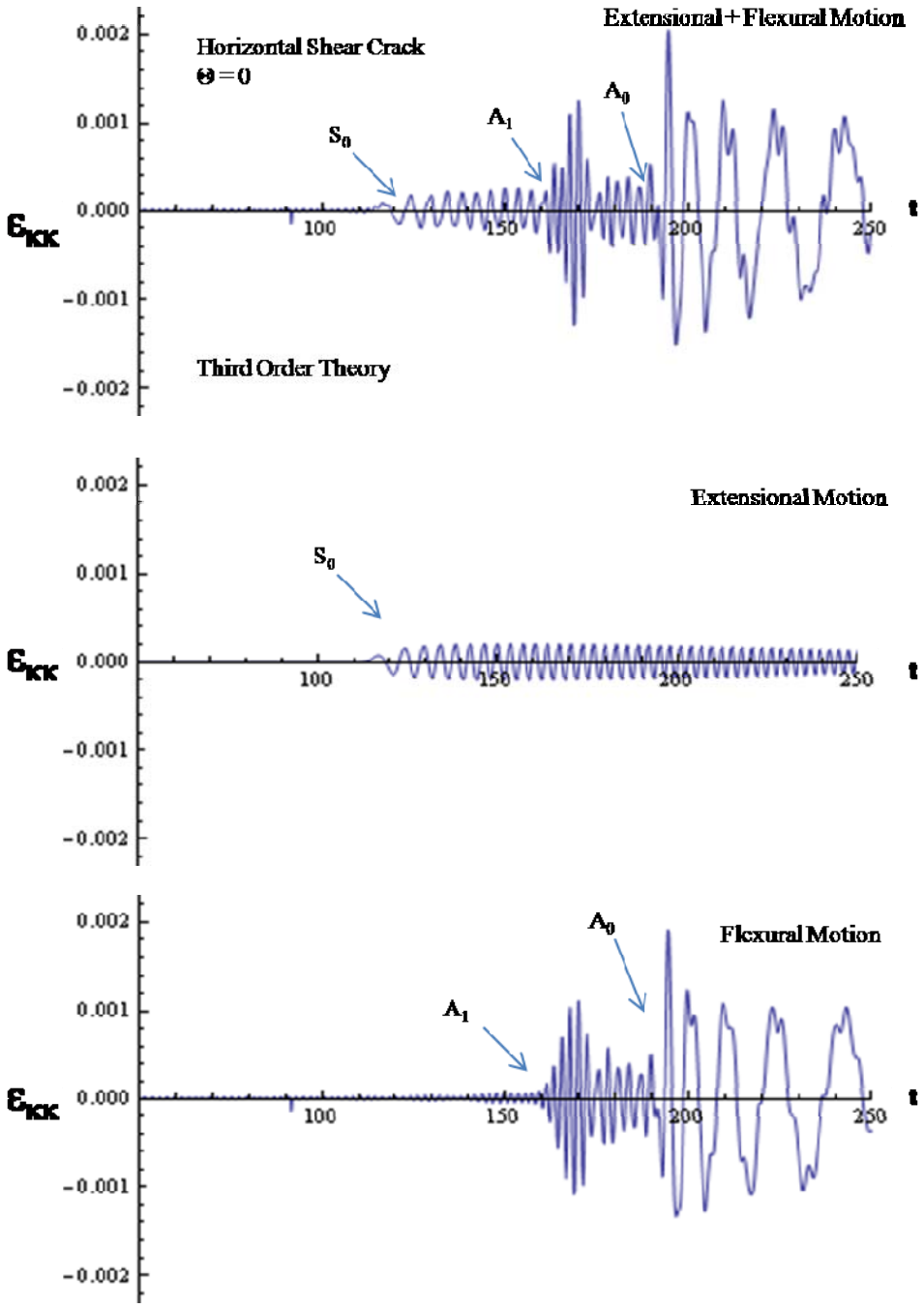

Figure 6.8 Surface strain transient response to source: Horizontal Shear Crack I $\theta = 0°$. **Third Order Theory.** The arrows indicate the corresponding modes near arrival. r=200, z_0=h/4

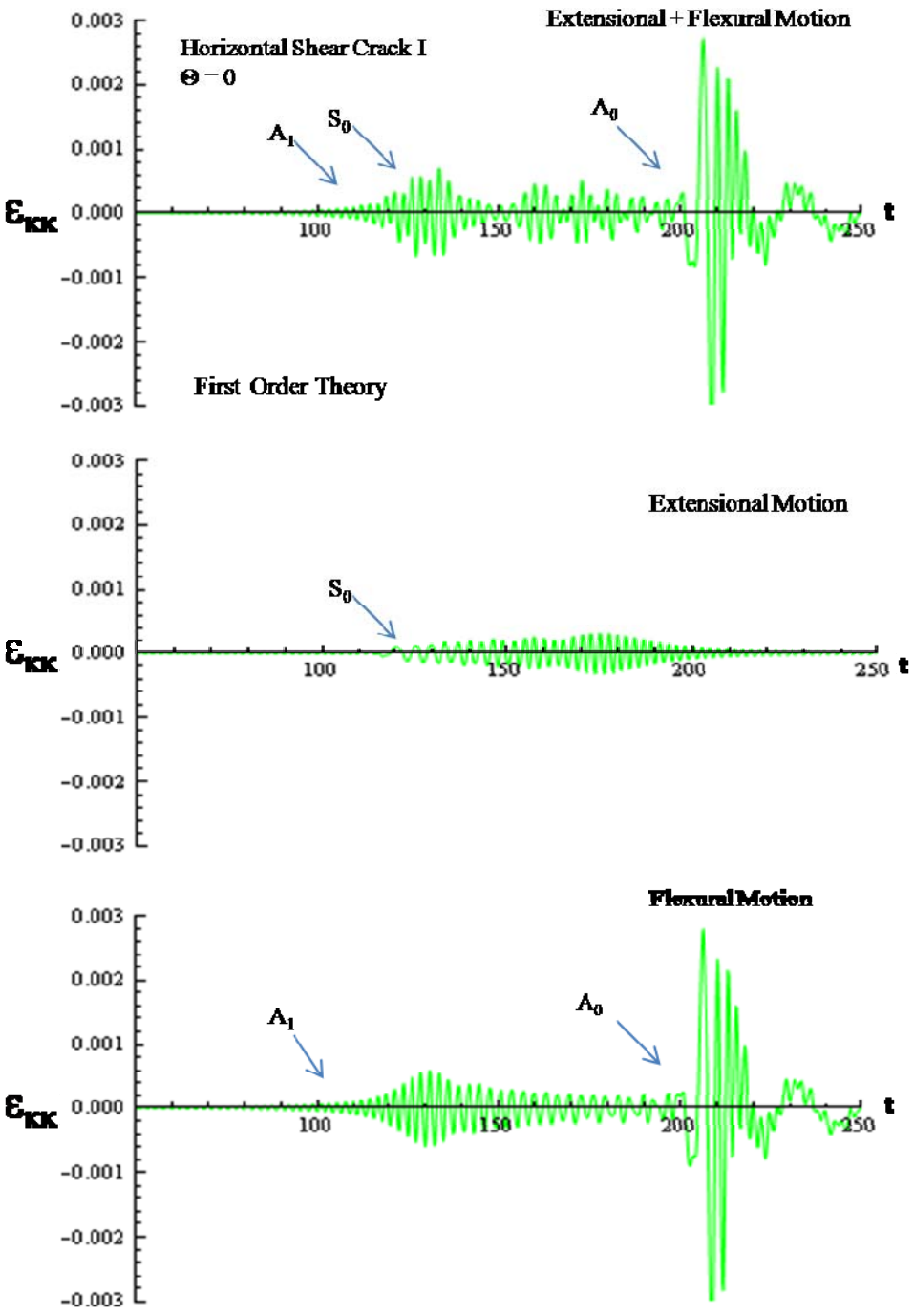

Figure 6.9 Surface strain transient response to source: Horizontal Shear Crack I $\theta = 0°$. **First Order Theory** The arrows indicate the corresponding modes near arrival. r=200, z_0=h/4

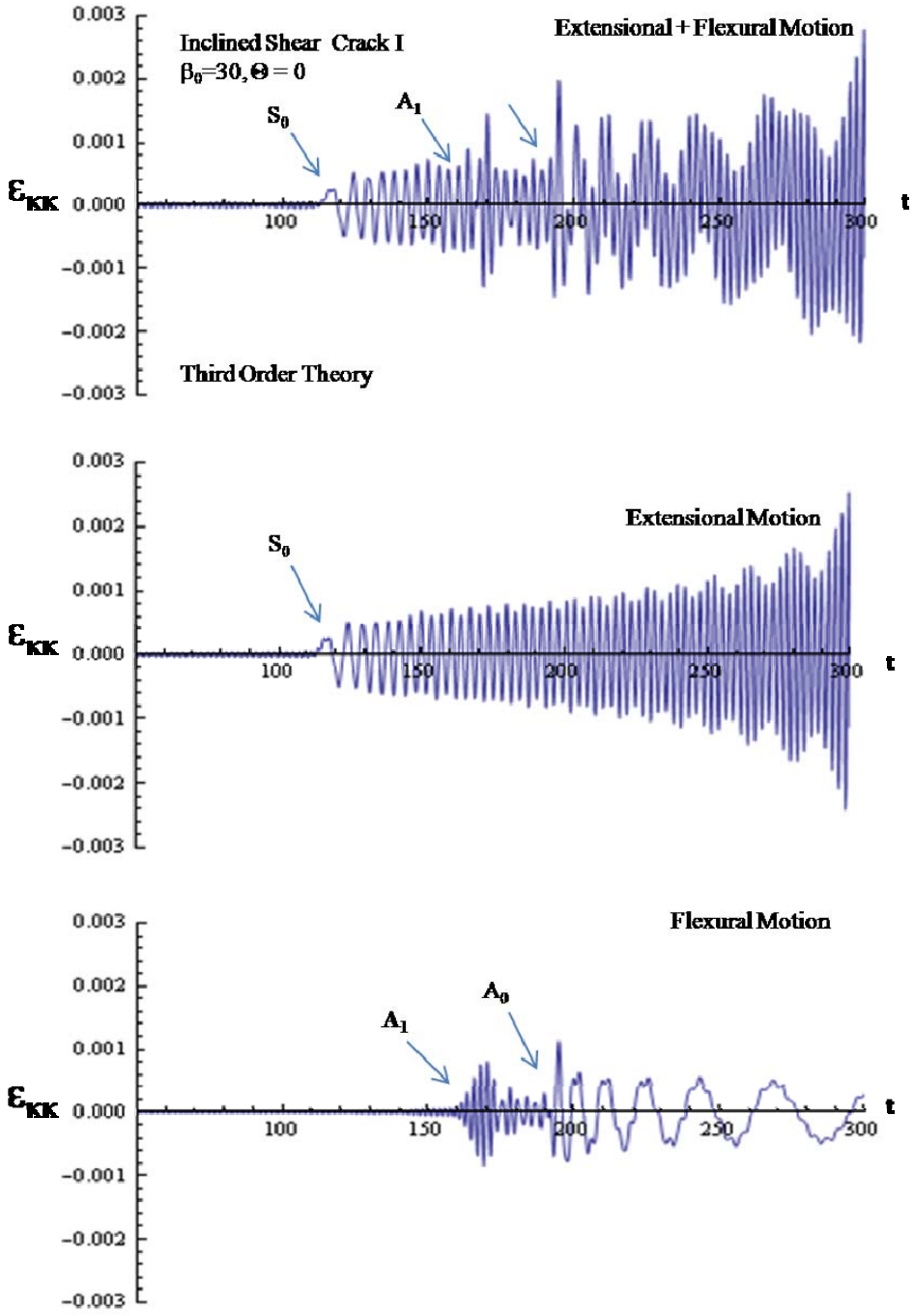

Figure 6.10 Surface strain transient response to source: Inclined Shear Crack I β_0=30°, θ = 0°. **Third Order Theory.** The arrows indicate the corresponding modes near arrival. r=200, z_0=h/4

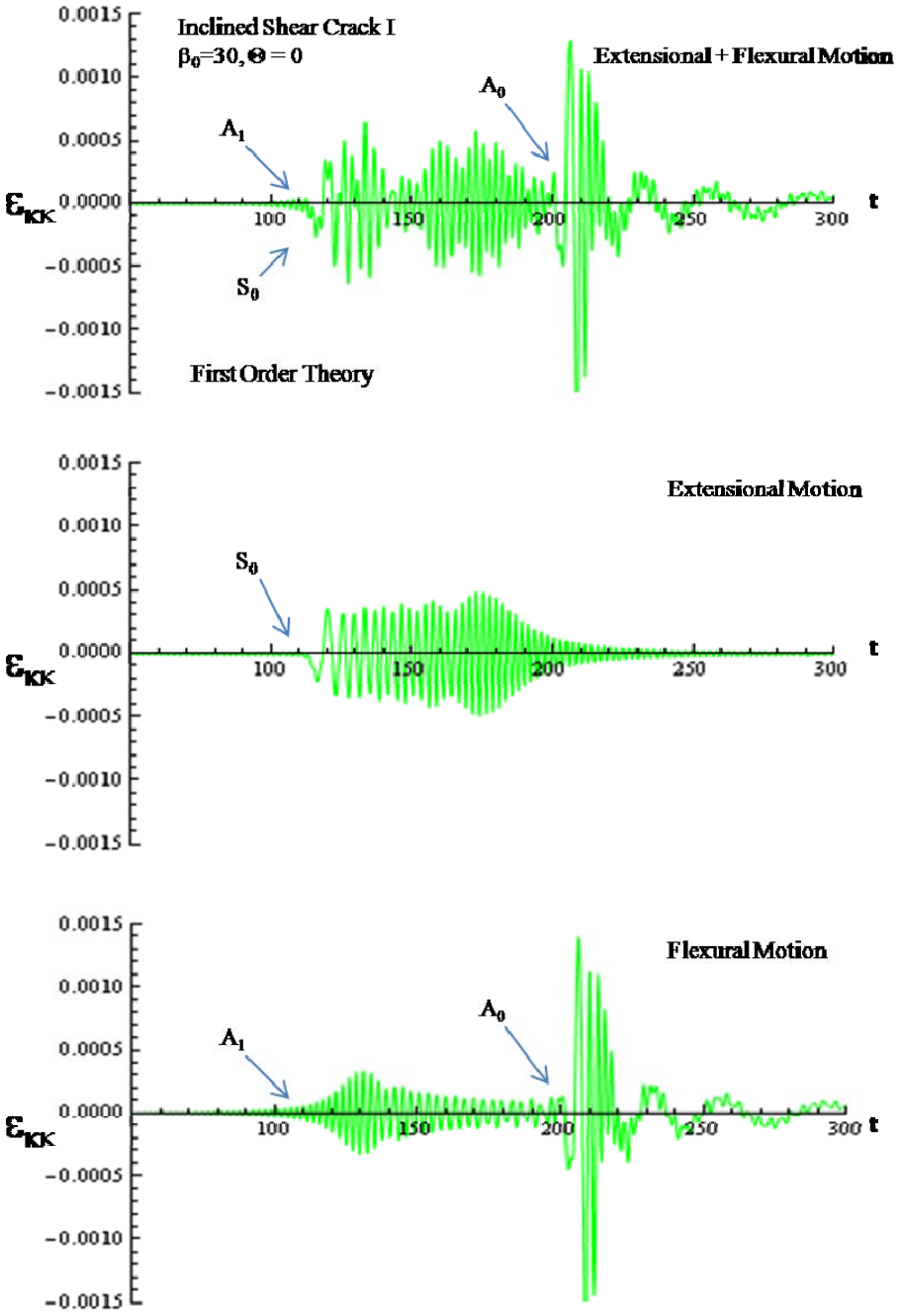

Figure 6.11 Surface strain transient response to source: Inclined Shear Crack I β_0=30° ,θ = 0°. **First Order Theory.** The arrows indicate the corresponding modes near arrival. r=200, z_0=h/4

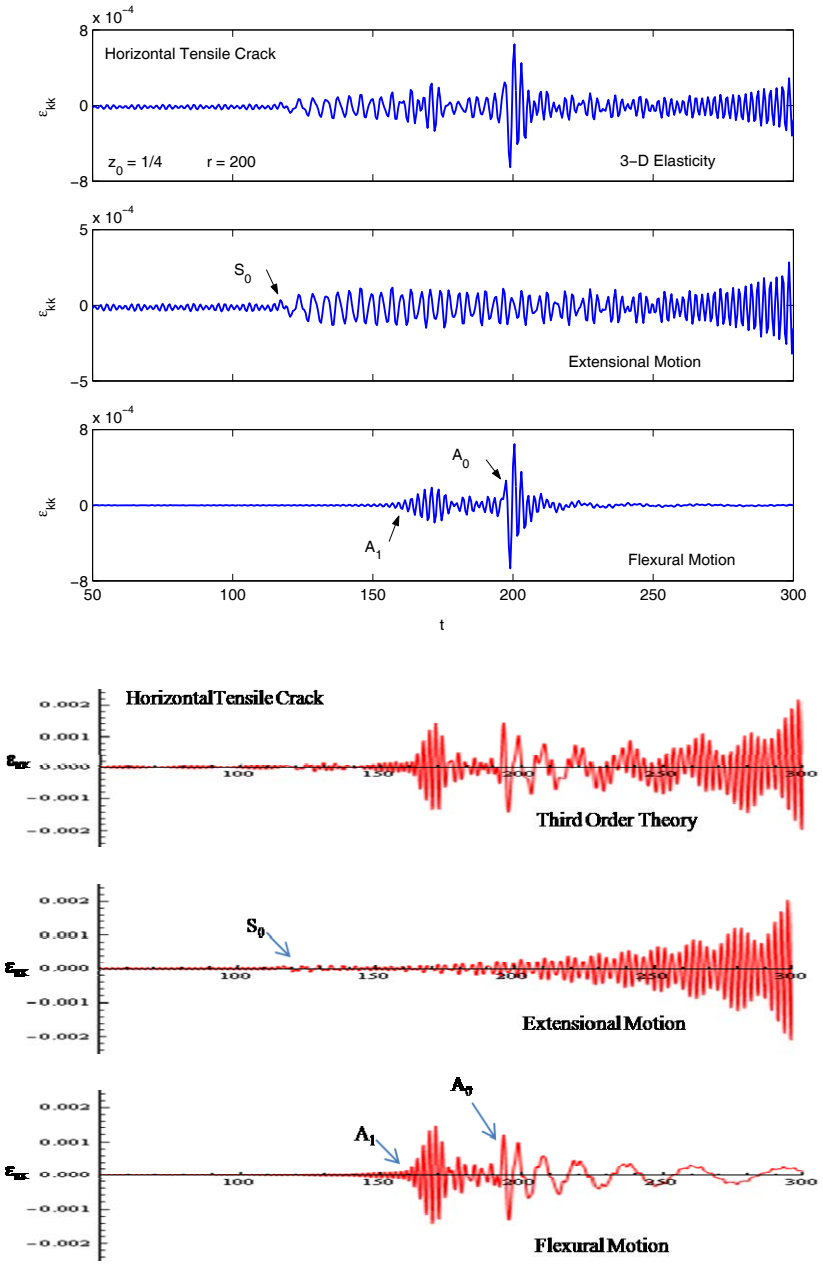

Figure 6.12 Surface strain waveform modeled by **Theory of Elasticity** and **Third Order Theory** from AE source: Horizontal Tensile Crack at z_0 = h/4, waveform observed at r = 200

CHAPTER 7.0

DISCUSSION AND CONCLUSIONS

The simulation of transient wave response for the point sources in an isotropic plate based on third-order plate theory provides physically reasonable solutions up to the given maximum frequency imposed in the numerical evaluation. This is evidenced by the fact that the higher order plate theory provides good approximation to the first arrival time from the AE source for the two fundamental modes ($\boldsymbol{A_0}$, $\boldsymbol{S_0}$) and also with the $\boldsymbol{A_1}$ mode, unlike the first order theory. These wave radiation patterns (or waveforms) due to point sources may serve as a set of references to locate and recognize the active damage in an isotropic plate.

In general, the flexural motion always plays an important role in the waveform emitted by AE source in plates. Thus, in most cases, the plate theory may give reasonable AE waveforms, or at least flexural waveforms, up to the first cut-off frequency ω_c for the higher-order mode $\boldsymbol{A_1}$.

The maximum frequency implemented in the numerical calculation may vary for generation of different micro-damage mechanisms. If the higher frequencies of the AE signals generated by the sources can be detected, such as signals from the higher-order $\boldsymbol{S_1}$ mode if a sensor (receiver) with high-frequency bandpass is used for measurement, then the value of maximum frequency should be increased in the plate theory for valid comparison with experiments.

Away from the low frequency region the third-order plate theory gives good results for the $\mathbf{S_0}$ mode. The wave behavior of the higher-order modes $\boldsymbol{S_1}$ and $\boldsymbol{A_1}$ provided by the first-order plate theory are not in good agreement with the corresponding modes from the elasticity theory. Substantial improvement in the dispersion relations are observed for both the lowest modes and the higher-order modes with the third order theory. Therefore, more accurate waveforms emitted from AE sources can are realized from a higher-order plate theory.

Applying the joint integral transforms, the transient response of the composite plate to a point source can be expressed as double inverse Fourier transform as well, although it cannot be reduced to the form of Hankel transform because of differing stiffnesses in the fiber and matrix directions. Performing numerical inversion of the integral solutions, the detailed wave patterns radiated from the sources in a composite plate can also be calculated with the higher order plate theory.

In summary, the higher order extensional theory has been extended to include AE loading, the reduced integration Bessel function transient solution concept was applied to the higher order extensional and bending solutions, and a higher order bending theory with general Cartesian AE loading solutions was developed and implemented.

Future development could include a general 3D elasticity semi-analytical solution with dipole loading, an anisotropic solution for composite material systems, verification by testing of the current theory starting with the plane stress solution developed in Appendix J, and most importantly, the solution of the inverse problem of reconstructing dipole damage

sources from measured strain signals. This, coupled with modern wireless sensor technology and current real-time data acquisition systems, could lead to a robust structural health monitoring system for future generation aircraft. Such a system would pinpoint and monitor damage formulation and accumulation continuously rather than requiring time-consuming scanning during infrequent tear down inspections. Early identification of potentially dangerous damage could enhance aircraft safety and minimize repair costs.

REFERENCES

1. M. Aberg and P. Gudmundson, "Micromechanical Modeling of Transient Waves from Matrix Cracking and Fiber Fracture in Laminated Beams," *International Journal of Solids and Structures*, Vol. 37, pp. 4083-4102, 2000.

2. J. D. Achenbach, *Wave Propagation in Elastic Solids,* North-Holland Publishing Company, Amsterdam, 1984.

3. T. Aizawa, T. Kishi, and F. Mudry, "Acoustic Emission Wave Characterization: A Numerical Simulation of the Experiments on Cracked and Uncracked Specimens," *Journal of Acoustic Emission*, Vol. 6, pp. 85-92, 1987.

4. K. Aki, "Estimation of Earthquake Movement, Released Energy, and Stress-strain Drop from G Wave Spectrum," *Bulletin of the Earthquake Research Institute*, Tokyo University, Vol. 44, pp. 23-88, 1966.

5. K. Aki and P. G. Richards, *Quantitative Seismology,* University Science Books, Sausalito, California, 1992.

6. D. E. Bray and D. McBride, *Nondestructive Testing Techniques*, John Wiley & Sons, Inc., New York, 1992.

7. R. Burridge and L. Knopoff, "Body Force Equivalents for Seismic Dislocations," *Bulletin of Seismological Society of America*, Vol. 54, pp. 1875-1888, 1964.

8. C. Chang and W. Sachse, "Analysis of Elastic Wave Signals from an Extended Source in a Plate," *Journal of the Acoustical Society of America*, Vol. 77, pp. 1335-1341, 1985.

9. L. Debnath, *Integral Transforms and Their Applications*, CRC Press Inc., Boca Raton, FL, 1995.

10. K. S. Downs and M. A. Hamstad, "Acoustic Emission from Depressurization to Detect/Evaluate Significance of Impact Damage to Graphite/Epoxy Pressure Vessels," *Journal of Composite Materials*, Vol. 32, No. 3, pp. 258-307, 1998.

11. Y. A. Dzenis and J. Qian, "Analysis of Microdamage Evolution Histories in Composites," *International Journal of Solids and Structures*, Vol. 38, pp. 1831-1854, 2001.

12. J. P. Favre and J. C. Laizet, "Amplitude and Counts per Event Analysis of the Acoustic Emission Generated by the Transverse Cracking of Cross-ply CFRP," *Composites Science and Technology,* Vol. 36, pp. 27-43, 1989.

13. T. J. Fowler, J. A. Blessing, P. J. Conlisk, and T. L. Swanson, "The MONPAC System," *Journal of Acoustic Emission*, Vol. 8, No. 3, pp. 1-8, 1989.

14. S. Ghaffari and J. Awerbuch, "On the Correlation between Acoustic Emission and Matrix Splitting in a Unidirectional Graphite/Epoxy Composite," *Acoustic Emission: Current Practice and Future Directions,* ASTM STP 1077, W, Sachse *et al*., Eds., ASTM, Philadelphia, pp. 404-415, 1991.

15. M. R. Gorman, "Plate Wave Acoustic Emission," *Journal of the Acoustic Society of America*, Vol. 90, No. 1, pp. 358-364, 1991.

16. M. R. Gorman and S. M. Ziola, "AE Source Orientation by Plated Wave Analysis," *Journal of Acoustic Emission*, Vol. 9, No. 4, pp. 283-288, 1990.

17. M. R. Gorman and S. M. Ziola, "Plate Waves produced by Transverse Matrix Cracking," *Ultrasonics*, Vol. 29, pp. 245-251, 1991.

18. P. J. de Groot, P. A. M. Wijnen, and R. B. F. Janssen, "Real-time Frequency Determination of Acoustic Emission for Different Fracture Mechanisms in Carbon/Epoxy Composites," *Composites Science and Technology*, Vol. 55, pp. 405-412, 1995.

19. D. Guo, A. Mal, and K. Ono, "Wave Theory of Acoustic Emission in Composite Laminates," *Journal of Acoustic Emission*, Vol. 14, pp. 19-46, 1996.

20. D. Guo, *Lamb Waves from Microfractures in Composite Plat*e, Doctoral thesis, University of California, Los Angeles, 1996.

21. M. A. Hamstad and K. S. Downs, "On Characterization and Location of Acoustic Emission Sources in Real Size Composite Structures – A Waveform Study,"

Journal of Acoustic Emission, Vol. 13, No. 1/2, pp. 31-41, 1995.

22. M. A. Hamstad, "Thirty Years of Advances and Some Remaining Challenges in the Application of Acoustic Emission to Composite Materials," *Acoustic Emission – Beyond the Millennium*, T. Kishi *et al*., Eds., Elsevier Science Ltd., UK, pp. 77-91, 2000.

23. M. A. Hamstad, A. O'Gallagher, and J. Gary, "Effects of Lateral Plate Dimensions on Acoustic Emission Signals from Dipole Sources," *Journal of Acoustic Emission*, Vol. 19, pp. 258-274, 2001.

24. N. A. Haskell, "Radiation Pattern of Surface Waves from Point Sources in Multi-layered medium," *Bulletin of the Seismological Society of America*, Vol. 54, pp. 377-394, 1964.

25. T. R. Kane and R. D. Mindlin, "High-frequency Extensional Vibrations of Plates," *ASME, Journal of Applied Mechanics*, Vol. 23, pp. 277-283, 1956.

26. B. V. Kostrov, "Seismic Moment and Energy of Earthquake, and Seismic Flow of Rock," *Izvestiya, Physics of the Solid Earth*, Vol. 10, pp. 13-21, 1974.

27. T. Maruyama, "On the Force Equivalents of Dynamic Elastic Dislocations with Reference to the Earthquake Mechanism," *Bulletin of the Earthquake Research Institute*, Tokyo, University, 41, 467-486, 1963.

28. J. E. Michaels, T. E. Michaels, and W. Sachse, "Application of Deconvolution to Acoustic Emission Signal Analysis," *Materials Evaluation*, Vol. 3, pp. 1032-1036, 1981.

29. R. D. Mindlin, "Influence of Rotatory Inertia and Shear in Flexural Motion of Isotropic Elastic Plate," *ASME, Journal of Applied Mechanics*, Vol. 18, pp. 31-38, 1951.

30. R. D. Mindlin and M. A. Medick, "Extensional Vibration of Elastic Plate," *ASME, Journal of Applied Mechanics*, Vol. 26, pp. 561-569, 1959.

31. M. Ohtsu, T. Okamoto, and S. Yuyama, "Moment Tensor Analysis of Acoustic Emissions for Cracking Mechanisms in Concrete," *ACI Structures Journal*, Vol. 95,

No. 2, pp. 87-95, 1998.

32. Y. H. Pao, R. R. Gajewski, and A. N. Ceranoglu, "Acoustic Emission and Transient Waves in an Elastic Plate," *Journal of the Acoustical Society of Americ*a, Vol. 65, pp. 96-105, 1979.

33. W. H. Prosser, "Applications of Advanced, Waveform based AE Techniques for Testing Composite Materials," *Proceedings of the SPIE Conference on Nondestructive Evaluation Techniques for Aging Infrastructure and Manufacturing: Materials and Composites*, SPIE, Scottsdale, AZ, pp. 146-153, 1996.

34. J. R. Rice, "Elastic Wave Emission from Damage Processes," *Journal of Nondestructive Evaluation*, Vol. 1, No. 4, pp. 215-224, 1980.

35. C. B. Scruby, "Quantitative Acoustic Emission Techniques," *Research Techniques in Nondestructive Testing,* Academic Press, Inc., London, Vol. 8, Chapter 8, pp. 141-208, 1985.

36. C. B. Scruby, G. R. Baldwin, and K. A. Stacey, "Characterization of Fatigue Crack Extension by Quantitative Acoustic Emission," *International Journal of Fracture*, Vol. 28, pp. 201-222, 1985.

37. K. R. Shah and J. F. Labuz, "Damage Mechanisms in Stressed Rock from Acoustic Emission," *Journal of Geophysical Research*, Vol. 100, No. R8, pp. 15527-15539, 1995.

38. J. J. Stamnes, *Waves in Focal Regions*, IOP Publishing Limited, England, 1986.

39. A. V. Vvedenskaya, "The Determination of the Displacement Fields by means of Dislocation Theory," *Izvestiya Akas, Nauk, S.S.S.R*., Ser. Geofiz., pp. 227-284, 1956.

40. S. Yang and F. G. Yuan, "Transient Wave Propagation of Isotropic Plates using a Higher-order Plate Theory," *International Journal of Solids and Structures*, Vol. 42, pp. 4115-4153, 2005.

41. R. L. Weaver and Y. H. Pao, "Axisymmetric Elastic Waves Excited by a Point Source in a Plate," ASME, *Journal of Applied Mechanics*, Vol. 49, pp. 821-836,

1982.

42. G. B. Whitham, *Linear and Nonlinear Waves*, John Wiley & Sons, Inc, 1999.

43. M. A. Hamstad, A. O'Gallagher, and J. Gary, "Modeling of Buried Monopole and Dipole Sources of Acoustic emission with a finite element Technique," *Journal of Acoustic Emission*, Vol. 17, pp. 97-110, 1999.

44. MATHEMATICA VERSION 7, Wolfram Research, Inc., 2009

45. P. Bogert, F.G. Yuan, S. Yang, "Transient Lamb waves from AE Sources in Isotropic Plates," *Internal Journal of Solids and Structures* (pending review), 2009

APPENDIX

APPENDIX A

FORMULATION OF THE HIGHER-ORDER PLATE THEORY

Displacement Field

In modeling the transient wave propagation in thin plate-like structures using two-dimensional plate theory, rather than three-dimensional elasticity theory, it is possible, in principle, to expand the displacement field of a plate in terms of the thickness coordinate up to any desired degree. To account for the effects of transverse shear deformation and rotary inertia and to improve the accuracy of the extensional wave motion by taking the third order normal and transverse shear strains into consideration, a consistent displacement field may be developed as follows. The extensional and bending degrees of freedom are:

$$[u, v, \varphi_1, \varphi_2, \psi_3]$$

$$[\psi_1, \psi_2, w, \chi_1, \chi_2, \varphi_3]$$

Respectively. The displacement field is:

$$\begin{aligned}
\mathbf{u}_1(\mathbf{x}, z, t) &= u(\mathbf{x}, t) + z\psi_1(\mathbf{x}, t) + z^2\varphi_1(\mathbf{x}, t) + z^3\chi_1(\mathbf{x}, t) \\
\mathbf{u}_2(\mathbf{x}, z, t) &= v(\mathbf{x}, t) + z\psi_2(\mathbf{x}, t) + z^2\varphi_2(\mathbf{x}, t) + z^3\chi_2(\mathbf{x}, t) \\
\mathbf{u}_3(\mathbf{x}, z, t) &= w(\mathbf{x}, t) + z\psi_3(\mathbf{x}, t) + z^2\varphi_3(\mathbf{x}, t)
\end{aligned} \tag{A.1}$$

where $\mathbf{x} = (x_1, x_2)$. The x_1-x_2 plane is chosen to lie along the mid-plane of the plate. The extensional and bending degrees of terms are recognizable by the degrees of freedom they contain. The displacement components (u, v, w, ψ_1, ψ_2, ψ_3) have the same physical meaning as in the first-order shear deformation theory (Mindlin, 1951[29]; Yuan and Yang[40]), and five additional linear, quadratic and cubic terms of z associated with φ_1, and

φ_2 , φ_3 for extension and χ_1, χ_2 for bending are added to the expansion of the displacement field. Note that the displacement field in Eq. (1.1) suggests that the transverse normal to the mid-plane will induce elongation or contraction (Kane and Mindlin, 1956[25]; Mindlin and Medick, 1959[30]). The linear strains associated with the displacement field Eq. (1.1) are

$$\begin{aligned}
\varepsilon_{11} &= \varepsilon_{11}^{(0)} + z\varepsilon_{11}^{(1)} + z^2\varepsilon_{11}^{(2)} + z^3\varepsilon_{11}^{(3)} \\
\varepsilon_{22} &= \varepsilon_{22}^{(0)} + z\varepsilon_{22}^{(1)} + z^2\varepsilon_{22}^{(2)} + z^3\varepsilon_{22}^{(3)} \\
\varepsilon_{33} &= \varepsilon_{33}^{(0)} + \varepsilon_{33}^{(1)} \\
\gamma_{12} &= \gamma_{12}^{(0)} + z\gamma_{12}^{(1)} + z^2\gamma_{12}^{(2)} + z^3\gamma_{12}^{(3)} \\
\gamma_{23} &= \gamma_{23}^{(0)} + z\gamma_{23}^{(1)} + z^2\gamma_{23}^{(2)} \\
\gamma_{13} &= \gamma_{13}^{(0)} + z\gamma_{13}^{(1)} + z^2\gamma_{13}^{(2)}
\end{aligned} \tag{A.2}$$

where

$$\begin{aligned}
&\varepsilon_{11}^{(0)} = u_{0,1}, && \varepsilon_{11}^{(1)} = \psi_{1,1}, && \varepsilon_{11}^{(2)} = \phi_{1,1}, && \varepsilon_{11}^{(3)} = \chi_{1,1} \\
&\varepsilon_{22}^{(0)} = v_{0,1}, && \varepsilon_{22}^{(1)} = \psi_{2,2}, && \varepsilon_{22}^{(2)} = \phi_{2,2}, && \varepsilon_{22}^{(3)} = \chi_{2.,2} \\
&\varepsilon_{33}^{(0)} = \psi_3, && \varepsilon_{33}^{(1)} = w_{,3} = 2z\phi_3 \\
&\gamma_{12}^{(0)} = u_{0,2} + v_{0,1}, && \gamma_1^{(1)} = \varphi_{1,2} + \varphi_{2,1}, && \gamma_{12}^{(2)} = \phi_{1,2} + \phi_{2,1}, && \gamma_{12}^{(3)} = \chi_{1,2} + \chi_{2,1} \\
&\gamma_{13}^{(0)} = \psi_1 + w_{,1}, && \gamma_{13}^{(1)} = 2\phi_1 + \psi_{3,1}, && \gamma_{13}^{(2)} = 3\chi_1 + \phi_{3,1} \\
&\gamma_{23}^{(0)} = \psi_2 + w_{,2}, && \gamma_{23}^{(1)} = 2\phi_2 + \psi_{3,2}, && \gamma_{23}^{(2)} = 3\chi_2 + \phi_{3,2}
\end{aligned} \tag{A.3}$$

The terms with extensional degrees of freedom are part of the extensional problem while the terms with bending degrees of freedom are part of the bending problem. Further, the discrepancies between the actual displacement field and that of the approximate plate theory need to be corrected by making the following substitutions related to the thickness strains

For extension

$$\begin{aligned}
&\kappa_3\varepsilon_{33}^{(0)} \text{ for } \varepsilon_{33}^{(0)}, \\
&\kappa_4\gamma_{\alpha 3}^{(i)} \text{ for } \gamma_{\alpha 3}^{(i)} \rightarrow \kappa_4\gamma_{13}^{(1)}, \kappa_4\gamma_{23}^{(1)}
\end{aligned} \tag{A.4a}$$

And for bending

$$\begin{aligned}
&\kappa_1\gamma_{\alpha 3}^{(i)} \text{ for } \gamma_{\alpha 3}^{(i)} \rightarrow \kappa_1\gamma_{13}^{(0)}, \kappa_1\gamma_{23}^{(0)}, \kappa_1\gamma_{13}^{(2)}, \kappa_1\gamma_{23}^{(2)} \\
&\kappa_6\varepsilon_{33}^{(1)} \text{ for } \varepsilon_{33}^{(1)}
\end{aligned} \tag{A.4b}$$

where κ_i are the corrected coefficients similar to those introduced by Mindlin and Medick (1959). Matching the cut-off frequencies of the following modes: (1) plate extensional modes and the first two symmetric modes of 3-D elasticity theory; (2) plate flexural mode with the second antisymmetric mode of 3-D elasticity theory, the corrected coefficients are chosen as $\kappa_3 = \sqrt{\pi^2/12}$, $\kappa_4 = \kappa_6 = \sqrt{\pi^2/15}$, $\kappa_1 = \pi/(\sqrt{90 - 2\sqrt{1605}})$ from matching cutoff frequencies. Calculation of the shear correction factors requires characteristic equation for the system and the dispersion relationship from elasticity. A derivation is shown In Appendix F.

Constitutive Equations for the Third Order Theory

The constitutive equations for a linear elastic plate may be derived from the strain energy density in the 3-D elasticity theory with the corrections made by Eqs. (A.4).

$$V_0 = \frac{1}{2}\lambda\varepsilon^2 + G[{\varepsilon_{11}}^2 + {\varepsilon_{22}}^2 + (\kappa_{3,6}\varepsilon_{33})^2] + \frac{1}{2}G[{\gamma_{12}}^2 + (\kappa_{4,1}\gamma_{23})^2 + (\kappa_{4,1}\gamma_{13})^2] \tag{A.5}$$

Where the $\kappa_{3,6}$ and $\kappa_{4,1}$ indicate the appropriate correction factor for the extensional and bending formulations, respectively. In Eq. (A.5) for the extensional formulation, using the correction factor subscript 3;

$$\begin{aligned}\varepsilon^2 &= (\varepsilon_{11} + \varepsilon_{22} + \kappa\varepsilon_{33})^2 = {\varepsilon_{11}}^2 + {\varepsilon_{22}}^2 + (\kappa_3\varepsilon_{33})^2 + 2\varepsilon_{11}\varepsilon_{22} \\ &+2\varepsilon_{11}(\kappa_3\varepsilon_{33}) + 2\varepsilon_{22}(\kappa_3\varepsilon_{33})\end{aligned} \tag{A.6}$$

λ and μ are Lame's constants for the material.

Note that the second Lame constant μ, is the shear modulus G. The two can be used interchangeably. Looking at the first plate extensional resultant force N_{11} for example, starting with the strain energy,

$$\sigma_{11} = \frac{\partial V_0}{\partial \varepsilon_{11}} = \lambda(\varepsilon_{11} + \varepsilon_{22} + \kappa_3 \varepsilon_{22}) + 2G\varepsilon_{11} \tag{A.7}$$

Now integrating through the thickness,

$$N_{11} = \int_{-h/2}^{h/2} \sigma_{11} dx_1 \tag{A.8}$$

Using the extensional strain contributions from Eq. (A.3),

$\varepsilon_{11}^{(0)}, \varepsilon_{11}^{(2)}, \varepsilon_{22}^{(0)}, \varepsilon_{22}^{(2)}$ *and* $\varepsilon_{33}^{(0)}$ the integral can be expanded to:

$$N_{11} = (\lambda + 2G) \int_{-h/2}^{h/2} (u_{,1} + z^2 \phi_{1,1}) dz + \lambda \int_{-h/2}^{h/2} (v_{,2} + z^2 \phi_{2,2} + \kappa_3 \varphi_3) dz \tag{A.9}$$

which after evaluation leads to the first plate constitutive equation in Eq. (A.11a), that is,

$$N_{11} = (\lambda + 2G)[h\, u_{,1} + \frac{h^3}{12} \phi_{1,1}] + \lambda[h\, v_{,1} + \frac{h^3}{12} \phi_{2,2} + h\, \kappa_3 \varphi_3] \tag{A.10}$$

The other extensional and flexural plate forces are developed in similar fashion and can be summarized for an isotropic plate as

<u>Extensional Wave</u>

$$\begin{Bmatrix} N_{11} \\ N_{22} \\ N_{12} \end{Bmatrix} = \begin{bmatrix} \lambda + 2G & \lambda & 0 \\ \lambda & \lambda + 2G & 0 \\ 0 & 0 & G \end{bmatrix} \left(h \begin{Bmatrix} u_{,1} \\ v_{,2} \\ u_{,2} + v_{,1} \end{Bmatrix} + \frac{h^3}{12} \begin{Bmatrix} \phi_{1,1} \\ \phi_{2,2} \\ \phi_{1,2} + \phi_{2,1} \end{Bmatrix} \right) + h\kappa_3 \lambda \begin{Bmatrix} 1 \\ 1 \\ 0 \end{Bmatrix} \psi_3 \tag{A.11a}$$

$$N_3 = h[\kappa_3 \lambda (u_{,1} + v_{,2}) + \kappa_3{}^2 (\lambda + 2G) \psi_3] + \frac{h^3}{12} \kappa_3 \lambda (\phi_{1,1} + \phi_{2,2})$$

(A.11b)

$$\begin{Bmatrix} R_2 \\ R_1 \end{Bmatrix} = \kappa_4^2 \frac{h^3}{12} G \begin{Bmatrix} 2\varphi_2 + \psi_{3,2} \\ 2\varphi_1 + \psi_{3,1} \end{Bmatrix} \tag{A.11c}$$

$$\begin{Bmatrix} S_{11} \\ S_{22} \\ S_{12} \end{Bmatrix} = \begin{bmatrix} \lambda+2G & \lambda & 0 \\ \lambda & \lambda+2G & 0 \\ 0 & 0 & G \end{bmatrix} \left(\frac{h^3}{12} \begin{Bmatrix} u_{,1} \\ v_{,2} \\ u_{,2}+v_{,1} \end{Bmatrix} + \frac{h^5}{80} \begin{Bmatrix} \phi_{1,1} \\ \phi_{2,2} \\ \phi_{1,2}+\phi_{2,1} \end{Bmatrix} \right) + \kappa_3 \frac{h^3}{12} \lambda \begin{Bmatrix} 1 \\ 1 \\ 0 \end{Bmatrix} \psi_3 \tag{A.11d}$$

Flexural Wave

$$\begin{Bmatrix} M_{11} \\ M_{22} \\ M_{12} \end{Bmatrix} = \frac{h^3}{12} \begin{bmatrix} \lambda+2G & \lambda & 0 \\ \lambda & \lambda+2G & 0 \\ 0 & 0 & G \end{bmatrix} \begin{Bmatrix} \psi_{1,1} \\ \psi_{2,2} \\ \psi_{1,2}+\psi_{2,1} \end{Bmatrix} + \frac{h^5}{80} \begin{bmatrix} \lambda+2G & \lambda & 0 \\ \lambda & \lambda+2G & 0 \\ 0 & 0 & G \end{bmatrix} \begin{Bmatrix} \chi_{1,1} \\ \chi_{2,2} \\ \chi_{1,2}+\chi_{2,1} \end{Bmatrix} \tag{A.12a}$$
$$+\kappa_6 \frac{h^3}{12} \lambda \begin{Bmatrix} 1 \\ 1 \\ 0 \end{Bmatrix} \phi_3$$

$$\begin{Bmatrix} Q_2 \\ Q_1 \end{Bmatrix} = \kappa_1^2 hG \begin{Bmatrix} w_{,1}+\psi_1 \\ w_{,2}+\psi_2 \end{Bmatrix} + G \frac{h^3}{12} \kappa_1^2 \begin{Bmatrix} 3(\chi_{1+}\phi_{3,1}) \\ 3(\chi_{2+}\phi_{2,2}) \end{Bmatrix} \tag{A.12b}$$

$$\begin{Bmatrix} P_2 \\ P_1 \end{Bmatrix} = \kappa_1^2 \frac{h^3}{12} G \begin{Bmatrix} w_{,1}+\psi_1 \\ w_{,1}+\psi_2 \end{Bmatrix} + G \frac{h^5}{80} \kappa_1^2 \begin{Bmatrix} 3(\chi_{1+}\phi_{3,1}) \\ 3(\chi_{2+}\phi 3_{,2}) \end{Bmatrix} \tag{A.12c}$$

$$M_3 = 2\kappa_6(\lambda+2G)\phi_3 \frac{h^3}{12} + \kappa_6 \lambda(\varphi_{1,2} + \varphi_{2,2)} \frac{h^3}{12} + \kappa_6 \lambda(\chi_{1,1} + \chi_{2,2}) \frac{h^5}{80} \tag{A.12d}$$

$$\begin{Bmatrix} T_{11} \\ T_{22} \\ T_{12} \end{Bmatrix} = \frac{h^5}{80} \begin{bmatrix} \lambda+2G & \lambda & 0 \\ \lambda & \lambda+2G & 0 \\ 0 & 0 & G \end{bmatrix} \begin{Bmatrix} \varphi_{1,1} \\ \varphi_{2,2} \\ \varphi_{1,2}+\varphi_{2,1} \end{Bmatrix} + \frac{h^7}{448} \begin{bmatrix} \lambda+2G & \lambda & 0 \\ \lambda & \lambda+2G & 0 \\ 0 & 0 & G \end{bmatrix} \begin{Bmatrix} \chi_{1,1} \\ \chi_{2,2} \\ \chi_{1,2}+\chi_{2,1} \end{Bmatrix} \tag{A12e}$$
$$+\kappa_6 \frac{h^5}{80} \lambda \begin{Bmatrix} 1 \\ 1 \\ 0 \end{Bmatrix} \phi_3$$

where h is the thickness of the plate, λ and G are the Lame's constants of elasticity, and the stress resultants are defined by

$$\begin{Bmatrix} N_{\alpha\beta} \\ M_{\alpha\beta} \\ S_{\alpha\beta} \\ T_{\alpha\beta} \end{Bmatrix} = \int_{-h/2}^{h/2} \sigma_{\alpha\beta} d \begin{Bmatrix} 1 \\ z \\ z^2/2 \\ z^3 \end{Bmatrix} z, \qquad \begin{Bmatrix} Q_\alpha \\ R_\alpha \\ P_\alpha \end{Bmatrix} = \int_{-h/2}^{h/2} \sigma_{\alpha 3} \begin{Bmatrix} 1 \\ z \\ z^2 \end{Bmatrix} dz, \qquad \begin{Bmatrix} N_3 \\ M_3 \end{Bmatrix} = \int_{-h/2}^{h/2} \begin{Bmatrix} 1 \\ z \end{Bmatrix} \sigma_{33} dz \tag{A.13}$$

Equations of Motion

With the linear strain-displacement relation, the equations of motion of the higher-order plate theory can be derived using the principle of virtual displacements or Hamilton's principle (e.g., Washizu, 1982)

$$0 = \int_{t_1}^{t_2} (\delta U + \delta V - \delta K) dt \tag{A.14}$$

where δU is the virtual strain energy, δV virtual work done by applied forces, and δK the virtual kinetic energy. Alternatively the Equations of motion can be derived using the elastodynamic equilibrium equations multiplied by powers of z and then integrated through the thickness to convert stresses to plate allowable. Starting with the classic elastodynamic equations of elasticity,

$$\begin{aligned} \frac{\partial \sigma_{11}}{\partial x_1} + \frac{\partial \sigma_{12}}{\partial x_2} + \frac{\partial \sigma_{13}}{\partial z} + f_1 &= \rho \ddot{u} \\ \frac{\partial \sigma_{22}}{\partial x_2} + \frac{\partial \sigma_{12}}{\partial x_1} + \frac{\partial \sigma_{23}}{\partial z} + f_2 &= \rho \ddot{v} \\ \frac{\partial \sigma_{33}}{\partial z} + \frac{\partial \sigma_{13}}{\partial x_1} + \frac{\partial \sigma_{23}}{\partial x_2} + f_3 &= \rho \ddot{w} \end{aligned} \tag{A.15}$$

The five extensional plate equations of motion are developed by integrating the first two equations through the thickness with respect to z, then multiplying the third equation by z and integrating through the thickness with respect to z, and finally by multiplying the first and second equations by z^2 and integrating through the thickness with respect to z . As an example look at the third equation of motion multiplied by z, noting that from Eq. (A.1) that the only inertial term associated with the total transverse displacement u_3 in extension is $z\ddot{\varphi}_3$ so $\ddot{w} = z\ddot{\varphi}_3$

$$\int_{-h/2}^{h/2} z \frac{\partial \sigma_3}{\partial z} dz + \int_{-h/2}^{h/2} z \frac{\partial \tau_{13}}{\partial x_1} + \int_{-h/2}^{h/2} z \frac{\partial \tau_{23}}{\partial x_2} + 0 = \int_{-h/2}^{h/2} \rho \ddot{w} z dz = \rho \int_{-h/2}^{h/2} z \ddot{\varphi}_3 z dz \tag{A.16}$$

After integration by parts the first term yield the plate force N_3 and the surface tractions (which will be subsequently replaced by the equivalent body forces) which by definition will be called the loading term *m*., i.e.

$$z\sigma_{33}\Big|_{-h/2}^{h/2} - \int_{-h/2}^{h/2} \sigma_{33} dz = \frac{h}{2}\left[\sigma_{33}\left(\frac{h}{2}\right) - \sigma_{33}\left(-\frac{h}{2}\right)\right] - N_z \tag{A.17}$$

The second term after integration by parts yields the plate force derivative definition of $R_{1,1}$ as defined in Eq. (a.13), which is:

$$\int_{-h/2}^{h/2} z\frac{\partial \tau_{13}}{\partial x_1} = \frac{\partial}{\partial x_1}\int_{-h/2}^{h/2} \tau_{13} z dz = \frac{\partial}{\partial x_1} R_1 = R_{1,1} \tag{A.18}$$

The third term yields $R_{2,2}$ in similar fashion. Putting the contributions of the four terms together and using the definition of inertial moments,
$I_j = \int_{-h/2}^{h/2} \rho(z)^j dz \qquad (j = 0, 2, 4, 6)$, the result yields the third extensional equation of motion in Eqs. (A.20) which is.

$$R_{1,1} + R_{2,2} - N_z + m = I_2 \ddot{\varphi}_3 \tag{A.19}$$

In similar fashion the other four extensional equations of motion are developed and the six bending equations of motion. For an isotropic plate with mid-plane parallel to the plane $z_0 = 0$, the complete equations of motion for the third order theory are:

Extension

$$\begin{aligned}
&N_{11,1} + N_{12,2} + q_1 = I_0 \ddot{u} + I_2 \ddot{\varphi}_1 \\
&N_{12,1} + N_{22,2} + q_2 = I_0 \ddot{v} + I_2 \ddot{\varphi}_2 \\
&R_{1,1} + R_{2,2} - N_{33} + m = I_2 \ddot{\psi}_3 \\
&S_{11,1} + S_{12,2} - R_1 + \frac{n_1}{2} = \frac{I_2}{2}\ddot{u} + \frac{I_4}{2}\ddot{\varphi}_1 \\
&S_{12,1} + S_{22,2} - R_2 + \frac{n_2}{2} = \frac{I_2}{2}\ddot{v} + \frac{I_4}{2}\ddot{\varphi}_2
\end{aligned} \tag{A.20}$$

Flexure

$$
\begin{aligned}
&M_{11,1} + M_{12,2} - Q_1 + m_1 = I_2\ddot{\psi}_1 + I_4\ddot{\chi}_1 \\
&M_{12,1} + M_{22,2} - Q_2 + m_2 = I_2\ddot{\psi}_2 + I_4\ddot{\chi}_2 \\
&Q_{x,x} + Q_{y,y} + q = I_0\ddot{w}_0 + I_2\ddot{\varphi}_3 \\
&T_{11,1} + T_{12.2} - 3P_1 + r_1 = I_4\ddot{\psi}_1 + I_6\ddot{\chi}_1 \\
&T_{12,1} + T_{22.2} - 3P_2 + r_2 = I_4\ddot{\psi}_2 + I_6\ddot{\chi}_2 \\
&P_{1,1} + P_{2,2} - 2M_3 + n_z = I_2\ddot{w} + I_4\ddot{\varphi}_3
\end{aligned}
\qquad \text{(A.21)}
$$

with a number of boundary conditions which must be specified on the plate edges; q_1, q_2, …, m_1, and m_2 are the loads related to the surface tractions and defined by

$$
\begin{Bmatrix} q_\alpha \\ n_\alpha \\ r_\alpha \end{Bmatrix} = [\sigma_{\alpha 3}(h/2) - \sigma_{\alpha 3}(-h/2)] \begin{Bmatrix} 1 \\ h^2/4 \\ h^3/8 \end{Bmatrix}, \quad m_\alpha = [\sigma_{\alpha 3}(h/2) + \sigma_{\alpha 3}(-h/2)]\frac{h}{2}
$$

$$
\begin{aligned}
&q = \sigma_{33}(h/2) - \sigma_{33}(-h/2), \quad m = [\sigma_{33}(h/2) + \sigma_{33}(-h/2)]\frac{h}{2} \\
&n_z = [\sigma_{33}(h/2) - \sigma_{33}(-h/2)]\frac{h^2}{4}
\end{aligned}
\qquad \text{(A.22)}
$$

where the subscript $\alpha = 1, 2$ and ρ is the mass density.

Equations of Motion in Terms of Displacement

The equations of motion in Eq. (A.20) and (A.21) can be expressed in terms of the displacements by substituting for the stress resultants from the constitutive equations, Eq. (A.12). The equations of motion and the plate constitutive equations indicate that the extensional or symmetric waves with five degrees of freedom (u, v, ψ_3, φ_1, φ_2) are decoupled from the flexural or anti-symmetric waves with three degrees of freedom ($\psi_1, \psi_2, w, \chi_1, \chi_2, \varphi_3$). The symmetric and anti-symmetric waves refer to the wave displacement profile symmetric and anti-symmetric with respect to the mid-plane of the plate ($z = 0$) respectively as shown in fig. 4.1. In the following these two wave motions are examined separately. For isotropic plates, the equations of motion take the form:

Extensional wave

$$\frac{I_0}{\rho}[(\lambda+2G)u_{,11}+(\lambda+G)v_{,12}+Gu_{,22}]+\frac{I_2}{\rho}[(\lambda+2G)\phi_{1,11}+(\lambda+G)\phi_{2,12}+G\phi_{1,22}] \\ +\kappa_3\frac{I_0}{\rho}\lambda\psi_{3,1}+q_1=I_0\ddot{u}+I_2\ddot{\phi}_1 \tag{A.23a}$$

$$\frac{I_0}{\rho}[Gv_{,11}+(\lambda+G)u_{,21}+(\lambda+2G)v_{,22}]+\frac{I_2}{\rho}[G\phi_{2,11}+(\lambda+G)\phi_{1,12}+(\lambda+2G)\phi_{2,22}] \\ +\kappa_3\frac{I_0}{\rho}\lambda\psi_{3,2}+q_2=I_0\ddot{v}+I_2\ddot{\phi}_2 \tag{A.23b}$$

$$\frac{I_2}{\rho}[\kappa_4^2G(\psi_{3,11}+\psi_{3,22})+(2\kappa_4^2G-\kappa_3\lambda)(\phi_{1,1}+\phi_{2,2})]-\frac{I_0}{\rho}\kappa_3[\lambda(u_{,1}+v_{,2}) \\ +\kappa_3(\lambda+2G)\psi_3]+m=I_2\ddot{\psi}_3 \tag{A.23c}$$

$$\frac{I_2}{2\rho}[(\lambda+2G)u_{,11}+(\lambda+G)v_{,12}+Gu_{,22}+(\kappa_3\lambda-2\kappa_4^2G)\psi_{3,1}-4\kappa_4^2G\phi_1]+ \\ \frac{I_4}{2\rho}[(\lambda+2G)\phi_{1,11}+(\lambda+G)\phi_{2,12}+G\phi_{1,22}]+n_1=\frac{I_2}{2}\ddot{u}+\frac{I_4}{2}\ddot{\phi}_1 \tag{A.23d}$$

$$\frac{I_2}{2\rho}[Gv_{,11}+(\lambda+G)u_{,12}+(\lambda+2G)v_{,22}+(\kappa_3\lambda-2\kappa_4^2G)\psi_{3,2}-4\kappa_4^2G\phi_2]+ \\ \frac{I_4}{2\rho}[G\phi_{2,11}+(\lambda+G)\phi_{1,12}+(\lambda+2G)\phi_{2,22}]+n_2=\frac{I_2}{2}\ddot{v}+\frac{I_4}{2}\ddot{\phi}_2 \tag{A.23e}$$

Flexural Wave

$$\frac{I_2}{\rho}[(\lambda+2G)\psi_{1,11}+(\lambda+G)\psi_{2,12}+G\psi_{1,22}-\kappa_1{}^2(3\chi_1+\phi_{3,1})]+-\frac{I_4}{\rho}[(\lambda+2G)\chi_{1,11} \\ +\lambda\chi_{2,12}+G(\chi_{1,22}+\chi_{2,12})]+2\kappa_6\frac{I_2}{\rho}\lambda\phi_{3,1}-\kappa_1{}^2\frac{I_0}{\rho}G(w_{,1}+\varphi_1)+m_1=I_2\ddot{\psi}_1+I_4\ddot{\chi}_1 \tag{A.24a}$$

$$\frac{I_2}{\rho}[(\lambda+2G)\psi_{2,22}+(\lambda+G)\psi_{1,12}+G\psi_{2,11}-\kappa_1^{\,2}(3\chi_2+\phi_{3,2})]+-\frac{I_4}{\rho}[(\lambda+2G)\chi_{2,22}$$
$$+\lambda\chi_{1,12}+G(\chi_{2,11}+\chi_{1,12})]+2\kappa_6\frac{I_2}{\rho}\lambda\phi_{3,2}-\kappa_1^{\,2}\frac{I_0}{\rho}G(w_{,2}+\varphi_2)+m_2=I_2\ddot{\psi}_2+I_4\ddot{\chi}_2 \quad \text{(A.24b)}$$

$$\frac{I_0}{\rho}\kappa_1^{\,2}G(w_{,11}+w_{,22}+\psi_{1,1}+\psi_{2,2})+\frac{I_2}{\rho}\kappa_1^{\,2}G[3(\chi_{1,1}+\chi_{2,2})+(\phi_{3,11}+\phi_{3,22})]$$
$$+q=I_0\ddot{w}+I_2\ddot{\phi}_3 \quad \text{(A.24c)}$$

$$\frac{I_4}{\rho}[(\lambda+2G)\psi_{1,11}+(\lambda+G)\psi_{2,12}+G\psi_{1,22}-3\kappa_1^{\,2}(3\chi_1+\phi_{3,1})]+\frac{I_6}{\rho}[(\lambda+2G)\chi_{1,11}$$
$$+\lambda\chi_{2,12}+G(\chi_{1,22}+\chi_{2,12})]+2\kappa_6\frac{I_4}{\rho}\lambda\phi_{3,1}-3\kappa_1^{\,2}\frac{I_2}{\rho}G(w_{,1}+\varphi_1)+r_1=I_4\ddot{\psi}_1+I_6\ddot{\chi}_1 \quad \text{(A.24d)}$$

$$\frac{I_4}{\rho}[(\lambda+2G)\psi_{2,22}+(\lambda+G)\psi_{1,12}+G\psi_{2,11}-3\kappa_1^{\,2}(3\chi_2+\phi_{3,2})]+\frac{I_6}{\rho}[(\lambda+2G)\chi_{2,22}$$
$$+\lambda\chi_{1,12}+G(\chi_{2,11}+\chi_{1,12})]+2\kappa_6\frac{I_4}{\rho}\lambda\phi_{3,2}-3\kappa_1^{\,2}\frac{I_2}{\rho}G(w_{,2}+\varphi_2)+r_2=I_4\ddot{\psi}_2+I_6\ddot{\chi}_2 \quad \text{(A.24e)}$$

$$\frac{I_2}{\rho}\{\kappa_1^{\,2}G(w_{,11}+w_{,22}+\psi_{1,1}+\psi_{2,2})-4\kappa_6^{\,2}(\lambda+2G)\phi_3-2\kappa_6\lambda(\varphi_{1,1}+\varphi_{2,2})]\}$$
$$+\frac{I_4}{\rho}\{\kappa_1^{\,2}G[3(\chi_{1,1}+\chi_{2,2})+(\phi_{3,11}+\phi_{3,22})]-2\kappa_6\lambda(\chi_{1,1}+\chi_{2,2})\}+n_z=I_2\ddot{w}+I_4\ddot{\phi}_3 \quad \text{(A.24f)}$$

In the following analysis it is convenient to make the variables dimensionless. To accomplish this step, we may introduce a representative length scale $h/2$, a typical time scale, $\tau = 0.5h/c_T$, where $c_T = \sqrt{G/\rho}$ is the velocity of bulk transverse or shear waves), and define the following non-dimensional variables and quantities

$$
\begin{aligned}
&x_i' = \frac{x_i}{h/2}, \qquad t' = \frac{t}{\tau}, \qquad w' = \frac{w}{h/2} \\
&u' = \frac{u}{h/2}, \qquad v' = \frac{v}{h/2}, \qquad \phi_\alpha' = \phi_\alpha h/2 \\
&\chi_i{}' = \chi_i \left(\frac{h}{2}\right)^2, \quad \varphi' = \varphi, \qquad p_i{}' = p_i \left(\frac{h}{3}\right)^3 \\
&q_\alpha' = \frac{q_\alpha}{2G}, \qquad n_\alpha' = \frac{n_\alpha}{Gh^2/10}, \quad m' = \frac{m}{Gh/3} \\
&q' = \frac{q}{2G}, \qquad m_\alpha' = \frac{m_\alpha}{Gh/3} \\
&k_j' = k_j h/2, \qquad \omega' = \omega\tau, \qquad \tau = \frac{h}{2C_T} = \frac{h}{2\sqrt{\frac{G}{\rho}}} \\
&\delta'(x_1) = \delta(x_1) l, \qquad \delta'^{(1)}(x_1) = \delta^{(1)}(x_1) l^2
\end{aligned}
\tag{A.25}
$$

where k_j', ω' are the nondimensional wave number and frequency which will be used in the dispersion relation. According to the non-dimensionalization, the phase velocity and group velocity are normalized by $c_T = \sqrt{G/\rho}$.

The bulk longitudinal wave velocity $c_L = \sqrt{(\lambda + 2G)/\rho}$, plate velocity $c_P = \sqrt{E/[(1-\nu^2)\rho]}$ and c_R (Rayleigh wave velocity) are also used and their dimensionless representations normalized by c_T are

$$
c_L' = \sqrt{\alpha}, \quad c_P' = 2\sqrt{\frac{\alpha - 1}{\alpha}} = \sqrt{\frac{2}{1-\nu}}, \quad c_R' = \frac{c_R}{c_T}, \quad c_T' = 1 \tag{A.26}
$$

where $\alpha = (c_L / c_T)^2 = 2 + \lambda / G = \dfrac{2G + \lambda}{G}$ and ν is Poisson's ratio. Note that the non-dimensional quantities will be used in the following wave analysis and all the "primes" will be dropped for convenience unless stated otherwise. Then the dimensionless equations of motion can be derived. To do so, the non-dimensionalized values are substituted into Eqs. (A.23) and (A.24) including the non-dimensionalized temporal and spatial derivitives, of the quantities in Eq. (A.25) as required. The equations are then divided by the shear modulus μ which gives rise to factors that are in the form α, α-1, or α-2, which simplify the equations. The inertial terms are then expressed as $\dfrac{I_0}{\rho} = h$, $\dfrac{I_2}{\rho} = \dfrac{h^3}{12}$, etc. as defined earlier, $I_j = \int_{-h/2}^{h/2} \rho z^j dz$ $(j = 0, 2, 4, 6)$. These substitutions along with

some algebraic manipulation lead to the non-dimensionalized equations of motion in terms of displacements:

Extensional wave

$$\alpha u_{,11}+(\alpha-1)v_{,12}+u_{,22}+[\alpha\phi_{1},_{11}+(\alpha-1)\phi_{2},_{12}+\phi_{1},_{22}]/3 \\ +\kappa_3(\alpha-2)\psi_{3},_{1}+q_1=\ddot{u}+\ddot{\phi}_1/3 \tag{A.27a}$$

$$v_{,11}+(\alpha-1)u_{,12}+\alpha v_{,22}+[\phi_{2},_{11}+(\alpha-1)\phi_{1},_{12}+\alpha\phi_{2},_{22}]/3 \\ +\kappa_3(\alpha-2)\psi_{3},_{2}+q_2=\ddot{v}+\ddot{\phi}_2/3 \tag{A.27b}$$

$$\kappa_4^2(\psi_{3},_{11}+\psi_{3},_{22})-[\kappa_4(\alpha-2)-2\kappa_4^2](\phi_{1},_{1}+\phi_{2},_{2})] \\ -3\kappa_3(\alpha-2)(u_{,1}+v_{,2})-3\kappa_3{}^2\alpha\psi_3+m=\ddot{\psi}_3 \tag{A.27c}$$

$$\{\alpha u_{,11}+(\alpha-1)v_{,12}+u_{,22}+[\kappa_3(\alpha-2)-2\kappa_4^2]\psi_{3},_{1}-4\kappa_4^2\phi_1\}\frac{5}{3} \\ +\alpha\phi_{1},_{11}+(\alpha-1)\phi_{2},_{12}+\phi_{1},_{22}+n_1=\frac{5}{3}\ddot{u}+\ddot{\phi}_1 \tag{A.27d}$$

$$\{v_{,11}+(\alpha-1)u_{,12}+\alpha v_{,22}+[\kappa_3(\alpha-2)-2\kappa_4^2]\psi_{3},_{2}-4\kappa_4^2\phi_2\}\frac{5}{3} \\ +\phi_{2},_{11}+(\alpha-1)\phi_{1},_{12}+\alpha\phi_{2},_{22}+n_2=\frac{5}{3}\ddot{v}+\ddot{\phi}_2 \tag{A.27e}$$

Flexural wave

$$\alpha\psi_{1,11}+(\alpha-1)\psi_{2,12}+\psi_{1,22}-\kappa_1{}^2(3\chi_1+\phi_{3,1})+\frac{3}{5}\left(\alpha\chi_{1,11}+(\alpha-1)\chi_{2,12}+\chi_{1,22}\right) \\ +2\kappa_6(\alpha-2)\phi_{3,1}-3\kappa_1{}^2(w,_1+\psi_1)+m_1=\ddot{\psi}_1+\frac{3}{5}\ddot{\chi}_1 \tag{A.28a}$$

$$\alpha\psi_{2,22}+(\alpha-1)\psi_{1,12}+\psi_{2,11}-\kappa_1{}^2(3\chi_2+\phi_{3,2})+\frac{3}{5}(\alpha\chi_{2,22}+(\alpha-1)\chi_{1,12}+\chi_{2,11}) \\ +2\kappa_6(\alpha-2)\phi_{3,2}-3\kappa_1{}^2(w,_2+\psi_2)+m_2=\ddot{\psi}_2+\frac{3}{5}\ddot{\chi}_2 \tag{A.28b}$$

$$\kappa_1^2(w_{,11}+w_{,22}+\psi_{1,1}+\psi_{2,2})+\kappa_1^2[\chi_{1,1}+\chi_{2,2}+\frac{1}{3}(\phi_{3,11}+\phi_{3,22})]+q=\ddot{w}+\frac{1}{3}\ddot{\phi}_3 \tag{A.28c}$$

$$\begin{aligned}&\alpha\psi_{1,11}+(\alpha-1)\psi_{2,12}+\psi_{1,22}-3\kappa_1^2(3\chi_1+\phi_{3,1})+\frac{5}{7}\alpha\chi_{1,11}+\frac{5}{7}(\alpha-1)\chi_{2,12}\\&+\frac{5}{7}\chi_{1,22}+2\kappa_6(\alpha-2)\phi_{3,1}-5\kappa_1^2(w_{,1}+\psi_1)+\frac{5}{7}r_1=\ddot{\psi}_1+\frac{5}{7}\ddot{\chi}_1\end{aligned} \tag{A.28d}$$

$$\begin{aligned}&\alpha\psi_{2,22}+(\alpha-1)\psi_{1,12}+\psi_{2,11}-3\kappa_1^2(3\chi_2+\phi_{3,2})+\frac{5}{7}\alpha\chi_{2,22}+\frac{5}{7}(\alpha-1)\chi_{1,12}\\&+\frac{5}{7}\chi_{2,11}+2\kappa_6(\alpha-2)\phi_{3,2}-5\kappa_1^2(w_{,2}+\psi_2)+\frac{5}{7}r_2=\ddot{\psi}_2+\frac{5}{7}\ddot{\chi}_2\end{aligned} \tag{A.28e}$$

$$\begin{aligned}&\kappa_1^2(w_{,11}+w_{,22}+\psi_{1,1}+\psi_{2,2})-4\kappa_6^2\alpha\phi_3-2\kappa_6(\alpha-2)(\varphi_{1,1}+\varphi_{2,2})+\frac{9}{5}\kappa_1(\chi_{1,1}+\chi_{2,2})\\&+\frac{3}{5}\kappa_1^2(\phi_{3,11}+\phi_{3,22})-\frac{6}{5}\kappa_6(\alpha-2)(\chi_{1,1}+\chi_{2,2})+\frac{3}{5}n_z=\ddot{w}+\frac{3}{5}\ddot{\phi}_3\end{aligned} \tag{A.28f}$$

The dimensionless equations depend only on a single parameter α except loading parameters, and thus the dispersion relation discussed below depends solely on the single parameter or Poisson's ratio. This is one advantage of this non-dimensionalization.

Equations of Motion in Vector and Matrix Form

Next, the vectorized equations of motion in terms of displacement will be established and the coefficients of the above equations will be used to form the constitutive matrices for extension and bending leading to a very compact form which will expedite the solution.

The plate motion, extensional or flexural, is governed by a system of second-order linear partial differential equations (PDE's). Transient wave solutions may be obtained by integral transforms.

Extensional motion

The dimensionless equations of motion of the plate with load $\boldsymbol{f}_E(\mathbf{x}, t)$ and zero initial conditions, as expressed in Eqs. (A.27) above can be written in the matrix notation as

$$\boldsymbol{I}\frac{\partial^2 \boldsymbol{V}}{\partial t^2}+\boldsymbol{T_{11}}\frac{\partial^2 \boldsymbol{V}}{\partial x_1^2}+\boldsymbol{T_{12}}\frac{\partial^2 \boldsymbol{V}}{\partial x_1 \partial x_2}+\boldsymbol{T_{22}}\frac{\partial^2 \boldsymbol{V}}{\partial x_2^2}+\boldsymbol{T_1}\frac{\partial \boldsymbol{V}}{\partial x_1}+\boldsymbol{T_2}\frac{\partial \boldsymbol{V}}{\partial x_2}+\boldsymbol{T_0}\boldsymbol{V}=\mathbf{f}_E, \quad t>0$$
$$\boldsymbol{V}=\frac{\partial \boldsymbol{V}}{\partial t}=\mathbf{0}, \quad at \;\; t=0 \tag{A.29}$$

Where

$\boldsymbol{V}=[u\,,v\;,\psi_3\,,\phi_1\,,\phi_2]^T$ and $\mathbf{f}_E=[q_1\,,q_2\,,m\,,n_1\,,n_2]^T$, and
$\boldsymbol{T}_{11}$, $\boldsymbol{T}_{12}$, $\boldsymbol{T}_{22}$, $\boldsymbol{T}_1$, $\boldsymbol{T}_2$, $\boldsymbol{T}_0$ are *5x5* constant matrices formed simply by isolating the coefficients of each displacement degree of freedom and its derivatives as indicated in Eqs. (A.27) to form Eq. (A.29) above. Note that the bolded quantities represent a vector or a matrix. To illustrate the formation of the coefficient matrices consider the element $\boldsymbol{T}_{11}$. This matrix picks up the coefficients of all terms in the normalized extensional displacement equations of motions, Eqs. (A.27a-A.27e), that multiply second derivatives with respect to x_1 of any of the five displacement degrees of freedom that comprise **V**. Mathematically then, the second term of Eq. (A.29) can be expressed as:

$$\mathbf{T}_{11}\frac{\partial^2 \boldsymbol{V}}{\partial x_1^2}=\begin{bmatrix} \alpha & 0 & 0 & \frac{\alpha}{3} & 0 \\ 0 & 1 & 0 & 0 & \frac{1}{3} \\ 0 & 0 & \kappa_4{}^2 & 0 & 0 \\ \frac{5}{3}\alpha & 0 & 0 & \alpha & 0 \\ 0 & \frac{5}{3} & 0 & 0 & 1 \end{bmatrix}\begin{pmatrix} u \\ v \\ \varphi_3 \\ \phi_1 \\ \varphi_2 \end{pmatrix}_{,11} \tag{A.30}$$

With $\mathbf{T_{11}}$ being the coefficient matrix. Also, consider the inertial terms that form the I matrix that multiply the temporal derivates of the displacement which is the first term of Eq. (A.29),

$$\mathbf{I}_{\text{ext}} = \begin{bmatrix} 1 & 0 & 0 & \frac{1}{3} & 0 \\ 0 & 1 & 0 & 0 & \frac{1}{3} \\ 0 & 0 & 1 & 0 & 0 \\ \frac{5}{3} & 0 & 0 & 1 & 0 \\ 0 & \frac{5}{3} & 0 & 0 & 1 \end{bmatrix} \begin{pmatrix} \ddot{u} + \frac{\ddot{\phi}_1}{3} \\ \ddot{v} + \frac{\ddot{\phi}_2}{3} \\ \ddot{\varphi}_3 \\ \frac{5}{3}\ddot{u} + \ddot{\varphi}_1 \\ \frac{5}{3}\ddot{v} + \ddot{\varphi}_{21} \end{pmatrix} \tag{A31}$$

The remaining coefficients, $\boldsymbol{T}_{12}$, $\boldsymbol{T}_{22}$, $\boldsymbol{T}_1$, $\boldsymbol{T}_2$, and $\boldsymbol{T}_0$ are assembled in similar fashion to those associated with the $\boldsymbol{T}_{11}$ term. The bending formulation uses the six bending normalized equations of motion, Eqs. (A.28a-A.28f) and will be summarized in the next section.

Equation of Motion in Compact Form

The equations of motion can be assembled into a very compact form that, albeit, a system of equations, has the appearance of a single degree of freedom system and is easier to manipulate in seeking a solution. In this form the coefficient matrices **T**ij can be formed into a single constitutive matrix **T** via the application of the Fourier transform.

This cannot be done prior to taking the transform in x_1,x_2 space by simply superimposing the terms from all of the individual **T**ij matrices in their assigned row and column similar in manner to the formation of a stiffness matrix in finite element analysis. The reason is, that the individual coefficient matrices multiply displacement derivatives that don't have a common denominator. This incompatibility will vanish with the application of the Fourier transform, which enables the establishment of the compact form.

Transformed Equations of Motion in Compact Form

In seeking both the homogeneous and inhomogeneous solutions of the system of equations of motion, a double transform approach will be employed. First the Fourier transform will be applied. The Fourier transformation of Eq. (A.29) with respect to the spatial variables x_1 and x_2 leads to:

$$\frac{\partial^2 \tilde{\boldsymbol{V}}}{\partial t^2} + \mathbf{T}(\mathbf{k})\,\tilde{\boldsymbol{V}} = \tilde{\mathbf{f}}_T\,, \quad t > 0 \tag{A.32}$$

$$\tilde{\boldsymbol{V}} = \frac{\partial \tilde{\boldsymbol{V}}}{\partial t} = \mathbf{0}, \quad at\ t = 0 \tag{A.33}$$

where $\mathbf{x} = (x_1, x_2)$ and the transformed variables $\mathbf{k} = (k_1, k_2)$, and

$$\tilde{\boldsymbol{V}}(\mathbf{k}, t) = \int_{-\infty}^{\infty} \boldsymbol{V}(\mathbf{x}, t) \exp(-i\mathbf{k} \cdot \mathbf{x})\, d\mathbf{x} \tag{A.34}$$
$$\tilde{\mathbf{f}}_E(\mathbf{k}, t) = \int_{-\infty}^{\infty} \mathbf{f}_E(\mathbf{x}, t) \exp(-i\mathbf{k} \cdot \mathbf{x})\, d\mathbf{x}$$

Addressing the aforementioned problem with assembling a compact coefficient matrix, advantage will be taken here of the formula for the n^{th} derivative of the transform,

$$\Im\left\langle \mathbf{V}^{(n)}(\mathbf{x}) \right\rangle = (-ik_i)^n\, \tilde{\mathbf{V}}(\mathbf{k}) \tag{A.35}$$

For the extensional problem this results in the following transformations of the coefficients in **k** space when the $(-ik_i)^n$ terms multiplying $\tilde{\mathbf{V}}(\mathbf{k})$ are grouped with the $\mathbf{T}_{ij}$ terms.

$$\begin{aligned}
&\mathbf{T}_{11}(\mathbf{k}) = -\mathrm{k}_1^{\,2}\mathbf{T}_{11} \\
&\mathbf{T}_{12}(\mathbf{k}) = -\mathrm{k}_1 k_2 \mathbf{T}_{12} \\
&\mathbf{T}_{22}(\mathbf{k}) = -\mathrm{k}_2^{\,2}\mathbf{T}_{22} \\
&\mathbf{T}_1(\mathbf{k}) = -\mathrm{i}\mathrm{k}_1\mathbf{T}_1 \\
&\mathbf{T}_2(\mathbf{k}) = -\mathrm{i}\mathrm{k}_2\mathbf{T}_2 \\
&\mathbf{T}_0(\mathbf{k}) = \mathbf{T}_0
\end{aligned} \tag{A.36}$$

When the above transformations and groupings are applied to each term of Eq. (A.29), the derivatives vanish and terms with like rows and columns terms can be superimposed from the five coefficient matrices into a single constitutive matrix.

Following the previous example then $\mathbf{T}_{11}(\mathbf{k})$, after applying the first of Eqs. (A.36) becomes;

$$-\mathrm{k}_1^{\,2}\mathbf{T}_{11} = \begin{bmatrix} \alpha k_1^{\,2} & 0 & 0 & \frac{\alpha}{3}k_1^{\,2} & 0 \\ 0 & k_1^{\,2} & 0 & 0 & \frac{k_1^{\,2}}{3} \\ 0 & 0 & \kappa_4^{\,2}k_1^{\,2} & 0 & 0 \\ \frac{5}{3}\alpha k_1^{\,2} & 0 & 0 & \alpha k_1^{\,2} & 0 \\ 0 & \frac{5}{3}k_1^{\,2} & 0 & 0 & k_1^{\,2} \end{bmatrix} \tag{A.37}$$

The other individual coefficient matrices are transformed in similar manner and then added together, resulting in the transformed master constitutive matrix.

$$\mathbf{T}(\mathbf{k}) = \begin{bmatrix} \alpha k_1^{\,2} + k_2^{\,2} & (\alpha-1)k_1k_2 & -i\kappa_3(\alpha-2)k_1 & \frac{\alpha k_1^{\,2} + k_2^{\,2}}{3} & \frac{(\alpha-1)}{3}k_1k_2 \\ (\alpha-1)k_1k_2 & k_1^{\,2} + \alpha k_2^{\,2} & -i\kappa_3(\alpha-2)k_2 & (\alpha-1)\frac{k_1k_2}{3} & \frac{k_1^{\,2} + \alpha k_2^{\,2}}{3} \\ 3i\kappa_3(\alpha-2)k_1 & 3i\kappa_3(\alpha-2)k_2 & \kappa_4^{\,2}(k_1^{\,2}+k_2^{\,2}) + 3\alpha\kappa_3^{\,2} & i[\kappa_3(\alpha-2) - 2\kappa_4^{\,2}]k_2 & i[\kappa_3(\alpha-2) - 2\kappa_4^{\,2}]k_2 \\ \frac{5}{3}(\alpha k_1^{\,2} + k_2^{\,2}) & \frac{5}{3}(\alpha-1)k_1k_2 & -\frac{5}{3}i[\kappa_3(\alpha-2) - 2\kappa_4^{\,2}]k_1 & \alpha k_1^{\,2} + k_2^{\,2} + \frac{20}{3}\kappa_4^{\,2} & (\alpha-1)k_1k_2 \\ \frac{5}{3}(\alpha-1)k_1k_2 & \frac{5}{3}(k_1^{\,2} + \alpha k_2^{\,2)} & -\frac{5}{3}i[\kappa_3(\alpha-2) - 2\kappa_4^{\,2}]k_2 & (\alpha-1)k_1k_2 & k_1^{\,2} + \alpha k_2^{\,2} + \frac{20}{3}\kappa_4^{\,2} \end{bmatrix} \tag{A.38}$$

The mass, or inertial, matrix is:

$$\boldsymbol{M} = \boldsymbol{I} = \begin{bmatrix} 1 & 0 & 0 & \frac{1}{3} & 0 \\ 0 & 1 & 0 & 0 & \frac{1}{3} \\ 0 & 0 & 1 & 0 & 0 \\ \frac{5}{3} & 0 & 0 & 1 & 0 \\ 0 & \frac{5}{3} & 0 & 0 & 1 \end{bmatrix} \tag{A.39}$$

Where $\alpha = (2G + \lambda)/G = 2(1-\nu)/(1-2\nu)$, where is Poisson's ratio, and λ and G are the Lame constants where the shear modulus G is identical to μ, the more traditional Lame constant.

Flexural motion

Employing the Fourier transforms and following similar procedures, the compact form of the equations of motion for flexure in the isotropic plate can be obtained from Eqs. (A.28). The equation of motion and the transformed solution for the flexural motion of the plate with bending load vector $\boldsymbol{f}_B$ **(x**, *t*) and zero initial conditions are

$$\begin{aligned} &\boldsymbol{I}\frac{\partial^2 \boldsymbol{U}}{\partial t^2}+\boldsymbol{A}_{11}\frac{\partial^2 \boldsymbol{U}}{\partial x_1^2}+\boldsymbol{A}_{12}\frac{\partial^2 \boldsymbol{U}}{\partial x_1 \partial x_2}+\boldsymbol{A}_{22}\frac{\partial^2 \boldsymbol{U}}{\partial x_2^2}+\boldsymbol{A}_1\frac{\partial \boldsymbol{U}}{\partial x_1}+\boldsymbol{A}_2\frac{\partial \boldsymbol{U}}{\partial x_2}+\boldsymbol{A}_0\boldsymbol{U}=\mathbf{f}_B, \quad t>0 \\ &\boldsymbol{U}=\frac{\partial \boldsymbol{U}}{\partial t}=\mathbf{0}, \quad at \;\; t=0 \end{aligned} \tag{A.40}$$

Where the flexural degrees of freedom and plate forces are:
$\boldsymbol{U}=[\psi_1, \;\; \psi_2, w, \chi_1, \;\; \chi_2, \varphi_3]^T$, $\mathbf{f}_B=[m_1, m_2, q, r_1, r_2, n_z]^T$,

The Fourier transformation of Eq. (A.40) with respect to the spatial variables x_1 and x_2 yields

$$\begin{aligned} &\frac{\partial^2 \tilde{\mathbf{U}}}{\partial t^2}+\mathbf{A}(\mathbf{k})\tilde{\mathbf{U}}=\tilde{\mathbf{f}}_B, \quad t>0 \\ &\tilde{\mathbf{U}}=\frac{\partial}{\partial t}\tilde{\mathbf{U}}=\mathbf{0}, \quad at \; t=0 \end{aligned} \tag{A.41}$$

where $\mathbf{x} = (x_1, x_2)$ and the transformed variables $\mathbf{k} = (k_1, k_2)$, and

$$\begin{aligned} \tilde{\mathbf{U}}(\mathbf{k},t)&=\int_{-\infty}^{\infty}\mathbf{U}(\mathbf{x},t)\exp(-i\mathbf{k}\cdot\mathbf{x})\,d\mathbf{x} \\ \tilde{\mathbf{f}}_B(\mathbf{k},t)&=\int_{-\infty}^{\infty}\mathbf{f}_B(\mathbf{x},t)\exp(-i\mathbf{k}\cdot\mathbf{x})\,d\mathbf{x} \end{aligned} \tag{A.42}$$

Where $\mathbf{A_{ij}}$ are 6x6 component matrices formed simply by isolating the coefficients of each displacement degree of freedom and its derivatives as indicated in Eqs. (A.28) and (A.40) above. These can be further combined into a single matrix **A(k)** to put the equations in their most compact form with **A**(**k**) representing the combined coefficient matrices with the k_i factors resulting from the transformed derivatives of **U** analogous to **T** for the extensional problem. This procedure is as outlined for the extensional wave using the extensional displacement equation of motion and will not be shown here for brevity. The results are:

$$\mathbf{A}=\begin{bmatrix}
\alpha k_1^{\,2}+k_2^{\,2}+3\kappa_1^{\,2} & k_1k_2(\alpha-1) & -3ik_1\kappa_1^{\,2} & \frac{3\alpha k_1^{\,2}}{5}+\frac{3k_2^{\,2}}{5}+3\kappa_1^{\,2} & \frac{3}{5}k_1k_2(\alpha-1) & ik_1(2(\alpha-2)\kappa_6-\kappa_1^{\,2}) \\
k_1k_2(\alpha-1) & k_1^{\,2}+\alpha k_2^{\,2}+3\kappa_1^{\,2} & -3ik_2\kappa_1^{\,2} & \frac{3}{5}k_1k_2(\alpha-1) & \frac{3k_1^{\,2}}{5}+\frac{3k_2^{\,2}\alpha}{5}+3\kappa_1^{\,2} & ik_2(2(\alpha-2)\kappa_6-\kappa_1^{\,2}) \\
ik_1\kappa_1^{\,2} & ik_2\kappa_1^{\,2} & k_1^{\,2}\kappa_1^{\,2}+k_2\kappa_1^{\,2} & ik_1\kappa_1^{\,2} & ik_2\kappa_1^{\,2} & \frac{k_1^{\,2}\kappa_1^{\,2}}{3}+\frac{k_2^{\,2}\kappa_1^{\,2}}{3} \\
\alpha k_1^{\,2}+k_2^{\,2}+5\kappa_1^{\,2} & k_1k_2(\alpha-1) & -5ik_1\kappa_1^{\,2} & \frac{5\alpha k_1^{\,2}}{7}+\frac{5k_2^{\,2}}{7}+9\kappa_1^{\,2} & k_1k_2(\frac{5}{7}(\alpha-2)+\frac{5}{7}) & ik_1(2(\alpha-2)\kappa_6-3\kappa_1^{\,2}) \\
k_1k_2(\alpha-1) & k_1^{\,2}+\alpha k_2^{\,2}+5\kappa_1^{\,2} & -5ik_2\kappa_1^{\,2} & k_1k_2\frac{5}{7}(\alpha-2)(+\frac{5}{7}) & \frac{5k_1^{\,2}}{7}+\frac{5k_2^{\,2}\alpha}{7}+9\kappa_1^{\,2} & ik_2(2(\alpha-2)\kappa_6-3\kappa_1^{\,2}) \\
ik_1(\kappa_1^{\,2}-2(\alpha-2)\kappa_6) & ik_1(\kappa_1^{\,2}-2(\alpha-2)\kappa_6) & k_1^{\,2}\kappa_1^{\,2}+k_2^{\,2}\kappa_1^{\,2}+3\kappa_1^{\,2} & ik_1(\frac{9\kappa_1^{\,2}}{5}-\frac{6(\alpha-2)}{5}\kappa_6) & ik_2(\frac{9\kappa_1^{\,2}}{5}-\frac{6}{5}(\alpha-2)\kappa_6) & \frac{3}{5}k_1^{\,2}\kappa_1^{\,2}+\frac{3}{5}k_2^{\,2}\kappa_1^{\,2}+4\alpha\kappa_6^{\,2}
\end{bmatrix} \quad \text{(A.43)}$$

and

$$\mathbf{I}=\mathbf{M}=\begin{bmatrix}
1 & 0 & 0 & \frac{3}{5} & 0 & 0 \\
0 & 1 & 0 & 0 & \frac{3}{5} & 0 \\
0 & 0 & 1 & 0 & 0 & \frac{1}{3} \\
1 & 0 & 0 & \frac{5}{7} & 0 & 0 \\
0 & 1 & 0 & 0 & \frac{5}{7} & 0 \\
0 & 0 & 1 & 0 & 0 & \frac{3}{5}
\end{bmatrix} \quad \text{(A.44)}$$

APPENDIX B –SAMPLE PLATE LOAD DERIVATION

Extensional Plate Load Example

Consider q_1 more closely. Before normalizing (actually for q it can be shown that $q'=q$, but all of the other loads must be normalized).

$$q_1 = \int_{-h/2}^{h/2} f_1 dz = \int_{-h/2}^{h/2} [-M_{11}\delta'(x_1)\delta(x_2)\delta^{(0)}(z-z_0) - M_{12}\delta(x_1)\delta'(x_2)\delta^{(0)}(z-z_0) - M_{13}\delta^{(1)}(z-z_0)\,\delta(x_1)\delta(x_2)]dz$$
$$= -M_{11}\delta'(x_1)\delta(x_2)\int_{-h/2}^{h/2}(1)\delta^{(0)}(z-z_0)dz - M_{12}\delta(x_1)\delta'(x_2)\int_{-h/2}^{h/2}(1)\delta^{(0)}(z-z_0)dz - M_{13}\delta(x_1)\delta(x_2)\int_{-h/2}^{h/2}(1)\delta^{(1)}(z-z_0)dz$$

where the superscripted primes indicating differentiation have been replaced by the order of differentiation in parentheses. Using the equality for the integral of a function times a derivative of a delta function, we note again that with $f(z)$ being the delta function,

$$f(z)=1$$
$$f(z_0)=f^{(0)}(z_0)=1$$
$$f^{(1)}(z_0)=0$$

then

$$q_1 = \int_{-h/2}^{h/2} f_1 dz = \int_{-h/2}^{h/2} [-M_{11}\delta'(x_1)\delta(x_2)[-1^0(1)] - M_{12}\delta(x_1)\delta'(x_2)[-1^0(1)] + M_{13}\delta(x_1)\delta(x_2)[-1(0)]$$
$$= -M_{11}\delta'(x_1)\delta(x_2) - M_{12}\delta(x_1)\delta'(x_2) + 0$$

As shown in Eq. (3.11) above.

Bending plate load example

consider n_z more closely. Before normalizing, n_z is defined as

$$f_6 = -M_{31}\frac{\partial}{\partial x_1}\delta(\mathbf{x}) - M_{32}\frac{\partial}{\partial x_2}\delta(\mathbf{x}) - M_{33}\frac{\partial}{\partial z}\delta(\mathbf{x})$$

$$n_z = \int_{-h/2}^{h/2} f_6 z^2 dz = \int_{-h/2}^{h/2}[-M_{31}\frac{\partial}{\partial x_1}\delta(\mathbf{x}) - M_{32}\frac{\partial}{\partial x_2}\delta(\mathbf{x}) - M_{33}\frac{\partial}{\partial z}\delta(\mathbf{x})]z^2 dz$$

Where the vector quantity $\delta(\mathbf{x}) = \delta(x_3)\delta(x_2)\delta(z)$. Then using the equality for the integral of a function times a derivative of a delta function we note that

$$f(z)=z^2$$
$$f(z_0)=f^{(0)}(z_0)=z^2$$
$$f^{(1)}(z_0)=2z_0$$

Then n_z can be expressed as:

$$
\begin{aligned}
n_z &= \int_{-h/2}^{h/2} [-M_{31}\delta'(x_1)\delta(x_2)\delta^{(0)}(z-z_0) - M_{32}\delta(x_1)\delta'(x_2)\delta^{(0)}(z-z_0) - M_{33}\delta^{(1)}(z-z_0)\,\delta(x_1)\delta(x_2)]z^2 dz \\
&= -M_{31}\delta'(x_1)\delta(x_2)[(-1)^0(z_0)^2] - M_{32}\delta(x_1)\delta'(x_2)[(-1)^0(z_0)^2] - M_{33}\delta(x_1)\delta(x_2)[(-1)^1(2z_0)] \\
&= -M_{31}\delta'(x_1)\delta(x_2)z_0^{\,2} - M_{32}\delta(x_1)\delta'(x_2)z_0^{\,2} + 2M_{33}\delta(x_1)\delta(x_2)z_0
\end{aligned}
$$

Above, the superscripted primes and the superscripted numbers in parentheses indicate differentiation, with the numbers in parentheses being the order of differentiation. The result is identical to the last equation in Eqs. (3.12).

APPENDIX C – PLATE LOAD NORMALIZATION EXAMPLE

Looking at *m* for example from Eq. (3.11) note that, from Appendix A, Eq. (A.25), that

$$m'_{\alpha} = \frac{m}{G\frac{2}{3}l}, \quad z'_0 = \frac{z_0}{l}, \quad x' = \frac{x}{l}, \quad \delta'(x_1) = \delta(x_1)l, \quad \delta'^{(1)}(x_1) = \delta^{(1)}(x_1)l^2$$

Here the primes indicate the normalized variable, not a derivative. The superscripted brackets with delta, i.e., $\delta^{(1)}$ indicate the first derivative of the delta function. A more complete list of normalization parameters is contained in Appendix A. Solving the above for the unprimed variables and subbing them into the third of (Eqs. 3.11) yields

$$m'G\frac{2l}{3} = -M_{31}z'_0 l\frac{1}{l^2}\delta'^{((1)}(x_1)\frac{1}{l}\delta'(x_2) - M_{32}z'_0 l\frac{1}{l}\delta'(x_1)\frac{1}{l^2}\delta'^{(1)}(x_2) + M_{33}\frac{1}{l}\delta(x_1)\frac{1}{l}\delta(x_2)$$

After collecting terms the above becomes

$$m' = -3\frac{M_{31}}{2Gl^3}z'_0\delta'^{((1)}(x_1)\delta'(x_2) + -3\frac{M_{32}}{2Gl^3}z'_0\delta'(x_1)\delta'^{(1)}(x_2) + 3M_{33}\delta'(x_1)\delta'(x_2)$$

Now we will define the normalized moment tensor component $M'_{ij} = \frac{M_{ij}}{2Gl^3}$

Leaving the normalized equation, after dropping the primes for convenience,

$m = -3M_{31}z_0\delta'(x_1)\delta(x_2) - 3M_{32}z_0\delta(x_1)\delta'(x_2) + 3M_{33}\delta(x_1)\delta(x_2)$ which becomes

The third of Eqs.(3.13) .

APPENDIX D – EXAMPLE CALCULATION OF MOMENT TENSOR FOR VERTICAL TENSILE CRACK

Computation of the moment tensor will be demonstrated for the vertical tensile crack case.

Recalling, $M_{ij} = [\lambda n_k \nu_k \delta_{ij} + G(n_i \nu_j + n_j \nu_i)]\Delta u \, \Delta\Sigma$ and defining the vectors in Fig. 2.3 and above for this load case, $n_k = [1,0,0]^T$, $\Delta u = [1,0,0]$, $\nu_k = [1,0,0]^T$ lead to

$$M_{ij} = M_{11} = \lambda[n_1\nu_1 + n_2\nu_2 + n_3\nu_3]\delta_{11} + G[n_1\nu_1 + n_1\nu_1]\Delta u$$
$$= (\lambda[1\cdot 1 + 0 + 0]\cdot 1 + G[1\cdot 1 + 1\cdot 1])\Delta u = (\lambda + 2G)\Delta u$$

In similar fashion it can be shown that

$$M_{22} = [\lambda + (0)G]\Delta u = \lambda\Delta u$$
$$M_{12} = [0 + (0 + 0)G]\Delta u = 0$$
$$M_{21} = M_{12} = 0$$

For the remaining off diagonal terms

$M_{13} = M_{31} = (\lambda[n_1\nu_1 + n_2\nu_2 + n_3\nu_3]\delta_{13} + G[n_1\nu_3 + n_3\nu_1])\Delta u = (\lambda[1 + 0 + 0]\cdot 0 + G[1\cdot 0 + 0\cdot 1])\Delta u = 0$

Finally for the last diagonal term,

$M_{33} = [\lambda + (0)G]\Delta u = \lambda \ \Delta u$

With a unit displacement discontinuity magnitude, the moment tensor for the vertical tensile crack with x_1 discontinuity is

$$\mathbf{Mij} = \begin{bmatrix} \lambda + 2G & 0 & 0 \\ 0 & \lambda & 0 \\ 0 & 0 & \lambda \end{bmatrix}$$

APPENDIX E – TRANSFORMING OF NORMALIZED PLATE FORCES EXAMPLE

Consider the third equation in Eq. (3.13). The plate force component m was used in Appendix C to illustrate the plate force normalization to it will be used as well to illustrate this final step. Applying the Fourier transform to the third of Eqs. (3.13)

$$\tilde{m} = \int_{-\infty}^{\infty} [\int_{-\infty}^{\infty} [-3M_{31}z_0\delta'(x_1)\delta(x_2) - 3M_{32}z_0\delta(x_1)\delta'(x_2) + 3M_{33}\delta(x_1)\delta(x_2)]e^{-ik_1x_1}dx_1]e^{-ik_2x_2}dx_2$$

Starting with the inside integral and using the identity Eq. (5.16)

$$\tilde{m} = \int_{-\infty}^{\infty} [-3M_{31}z_0\delta(x_2)ik_1 - 3M_{32}z_0\delta'(x_2)(1) + 3M_{33}\delta(x_2)(1)]e^{-ik_2x_2}dx_2$$

And now integrating terms that are a function of x_2 the transformed force is

$$\begin{aligned}\tilde{m} &= -3M_{31}z_0\delta(x_2)ik_1(1) - 3M_{32}z_0ik_2(1) + 3M_{33}(1) \\ &= -i3k_1M_{31}z_0 - -i3k_2M_{32}z_0 + 3M_{33}\end{aligned}$$

This is the third of Eqs. (5.13). The other four extensional normalized plate forces are transformed in similar manner.

APPENDIX F - SHAPE CORRECTION FACTORS

Extensional wave

Defining the characteristic determinant of the system using the isotropic form of the extensional constitutive matrix, since the modes are not a function of orientation in an isotropic material,

$$\begin{bmatrix} k^2-\lambda & 0 & -ik(\alpha\kappa_3-2) & \frac{1}{3}(k^2\alpha-\lambda) & 0 \\ 0 & k^2-\lambda & 0 & 0 & \frac{1}{3}(k^2-\lambda) \\ 3ik(\alpha-2)\kappa_3 & 0 & 3\alpha\kappa_3{}^2+k^2\kappa_4{}^2-\lambda & ik((\alpha-2)\kappa_3-2\kappa_4{}^2) & 0 \\ \frac{5}{3}(k^2\alpha-\lambda) & 0 & -\frac{5}{3}ik((\alpha-2)\kappa_3-2\kappa_4{}^2) & \alpha k^2+\frac{20}{3}\kappa_4{}^2-\lambda & 0 \\ 0 & \frac{5}{3}(k^2-\lambda) & 0 & 0 & k^2+\frac{20}{3}\kappa_4{}^2-\lambda \end{bmatrix}$$

Now, letting k=o which is the value corresponding to the cutoff value of omega, ω_c

Now, setting the non trivial equations equal to the cutoff frequencies from the elasticity formulation for the corresponding modes as shown in Ref. (40) and Fig. 4.7;

Cutoff frequency for extensional modes SH0 and S0
$\{c_1 = (\pi/2)\sqrt{\alpha}, c_2 = \pi\}$

$$\begin{bmatrix} \lambda & 0 & 0 & -\frac{\lambda}{3} & 0 \\ 0 & -\lambda & 0 & 0 & \frac{-\lambda}{3} \\ 0 & 0 & 3\alpha\kappa_3{}^2-\lambda & 0 & 0 \\ -\frac{5}{3}\lambda & 0 & 0 & \frac{20}{3}\kappa_4{}^2-\lambda & 0 \\ 0 & -\frac{5}{3}\lambda & 0 & 0 & \frac{20}{3}\kappa_4{}^2-\lambda \end{bmatrix}$$

Gives the equations,

$$3\alpha\kappa_3^{\,2} = c_1^{\,2}$$
$$15\kappa_4^{\,2} = c_2^{\,2}$$

They yield the correction factors

$$\kappa_3 = \frac{\pi}{\sqrt{12}} \qquad \kappa_4 = \frac{\pi}{\sqrt{15}}$$

Which are identical to those used my Mindlin and Medick [30].

Flexural wave

Defining the characteristic determinant of the system using the isotropic form of the bending constitutive matrix, since the modes are not a function of orientation in an isotropic material;

$$\begin{bmatrix}
\alpha k^2 + 3\kappa_1^{\,2} - \lambda & 0 & -3ik\kappa_1^{\,2} & \frac{3}{5}(\alpha k^2 + 5\kappa_1^{\,2} - \lambda) & 0 & ik(2(\alpha-2)\kappa_6 - \kappa_1^{\,2}) \\
0 & k^2 + 3\kappa_1^{\,2} - \lambda & 0 & 0 & \frac{3}{5}(k^2 + 5\kappa_1^{\,2} - \lambda) & 0 \\
ik\kappa_1^{\,2} & 0 & k^2\kappa_1^{\,2} - \lambda & ik\kappa_1^{\,2} & 0 & \frac{1}{3}(k\kappa_1^{\,2} - \lambda) \\
\alpha k^2 + 5\kappa_1^{\,2} - \lambda & 0 & -5ik\kappa_1^{\,2} & 9\kappa_1^{\,2} + \frac{5}{7}(k^2\alpha - \lambda) & 0 & ik(2(\alpha-2)\kappa_6 - 3\kappa_1^{\,2}) \\
0 & k^2 + 5\kappa_1^{\,2} - \lambda & 0 & 0 & 9\kappa_1^{\,2} + \frac{5}{7}(k^2 - \lambda) & 0 \\
ik(\kappa_1^{\,2} - 2(\alpha-2)\kappa_6) & 0 & k^2\kappa_1^{\,2} - \lambda & \frac{3}{5}ik(3\kappa_1^{\,2} - 2(\alpha-2)\kappa_6) & 0 & \frac{3}{5}k^2\kappa_1^{\,2} + 4\alpha\kappa_6^{\,2} - \frac{3}{5}\alpha
\end{bmatrix}$$

Now setting the non trivial equations equal to the cutoff frequencies from the elasticity formulation for the corresponding modes,

$$\begin{bmatrix}
3\kappa_1^{\,2} - \lambda & 0 & 0 & 3\kappa_1^{\,2} - \frac{3}{5}\lambda & 0 & 0 \\
0 & 3\kappa_1^{\,2} - \lambda & 0 & 0 & 3\kappa_1^{\,2} - \frac{3}{5}\lambda & 0 \\
0 & 0 & -\lambda & 0 & 0 & -\frac{\lambda}{3} \\
5\kappa_1^{\,2} - \lambda & 0 & 0 & 9\kappa_1^{\,2} - \frac{5}{7}\lambda & 0 & 0 \\
0 & 5\kappa_1^{\,2} - \lambda & 0 & 0 & 9\kappa_1^{\,2} - \frac{5}{7}\lambda & 0 \\
0 & 0 & -\lambda & 0 & 0 & 4\alpha\kappa_6^{\,2} - \frac{3}{5}\alpha
\end{bmatrix}$$

Gives the equations

$$\{\{\lambda \to 0\}, \{\lambda \to -\frac{1}{2}(\sqrt{1605} - 45)\kappa_1^2\}, \{\lambda \to -\frac{1}{2}(\sqrt{1605} - 45)\kappa_1^2\},$$
$$\{\lambda \to \frac{1}{2}(45 - \sqrt{1605})\kappa_1^2\}, \{\lambda \to \frac{1}{2}(45 + \sqrt{1605})\kappa_1^2\}, \{\lambda \to 15\alpha\kappa_6^2\}$$

Using the cutoff frequencies for bending modes **A_1** and **A_2**

$$\{c_1 = \pi\sqrt{\alpha}, c_2 = \pi / 2\}$$

in

$$c_2^2 = \frac{1}{2}(45 + \sqrt{1605})\kappa_1^2$$

and

$$c_1^2 = 15\kappa_6^2\alpha$$

yields the shape correction factors

$$\kappa_1 = \frac{\pi}{\sqrt{90 + 2\sqrt{1605}}}$$
$$\kappa_6 = \frac{\pi}{\sqrt{15}}$$

APPENDIX G – STRAINS FROM DISPLACEMENTS FORMULATION

Extensional Surface Strain

For an isotropic material strain gages are likely to be located on the surface. Piezoelectric gages measure the total strain $\varepsilon_{kk} = \varepsilon_{11} + \varepsilon_{22}$ where $\varepsilon_{11}=d\mathbf{u}/dx_1$ and $\varepsilon_{22}=d\mathbf{v}/dx_2$. It is important to note that **u** and **v** are functions of the transverse variable z and involve multiple degrees of freedon as per the displacement field equations, Eq. (A.1). Selecting only the terms required to define ε_{11} and ε_{22} associated with extensional motion leaves:

$$\begin{aligned}\mathbf{u}_1(\mathbf{x},z,t) &= u(\mathbf{x},t) + z^2\varphi_1(\mathbf{x},t)\\ \mathbf{u}_2(\mathbf{x},z,t) &= v(\mathbf{x},t) + z^2\varphi_2(\mathbf{x},t)\end{aligned} \tag{G.1}$$

Looking at the individual degrees of freedom above contributing to the displacements from which ε_{kk} is defined , prior to the conversion to polar coordinates, starting with Eq. (5.29):

$$\mathbf{u}_1(\mathbf{x},z,t) = \frac{-i}{4\pi^2}\sum_{m=1}^{5}\int_{-\infty}^{\infty}\Big(\sum_{i=1}^{5}[\mathbf{Q}_m^{1i} + z^2\mathbf{Q}_m^{3i}]\{F_i\}\Big)\frac{H_m}{D'_m}\exp(i\mathbf{k}\cdot\mathbf{x})d\mathbf{k}$$

(G.2)

$$\mathbf{u}_2(\mathbf{x},z,t) = \frac{-i}{4\pi^2}\sum_{m=1}^{5}\int_{-\infty}^{\infty}\Big(\sum_{i=1}^{5}[\mathbf{Q}_m^{2i} + z^2\mathbf{Q}_m^{4i}]\{F_i\}\Big)\frac{H_m}{D'_m}\exp(i\mathbf{k}\cdot\mathbf{x})d\mathbf{k}$$

(G.3)

Recognizing that the Q^{ij} components from (Eq. 5.29) not present above are considered zero above, only the F_i terms that multiply the components of Q^{ij} that are present produce a nonzero contribution.

Combining the **u** and **v** displacement components and differentiating according to the strain definition, and expanding the dot products in the exponential superscript, and the integration variable **k**:

$$\varepsilon_{kk} = \frac{-\boldsymbol{i}}{4\pi^2}\sum_{\boldsymbol{m}=1}^{5}\int_{-\infty}^{\infty}\left(\begin{aligned}&\frac{\boldsymbol{du}_1}{\boldsymbol{dx}_1}\left\{\sum_{\boldsymbol{i}=1}^{5}[\mathbf{Q}_{\boldsymbol{m}}^{1\boldsymbol{i}} + \boldsymbol{z}^2\mathbf{Q}_{\boldsymbol{m}}^{3\boldsymbol{i}}]\{\boldsymbol{F}_{\boldsymbol{i}}\}\frac{\boldsymbol{H}_{\boldsymbol{m}}}{\boldsymbol{D}'_{\boldsymbol{m}}}\exp(\boldsymbol{i}[\boldsymbol{k}_1\boldsymbol{x}_1 + \boldsymbol{k}_2\boldsymbol{x}_2])\right\}\\ &+\frac{\boldsymbol{du}_2}{\boldsymbol{dx}_2}\left\{\sum_{\boldsymbol{i}=1}^{5}[\mathbf{Q}_{\boldsymbol{m}}^{2\boldsymbol{i}} + \boldsymbol{z}^2\mathbf{Q}_{\boldsymbol{m}}^{4\boldsymbol{i}}]\{\boldsymbol{F}_{\boldsymbol{i}}\}\right\}\frac{\boldsymbol{H}_{\boldsymbol{m}}}{\boldsymbol{D}'_{\boldsymbol{m}}}\exp(\boldsymbol{i}[\boldsymbol{k}_1\boldsymbol{x}_1 + \boldsymbol{k}_2\boldsymbol{x}_2])\end{aligned}\right)\boldsymbol{dk}_1\boldsymbol{k}_2 \tag{G.4}$$

Observing that only the exponential terms are function of the differentiation variables x_1 and x_2, the expression becomes

$$\varepsilon_{kk} = \frac{-\boldsymbol{i}(\boldsymbol{i})}{4\pi^2}\sum_{\boldsymbol{m}=1}^{5}\int_{-\infty}^{\infty}\sum_{\boldsymbol{i}=1}^{5}\left\{k_1[\mathbf{Q}_{\boldsymbol{m}}^{1\boldsymbol{i}}+\boldsymbol{z}^2\mathbf{Q}_{\boldsymbol{m}}^{3\boldsymbol{i}}]+k_2[\mathbf{Q}_{\boldsymbol{m}}^{2\boldsymbol{i}}+\boldsymbol{z}^2\mathbf{Q}_{\boldsymbol{m}}^{4\boldsymbol{i}}]\{\boldsymbol{F}_{\boldsymbol{i}}\}\right\}\frac{\boldsymbol{H}_{\boldsymbol{m}}}{\boldsymbol{D}'_{\boldsymbol{m}}}\exp(\boldsymbol{i}[\boldsymbol{k}\boldsymbol{x}])\boldsymbol{dk} \qquad \text{(G.6)}$$

Expanding the terms of the inner summation the extensional surface strain becomes

$$\varepsilon_{kk} = \frac{1}{4\pi^2}\sum_{\boldsymbol{m}=1}^{5}\int_{-\infty}^{\infty}\begin{Bmatrix} k_1[\mathbf{Q}_{\boldsymbol{m}}^{11}\boldsymbol{F}_1+\mathbf{Q}_{\boldsymbol{m}}^{12}\boldsymbol{F}_2+\mathbf{Q}_{\boldsymbol{m}}^{13}\boldsymbol{F}_3+\mathbf{Q}_{\boldsymbol{m}}^{14}\boldsymbol{F}_4+\mathbf{Q}_{\boldsymbol{m}}^{15}\boldsymbol{F}_5] \\ +k_1\boldsymbol{z}^2[\mathbf{Q}_{\boldsymbol{m}}^{31}\boldsymbol{F}_1+\mathbf{Q}_{\boldsymbol{m}}^{32}\boldsymbol{F}_2+\mathbf{Q}_{\boldsymbol{m}}^{33}\boldsymbol{F}_3+\mathbf{Q}_{\boldsymbol{m}}^{34}\boldsymbol{F}_4+\mathbf{Q}_{\boldsymbol{m}}^{35}\boldsymbol{F}_5]+ \\ k_2[\mathbf{Q}_{\boldsymbol{m}}^{21}\boldsymbol{F}_1+\mathbf{Q}_{\boldsymbol{m}}^{22}\boldsymbol{F}_2+\mathbf{Q}_{\boldsymbol{m}}^{23}\boldsymbol{F}_3+\mathbf{Q}_{\boldsymbol{m}}^{24}\boldsymbol{F}_4+\mathbf{Q}_{\boldsymbol{m}}^{25}\boldsymbol{F}_5] \\ +k_2\boldsymbol{z}^2[\mathbf{Q}_{\boldsymbol{m}}^{41}\boldsymbol{F}_1+\mathbf{Q}^{42}\boldsymbol{F}_2+\mathbf{Q}_{\boldsymbol{m}}^{43}\boldsymbol{F}_3+\mathbf{Q}_{\boldsymbol{m}}^{44}\boldsymbol{F}_4+\mathbf{Q}_{\boldsymbol{m}}^{45}\boldsymbol{F}_5] \end{Bmatrix}\frac{\boldsymbol{H}_{\boldsymbol{m}}}{\boldsymbol{D}'_{\boldsymbol{m}}}\exp(\boldsymbol{i}[\boldsymbol{k}\boldsymbol{x}])\boldsymbol{dk} \qquad \text{(G.7)}$$

With length scale l=h/2 or h=2l then the z coordinate, when normalized, becomes z'=z/l=z/(h/2) so at the surface with z_0=h/2 the normalized value becomes z'(h/2)=(h/2)/(h/2)=1. Therefore it is not necessary to carry the z^2 terms, which are unity, in the extensional displacement field equations above for surface strains. Of course for strains at other locations, such as z=h/4, the normalized z coordinate would not be 1 and z must remain in the general strain formula.

Eq. (5.32) is the above expression written more compactly by not expanding the inner summation over i. The strain expression can be expressed even more compactly by following the procedure outlined in Section 5.7 where a polar conversion reduces the order of integration to the single variable k with the trigonometric reduction of the products in the strain expression above, when coupled with the introduction of a change of variable similar to that of the displacement formulation. The resulting Bessel function form and coefficients that are a function of the polar output location variable θ are:

$$\varepsilon_{\alpha\alpha_E} = \frac{1}{2\pi}\sum_{m=1}^{5}\sum_{n=0}^{5}\int_0^{\infty}\frac{H_m(k,t)}{D'_m(k)}E_{mn}(k,\theta)J_n(kr)kdk \qquad \text{(G.8)}$$

As in Eq. 5.43, where the E subscript indicates extension and the strain coefficients

$$E_{mn} = E_{mnc}(k)\cos n\theta + E_{mns}(k)\sin n\theta \qquad \text{(G.9)}$$

are very lengthy for the third order theory and are calculated symbolically by MATHEMATICA.

Flexural Surface Strains

Following the same procedure using the bending terms from the displacements field equations:

$$\mathbf{u_1}(\mathbf{x},z,t) = z\psi_1(\mathbf{x},t) + z^3\chi_1(\mathbf{x},t)$$
$$\mathbf{u_2}(\mathbf{x},z,t) = z\psi_2(\mathbf{x},t) + z^3\chi_2(\mathbf{x},t) \qquad \text{(G.10)}$$

The expression for bending strain after differentiation is

$$\varepsilon_{\mathrm{kk}} = \frac{1}{4\pi^2}\sum_{\boldsymbol{m}=1}^{6}\int_{-\infty}^{\infty}\sum_{\boldsymbol{i}=1}^{5}\left\{\mathrm{k}_1[\boldsymbol{z}\mathbf{Q}_{\boldsymbol{m}}^{1\boldsymbol{i}} + \boldsymbol{z}^3\mathbf{Q}_{\boldsymbol{m}}^{4\boldsymbol{i}}] + \mathrm{k}_2[\boldsymbol{z}\mathbf{Q}_{\boldsymbol{m}}^{2\boldsymbol{i}} + \boldsymbol{z}^3\mathbf{Q}_{\boldsymbol{m}}^{5\boldsymbol{i}}]\{\boldsymbol{F}_{\boldsymbol{i}}\}\right\}\frac{\boldsymbol{H}_{\boldsymbol{m}}}{\boldsymbol{D}'_{\boldsymbol{m}}}\exp(\boldsymbol{i}[\boldsymbol{k}\boldsymbol{x}])\boldsymbol{dk} \qquad \text{(G.11)}$$

Where the degrees of freedom in the first of each superscript pair above are those corresponding to the flexural degrees of freedom that contribute to **u** and **v** which are those degrees of freedom multiplying odd powers of z shown in Eq. (G.10) above, excerpted from the total displacement field equations in Eq. (A.1), namely, degrees of freedom $\psi_{1,}\psi_{2,}\chi_1,\chi$. The expanded expression analogous to the extensional formulation becomes:

$$\varepsilon_{\mathrm{kk}} = \frac{1}{4\pi^2}\sum_{\boldsymbol{m}=1}^{6}\int_{-\infty}^{\infty}\left\{\begin{array}{l}\mathrm{k}_1\boldsymbol{z}[\mathbf{Q}_{\boldsymbol{m}}^{11}\boldsymbol{F}_1 + \mathbf{Q}_{\boldsymbol{m}}^{12}\boldsymbol{F}_2 + \mathbf{Q}_{\boldsymbol{m}}^{13}\boldsymbol{F}_3 + \mathbf{Q}_{\boldsymbol{m}}^{14}\boldsymbol{F}_4 + \mathbf{Q}_{\boldsymbol{m}}^{15}\boldsymbol{F}_5 + \mathbf{Q}_{\boldsymbol{m}}^{16}\boldsymbol{F}_6] \\ +\mathrm{k}_1\boldsymbol{z}^3[\mathbf{Q}_{\boldsymbol{m}}^{41}\boldsymbol{F}_1 + \mathbf{Q}_{\boldsymbol{m}}^{42}\boldsymbol{F}_2 + \mathbf{Q}_{\boldsymbol{m}}^{43}\boldsymbol{F}_3 + \mathbf{Q}_{\boldsymbol{m}}^{44}\boldsymbol{F}_4 + \mathbf{Q}_{\boldsymbol{m}}^{45}\boldsymbol{F}_5 + \mathbf{Q}_{\boldsymbol{m}}^{46}\boldsymbol{F}_6] + \\ \mathrm{k}_2\boldsymbol{z}[\mathbf{Q}_{\boldsymbol{m}}^{21}\boldsymbol{F}_1 + \mathbf{Q}_{\boldsymbol{m}}^{22}\boldsymbol{F}_2 + \mathbf{Q}_{\boldsymbol{m}}^{23}\boldsymbol{F}_3 + \mathbf{Q}_{\boldsymbol{m}}^{24}\boldsymbol{F}_4 + \mathbf{Q}_{\boldsymbol{m}}^{25}\boldsymbol{F}_5 + \mathbf{Q}_{\boldsymbol{m}}^{26}\boldsymbol{F}6] \\ +\mathrm{k}_2\boldsymbol{z}^3[\mathbf{Q}_{\boldsymbol{m}}^{51}\boldsymbol{F}_1 + \mathbf{Q}^{52}\boldsymbol{F}_2 + \mathbf{Q}_{\boldsymbol{m}}^{53}\boldsymbol{F}_3 + \mathbf{Q}_{\boldsymbol{m}}^{54}\boldsymbol{F}_4 + \mathbf{Q}_{\boldsymbol{m}}^{55}\boldsymbol{F}_5 + \mathbf{Q}_{\boldsymbol{m}}^{56}\boldsymbol{F}_6]\end{array}\right\}\frac{\boldsymbol{H}_{\boldsymbol{m}}}{\boldsymbol{D}'_{\boldsymbol{m}}}\exp(\boldsymbol{i}[\boldsymbol{k}\boldsymbol{x}])\boldsymbol{dk} \qquad \text{(G.12)}$$

Eq. (5.33) is the above expression written more compactly by not expanding the inner summation over i. The strain expression can be expressed even more compactly as in the case of extension with the reduction of integration order of Section 5.7. The result is

$$\varepsilon_{\alpha\alpha_B} = \frac{1}{2\pi}\sum_{m=1}^{6}\sum_{n=0}^{5}\int_0^{\infty}\frac{H_m(k,t)}{D'(k)}E_{mn}(k,\theta)J_n(kr)kdk \qquad \text{(G.13)}$$

which is Eq. 5.46.

APPENDIX H-HEAVYSIDE TEMPORAL LOADING

The Heavyside loading function represents an instantly applied force with no rise time that is applied constantly throughout the loading history. It as a mathematical construct as almost all forces have some ramp up time even if very short. It is a useful mathematical representation that tends to excite virtually all of the frequencis of a structure.

Recall the total loading $\mathbf{f}(\mathbf{x},t)=M_{ij}^{0} f(t)$ where the spatial part M_{ij}^{0} was defined in Eqs. (2.9) and (2.10) and further developed in Section 3.4. Mij^{0} is the moment tensor and contributes to the equivalent body forces Eqs. (2.6b) and (2.6b) and the to the dimensionless equivalent plate loads eqs. (3.13) and (3.14) for extension and flexure respectively. This contribution is already in the formulation through the plate loads and it is the temporal portion that is of concern here.

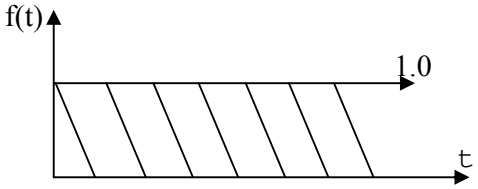

For the unit Heavyside loading shown above f(t)=1 and its Laplace transform $\overline{f}=\frac{1}{s}$

Looking at Eq. (5.8) for extension,

$$\overline{\overline{\tilde{\boldsymbol{V}}}}=\sum_{m=1}^{5}\left[\frac{Q_m^{ij}}{D_m'}\frac{1}{(s^2-s_m^2)}\right]_{5x5}\overline{\overline{\mathbf{f}}}_E$$

noting that the Laplace transform of $\overline{\overline{\mathbf{f}}}_E(\mathbf{k},t)$ which applies to the temporal portion t, for the Heavyside loading, is simply 1/s, then the inverse Laplace transform is given by the convolution theorem.

From Eq. (5.8) recogniozing the form

$$L^{-1}\left\{\frac{1}{s^2-\omega_m{}^2}\cdot\frac{1}{s}\right\}=\int_0^t\frac{\sin\omega_m(t-\xi)}{\omega_m}*f(\xi)d\xi \qquad \text{(H.1)}$$

Examining the portion of Eq. (5.9) for extension, (or Eq. (5.23) for flexure), that comes from the inverse Laplace transform of Eq. (5.28), it remains to evaluate the resulting convolution integral for the Heavyside loading.

$$\frac{\sin(\omega_m t) * \tilde{\mathbf{f}}_E(\mathbf{k},t)}{\omega_m} \tag{H.2}$$

Which by definition is:

$$\sin(\omega_m t) * \tilde{\mathbf{f}}_B(\mathbf{k}.t) = \int_0^t \tilde{\mathbf{f}}_B(\mathbf{k},\xi)\sin\omega_m(t-\xi)d\xi \tag{H.3}$$

But, as can be seen from Eq. (5.11) for extension (or Eq. (5.25) for bending), with Eq. (5.11) repeated here for convenience,

$$\begin{aligned}\tilde{\mathbf{V}}(\mathbf{k},t) &= \sum_{m=1}^{5}\frac{[Q_m^{ij}]_{5x5}}{D'_m}\frac{\sin(\omega_m t) * \tilde{\mathbf{f}}_E(\mathbf{k},t)}{\omega_m} \\ &= \sum_{m=1}^{3}[\,\mathbf{Q}_m^1\,\tilde{q}_1 + \mathbf{Q}_m^2\,\tilde{q}_2 + \mathbf{Q}_m^3\,\tilde{m} + \mathbf{Q}_m^4\,\tilde{n}_1 + \mathbf{Q}_m^5\,\tilde{n}_2\,] * \frac{\sin(\omega_m t)}{D'_m\omega_m}\end{aligned} \tag{H.4}$$

the transformed spatial portion of $\mathbf{f}_E$ or $\mathbf{f}_B$ multiplies the **Q** matrix, leaving only the temporal portion of **f** in the convolution so what remains is,

$$f(t) * \frac{\sin(\omega_m t)}{\omega_m} = \frac{1}{\omega_m}\int_0^t f(\xi) * \sin\omega_m(t-\xi)d\xi \tag{H.5}$$

This can be evaluated by introducing a change in variable, T= t-ξ and consequently dξ=-dT. Then, calling the result $H_m(\mathbf{k},t)$, since the wave number **k** is still present in the roots, the temporal portion of the force is given by,

$$\begin{aligned}H_m(\mathbf{k},t) &= -\frac{1}{\omega_m}\int_0^t \sin\omega_m T dT = \frac{1}{\omega_m^{\,2}}\cos\omega_m\Big|_0^t \\ &= \frac{1}{\omega_m^{\,2}}(1-\cos\omega_m t) \\ &= \frac{1}{\omega_m^{\,2}} - \frac{\cos\omega_m t}{\omega_m^{\,2}}\end{aligned} \tag{H.6}$$

Where the first term represents the stead state load and the second term represents the more dominant transient portion of the temporal loading.

APPENDIX I – SUMMARY OF MINDLIN (FIRST ORDER) KEY EQUATIONS

Displacement Field

$$u_1(\mathbf{x},z,t) = u(\mathbf{x},t) + z\psi_1(\mathbf{x},t)$$
$$u_2(\mathbf{x},z,t) = v(\mathbf{x},t) + z\psi_2(\mathbf{x},t)$$
$$u_3(\mathbf{x},z,t) = w(\mathbf{x},t) + z\psi(\mathbf{x},t)$$

Extensional Degrees of freedom

$u,\ v,\ \psi$

Flexural Degrees of Freedom

$w,\ \psi_1,\ \psi_2$

Plate Equations of Motion - Extension

$$N_{11,1} + N_{12,2} + q_1 = \rho I_0 \ddot{u}$$
$$N_{12,1} + N_{22,2} + q_2 = \rho I_0 \ddot{v}$$
$$R_{1,1} + R_{2,2} - N_{33} + m = \rho I_2 \ddot{\psi}$$

Plate Resultants Definitions – Extension and Flexure

$$\begin{Bmatrix} N_{\alpha\beta} \\ M_{\alpha\beta} \\ S_{\alpha\beta} \end{Bmatrix} = \int_{-h/2}^{h/2} \sigma_{\alpha\beta} \begin{Bmatrix} 1 \\ z \\ z^2/2 \end{Bmatrix} dz, \quad \begin{Bmatrix} Q_\alpha \\ R_\alpha \end{Bmatrix} = \int_{-h/2}^{h/2} \sigma_{\alpha 3} \begin{Bmatrix} 1 \\ z \end{Bmatrix} dz, \quad N_3 = \int_{-h/2}^{h/2} \sigma_{33} dz$$

Plate Forces - Extensional

$$q_1 = -M_{11}\delta'(x_1)\delta(x_2) - M_{12}\delta(x_1)\delta'(x_2) + M_{13} \times 0$$
$$q_2 = -M_{21}\delta'(x_1)\delta(x_2) - M_{22}\delta(x_1)\delta'(x_2) + M_{23} \times 0$$
$$m = -M_{31}z_0\delta'(x_1)\delta(x_2) - M_{32}z_0\delta(x_1)\delta'(x_2) + M_{33}\delta(x_1)\delta(x_2)$$

Plate Forces – Extensional – Transformed Dimensionless

$$\tilde{q}_1 = -ik_1 M_{11} \quad - ik_2 M_{12}$$
$$\tilde{q}_2 = -ik_1 M_{21} \quad - ik_2 M_{22}$$
$$\tilde{m} = -i3k_1 M_{31} z_0 - ik_2 3M_{32} z_0 \quad + 3M_{33}$$

Plate Equation of Motion - Flexure

$$M_{xx,x} + M_{xy,y} - Q_x + m_1 = I_2 \ddot{\psi}_1$$
$$M_{xy,x} + M_{yy,y} - Q_y + m_2 = I_2 \ddot{\psi}_2$$
$$Q_{x,x} + Q_{y,y} + q = \rho I_0 \ddot{w}$$

Plate Forces – Flexural

$$m_1 = -M_{11} z_0 \delta'(x_1)\delta(x_2) - M_{12} z_0 \delta(x_1)\delta'(x_2) + M_{13}\delta(x_1)\delta(x_2)$$
$$m_2 = -M_{21} z_0 \delta'(x_1)\delta(x_2) - M_{22} z_0 \delta(x_1)\delta'(x_2) + M_{23}\delta(x_1)\delta(x_2)$$
$$q \quad = -M_{31}\delta'(x_1)\delta(x_2) \quad - M_{32}\delta(x_1)\delta'(x_2) \quad + M_{33} \times 0$$

Plate Forces – Flexural – Transformed Dimensional

$$\tilde{m}_1 = -i3k_1 M_{11} z_0 - i3k_2 M_{12} z_0 + 3M_{13}$$
$$\tilde{m}_2 = -i3k_1 M_{21} z_0 - i3k_2 M_{22} z_0 + 3M_{23}$$
$$\tilde{q} \quad = -ik_1 M_{31} \quad - ik_2 M_{32}$$

Constitutive Equations – Extension

$$\tilde{\mathbf{T}} = \begin{bmatrix} \alpha k_1^2 + k_2^2 & (\alpha - 1)k_1 k_2 & -ip(\alpha - 2)k_1 \\ (\alpha - 1)k_1 k_2 & k_1^2 + \alpha k_2^2 & -ip(\alpha - 2)k_2 \\ i3p(\alpha - 2)k_1 & i3p(\alpha - 2)k_2 & k_1^2 + k_2^2 + 3p^2\alpha \end{bmatrix}$$

$$\mathbf{I} = \begin{bmatrix} 1 & 0 & 0 \\ 0 & 1 & 0 \\ 0 & 0 & 1 \end{bmatrix}$$

Constitutive Equations – Flexural

$$\mathbf{A} = \begin{bmatrix} \alpha k_1^2 + k_2^2 + 3\kappa & (\alpha - 1)k_1 k_2 & i3\kappa k_1 \\ (\alpha - 1)k_1 k_2 & k_1^2 + \alpha k_2^2 + 3\kappa & i3\kappa i k_2 \\ -i\kappa k_1 & -i\kappa k_2 & \kappa(k_1^2 + k_2^2) \end{bmatrix}$$

$$\mathbf{I} = \begin{bmatrix} 1 & 0 & 0 \\ 0 & 1 & 0 \\ 0 & 0 & 1 \end{bmatrix}$$

Transient Displacement Solution – Extension

$$\mathbf{V} = \frac{-i}{4\pi^2} \sum_{m=1}^{3} \int_{-\infty}^{\infty} [F_1 \mathbf{Q}_m^1 + F_2 \mathbf{Q}_m^2 + 3(z_0 F_3 + iM_{33}^0)\mathbf{Q}_m^3] \frac{H_m}{D_m'} \exp(i\mathbf{k} \cdot \mathbf{x}) d\mathbf{k}$$

Transient Displacement Solution – Extension

$$\mathbf{U} = \frac{-i}{4\pi^2} \sum_{m=1}^{3} \int_{-\infty}^{\infty} [3z_0(F_1 + iM_{13}^0)\mathbf{Q}_m^1 + 3z_0(F_2 + iM_{23}^0)\mathbf{Q}_m^2 + F_3 \mathbf{Q}_m^3] \frac{H_m}{D_m'} \exp(i\mathbf{k} \cdot \mathbf{x}) d\mathbf{k}$$

Transient Strain Solution – Extension

$$\varepsilon_{kk} = \frac{1}{4\pi^2} \sum_{m=1}^{3} \int_{-\infty}^{\infty} [(k_1 Q_m^{11} + k_2 Q_m^{21})F_1 + (k_1 Q_m^{12} + k_2 Q_m^{22})F_2 + 3(k_1 Q_m^{13} + k_2 Q_m^{23})(z_0 F_3 + iM_{33}^0)] \frac{H_m}{D_m'} \exp(i\mathbf{k} \cdot \mathbf{x}) d\mathbf{k}$$

Transient Strain Solution – Extension

$$\varepsilon_{\alpha\alpha} = \frac{1}{4\pi^2} \sum_{m=1}^{3} \int_{-\infty}^{\infty} [3(k_1 Q_m^{11} + k_2 Q_m^{21})(z_0 F_1 + iM_{13}^0) + 3(k_1 Q_m^{12} + k_2 Q_m^{22})(z_0 F_2 + iM_{23}^0) + (k_1 Q_m^{13} + k_2 Q_m^{23})F_3] \frac{H_m}{D_m'} \exp(i\mathbf{k} \cdot \mathbf{x}) d\mathbf{k}$$

Transient Strain Solution – Extension Bessel Representation

$$\begin{Bmatrix} u \\ v \\ \psi \end{Bmatrix} = \frac{1}{2\pi} \sum_{m=1}^{3} \sum_{n=0}^{5} \int_0^{\infty} \frac{H_m(k,t)}{D_m'(k)} \begin{Bmatrix} U_{mn}(k,\theta) \\ V_{mn}(k,\theta) \\ \Psi_{mn}(k,\theta) \end{Bmatrix} J_n(kr)kdk$$

$$\begin{Bmatrix} U_{mn} \\ V_{mn} \\ \Psi_{mn} \end{Bmatrix} = \begin{Bmatrix} U_{mnc}(k) \\ V_{mnc}(k) \\ \Psi_{mnc}(k) \end{Bmatrix} \cos n\theta + \begin{Bmatrix} U_{mns}(k) \\ V_{mns}(k) \\ \Psi_{mns}(k) \end{Bmatrix} \sin n\theta$$

Transient Strain Solution – Extension Bessel- Representation

$$\varepsilon_{kk} = \frac{1}{2\pi} \sum_{m=1}^{3} \sum_{n=0}^{2} \int_0^{\infty} \frac{H_m(k,t)}{D_m'(k)} E_{mn}(k,\theta) J_n(kr)kdk$$

$$E_{mn} \equiv E_{mnc}(k)\cos n\theta + E_{mns}(k)\sin n\theta$$

Transient Displacement Solution – Flexure - Bessel Representation

$$\begin{Bmatrix} \psi_1 \\ \psi_2 \\ w \end{Bmatrix} = \frac{1}{2\pi} \sum_{m=1}^{3} \sum_{n=0}^{5} \int_0^{\infty} \frac{H_m(k,t)}{D'(k)} \begin{Bmatrix} \alpha_{mn}(k,\theta) \\ \beta_{mn}(k,\theta) \\ \gamma_{mn}(k,\theta) \end{Bmatrix} J_n(kr)kdk$$

$$\begin{Bmatrix} \alpha_{mn} \\ \beta_{mn} \\ \gamma_{mn} \end{Bmatrix} = \begin{Bmatrix} \alpha_{mnc}(k) \\ \beta_{mnc}(k) \\ \gamma_{mnc}(k) \end{Bmatrix} \cos n\theta + \begin{Bmatrix} \alpha_{mns}(k) \\ \beta_{mns}(k) \\ \gamma_{mns}(k) \end{Bmatrix} \sin n\theta$$

Transient Strain Solution – Flexure - Bessel Representation

$$\varepsilon_{kk} = \frac{1}{2\pi} \sum_{m=1}^{3} \sum_{n=0}^{2} \int_0^{\infty} \frac{H_m(k,t)}{D'(k)} E_{mn}(k,\theta) J_n(kr)kdk$$

$$E_{mn} \equiv E_{mnc}(k)\cos n\theta + E_{mns}(k)\sin n\theta$$

Explicit Expressions for Strain Coefficients E_{mn}

The total response of the surface strains to the point source is the summation of two parts: one due to extensional motion, and the other due to flexural motion. The two responses can be conveniently expressed as in the form

$$\varepsilon_{\alpha\alpha} = \frac{1}{2\pi}\sum_{m=1}^{3}\sum_{n=0}^{4}\int_0^\infty \frac{H_m(k,t)}{D'_m(k)} E_{mn}(k,\theta) J_n(kr) k dk$$

where

$$E_{mn} = E_{mnc}(k)\cos n\theta + E_{mns}(k)\sin n\theta$$

However, the quantities, $H_m(k,t)$, $D'_m(k)$, $\omega_m(k)$, $E_{mnc}(k)$, $E_{mns}(k)$, are different for each motion. Hence, the expressions for E_{mnc} and E_{mns} are given separately:

Extensional motion

From Eq. (4.22),

$$E_{m0c}/k^2 = \tfrac{1}{2}[M^0_{11}(q_{11}+q_{12}) + M^0_{22}q_{22}] + 3M^0_{33}q_{13}/k$$
$$E_{m1c}/k^2 = -i3z_0M^0_{31}q_{13}, \quad E_{m1s}/k^2 = -i3z_0M^0_{32}q_{13}$$
$$E_{m2c}/k^2 = \tfrac{1}{2}[M^0_{11}(q_{11}+q_{12}) - M^0_{22}q_{22}]$$
$$E_{m2s}/k^2 = \tfrac{1}{2}M^0_{12}(q_{11}+q_{12}+q_{22})$$

with

$$q_{11} = \omega_m^4 - (\alpha k^2 + A_{33})\omega_m^2 + [\alpha A_{33} - 3(a-2)^2 p^2]k^2$$
$$q_{12} = [(\alpha-1)(\omega_m^2 - A_{33}) + 3(\alpha-2)^2 p^2]k^2$$
$$q_{22} = \omega_m^4 - (k^2 + A_{33})\omega_m^2 + A_{33}k^2$$
$$q_{13} = (\alpha-2)(\omega_m^2 - k^2)pk$$
$$A_{33} = k^2 + 3\alpha p^2$$

where $\omega = \omega_m(k)$ is the dispersion relation for the m^{th} extensional mode.

Flexural motion

From Eq. (4.24),

$$E_{m0c}/k^2 = \tfrac{3}{2}z_0[M^0_{11}(q_{11}+q_{12}) + M^0_{22}q_{22}]$$
$$E_{m1c}/k^2 = -iM^0_{13}[q_{13} - \tfrac{3}{k}(q_{11}+q_{12})]$$
$$E_{m1s}/k^2 = -iM^0_{23}(q_{13} - \tfrac{3}{k}q_{22})$$
$$E_{m2c}/k^2 = \tfrac{3}{2}z_0[M^0_{11}(q_{11}+q_{12}) - M^0_{22}q_{22}]$$
$$E_{m2s}/k^2 = \tfrac{3}{2}z_0M^0_{12}(q_{11}+q_{12}+q_{22})$$

with

$$q_{11} = \omega_m^4 - (\alpha k^2 + 3p^2 + p^2k^2)\omega_m^2 + \alpha p^2 k^4$$
$$q_{12} = [(\alpha-1)(\omega_m^2 - p^2k^2) + 3p^4]k^2$$
$$q_{22} = \omega_m^4 - (k^2 + 3p^2 + p^2k^2)\omega_m^2 + (k^2+3p^2)p^2k^2$$
$$q_{13} = 3p^2(k^2 + 3p^2 - \omega_m^2)k$$

Note that in the above formulation the equivalent plate loads for the point source are normalized according to the plate theory, as are the components of the moment tensor.

APPENDIX J - PLANE STRESS FORMULATION

Using the concept of moment tensor (or derived "equivalent" body-forces) in seismology for a point source with displacement discontinuities on the fracture surface in three-dimensional elastodynamics, this paper first presents equivalent loads for the point source and then derives transient wave response to a general acoustic emission (AE) point source with an arbitrary moment tensor in isotropic plates under plane stress condition. The transient response which represents waves propagating from the general AE point source in the plate is expressed in an explicit integral form. It is shown that the transient response which is given by the double inverse Fourier transforms can be simplified into a finite series involving inverse Hankel transforms which is one-dimensional inversion in isotropic plates. Exact solutions of the AE sources have been obtained. Three types of AE sources representing different micro-damages and their corresponding plate loads are discussed. Numerical results for nine of the AE point sources with Heaviside time history are presented.

1 . The equivalent body-forces in the thin plate

In the elastodynamic problem of a thin plate under plane stress condition, the displacement field (u, v) is a function of $\mathbf{x} = (x_1, x_2)$ and t. The equations of motion are written as

$$\begin{aligned} \sigma_{11,1} + \sigma_{12,2} + f_1 &= \rho\ddot{u} \\ \sigma_{21,1} + \sigma_{22,2} + f_2 &= \rho\ddot{v} \end{aligned} \tag{J.1.1}$$

where (σ_{11}, σ_{22}, σ_{12}) are stress components, and (f_1, f_2) are the equivalent body-forces acting at $\boldsymbol{\xi}$ expressed as

$$\begin{aligned} f_1 &= -M_{11}\delta_{,1}(\mathbf{x}-\boldsymbol{\xi}) - M_{12}\delta_{,2}(\mathbf{x}-\boldsymbol{\xi}) \\ f_2 &= -M_{21}\delta_{,1}(\mathbf{x}-\boldsymbol{\xi}) - M_{22}\delta_{,2}(\mathbf{x}-\boldsymbol{\xi}) \end{aligned} \tag{J.1.2}$$

where $\boldsymbol{\xi} = (\xi_1, \xi_2)$.

Without loss of generality it is assumed that the dipoles are applied at the origin (0, 0), the body forces can be conveniently expressed as

$$\begin{aligned} f_1 &= -M_{11}\delta'(x_1)\delta(x_2) - M_{12}\delta(x_1)\delta'(x_2) \\ f_2 &= -M_{21}\delta'(x_1)\delta(x_2) - M_{22}\delta(x_1)\delta'(x_2) \end{aligned} \tag{J.1.3}$$

2. AE waves in thin isotropic plates

The 2-D equations of motion under plane stress can be expressed in terms of displacements as

$$\begin{aligned} \mu(u_{,11} + u_{,22}) + (\lambda+\mu)(u_{,11} + v_{,12}) + f_1 &= \rho\ddot{u} \\ \mu(v_{,11} + v_{,22}) + (\lambda+\mu)(u_{,12} + v_{,22}) + f_2 &= \rho\ddot{v} \end{aligned} \tag{J.2.1}$$

or in a matrix form

$$\begin{bmatrix} \lambda+2\mu & 0 \\ 0 & \mu \end{bmatrix} \frac{\partial^2}{\partial x_1^2} \begin{Bmatrix} u \\ v \end{Bmatrix} + \begin{bmatrix} 0 & \lambda+\mu \\ \lambda+\mu & 0 \end{bmatrix} \frac{\partial^2}{\partial x_1 \partial x_2} \begin{Bmatrix} u \\ v \end{Bmatrix} + \begin{bmatrix} \mu & 0 \\ 0 & \lambda+2\mu \end{bmatrix} \frac{\partial^2}{\partial x_2^2} \begin{Bmatrix} u \\ v \end{Bmatrix} + \begin{Bmatrix} f_1 \\ f_2 \end{Bmatrix} = \rho \begin{Bmatrix} \ddot{u} \\ \ddot{v} \end{Bmatrix} \tag{J.2.2}$$

To make the variables dimensionless, a representative length scale $l = h$ (h is the thickness of the plate) and a typical time scale $\tau_0 = l / c_T$ ($c_T = \sqrt{\mu / \rho}$) is the velocity of bulk transverse or shear vertical waves) are introduced and the following nondimensional variables and quantities are defines by

$$x_i' = x_i / l, \quad t' = t / \tau_0, \quad u' = u / l, \quad v' = v / l, \quad k_i' = k_i l, \quad \omega' = \omega \tau_0, \quad f_i' = f_i l / \mu \text{ (J.2.3)}$$

The nondimensional quantities will be used and the "primes" will be dropped hereafter. The equations of motion Eq. (J.2.2) can be written in nondimensional form together with zero initial conditions:

$$\begin{aligned} &\mathbf{I}\frac{\partial^2 \mathbf{V}}{\partial t^2} + \mathbf{T}_{11}\frac{\partial^2 \mathbf{V}}{\partial x_1^{\,2}} + \mathbf{T}_{12}\frac{\partial^2 \mathbf{V}}{\partial x_1 \partial x_2} + \mathbf{T}_{22}\frac{\partial^2 \mathbf{V}}{\partial x_2^{\,2}} = \mathbf{f}_T, t > 0 \\ &\mathbf{V} = \frac{\partial \mathbf{V}}{\partial t} = 0, \quad at \ t = 0 \end{aligned} \tag{J.2.4}$$

where $\mathbf{V} = [u, v]^T, \mathbf{f} = [f_1, f_2]^T$, and $\mathbf{T}_{11}, \mathbf{T}_{12}$ and $\mathbf{T}_{22}$ are 2×2 constant matrices. The Fourier transformation of Eq. (J.2.4) with respect to x_1 and x_2 yields

$$\begin{aligned} &\ddot{\tilde{\mathbf{V}}} + \mathbf{T}(\mathbf{k})\tilde{\mathbf{V}} = \tilde{\mathbf{f}}, \quad t > 0 \\ &\tilde{\mathbf{V}} = \dot{\tilde{\mathbf{V}}} = \mathbf{0}, \quad \text{at} \quad t = 0 \end{aligned} \tag{J.2.5}$$

where $\mathbf{k} = (k_1, k_2)$,

$$\tilde{\mathbf{V}}(\mathbf{k}, t) = \int_{-\infty}^{\infty} \mathbf{V}(\mathbf{x}, t) \exp(-i\mathbf{k} \cdot \mathbf{x}) d\mathbf{x}, \quad \tilde{\mathbf{f}}(\mathbf{k}, t) = \int_{-\infty}^{\infty} \mathbf{f}(\mathbf{x}, t) \exp(-i\mathbf{k} \cdot \mathbf{x}) d\mathbf{x} \tag{J.2.6}$$

$$\mathbf{T} = \begin{bmatrix} \alpha k_1^2 + k_2^2 & (\alpha - 1) k_1 k_2 \\ (\alpha - 1) k_1 k_2 & k_1^2 + \alpha k_2^2 \end{bmatrix}$$

where $\alpha = (\lambda + 2\mu) / \mu = 2(1 - \nu) / (1 - 2\nu)$, ν is Poisson's ratio, and λ and μ are the Lame constants. The application of Laplace transformation of Eq. (J.2.5) with respect to t leads to

$$(\mathbf{T} + s^2 \mathbf{I})\bar{\tilde{\mathbf{V}}} = \bar{\tilde{\mathbf{f}}} \tag{J.2.7}$$

where

$$\bar{\tilde{\mathbf{V}}}(\mathbf{k}, s) = \int_0^{\infty} \tilde{\mathbf{V}}(\mathbf{k}, t) \exp(-st) dt, \quad \bar{\tilde{\mathbf{f}}}(\mathbf{k}, s) = \int_0^{\infty} \mathbf{f}(\mathbf{k}, s) \exp(-st) dt \tag{J.2.8}$$

The solution of Eq. (J.2.7) can be simply obtained by matrix inversion:

$$\bar{\tilde{\mathbf{V}}} = (\mathbf{T} + s^2 \mathbf{I})^{-1} \bar{\tilde{\mathbf{f}}} = \frac{adj(\mathbf{T} + s^2 \mathbf{I})}{\left|\mathbf{T} + s^2 \mathbf{I}\right|} \bar{\tilde{\mathbf{f}}} = \frac{adj(\mathbf{T} + s^2 \mathbf{I})}{(s^2 - s_1^2)(s^2 - s_2^2)} \bar{\tilde{\mathbf{f}}} \tag{J.2.9}$$

where $s_1^2(\mathbf{k})$ and $s_2^2(\mathbf{k})$ are roots of the equation

$$\left|\mathbf{T} + s^2 \mathbf{I}\right| = 0 \tag{J.2.10}$$

Let $s^2 = -\omega^2$, we have

$$\left|\mathbf{T}(\mathbf{k}) - \omega^2 \mathbf{I}\right| = 0 \tag{J.2.11}$$

which is the dispersion relation of the plate with $\mathbf{k}$ being the wave number vector, and ω the frequency. The roots associated with two wave modes may be expressed in the form

$$\omega^2 \equiv W_1^2(\mathbf{k}) = k^2$$
$$\omega^2 \equiv W_2^2(\mathbf{k}) = \alpha k^2 \tag{J.2.12}$$

The phase velocities of the two non-dispersive wave modes are 1 and $\sqrt{\alpha}$ respectively. Let

$$D(s^2) = \left|\mathbf{T} + s^2\mathbf{I}\right| = (s^2 + k^2)(s^2 + \alpha k^2)$$
$$\mathbf{Q} = [Q^{ij}] = adj(\mathbf{T} + s^2\mathbf{I}) = \begin{bmatrix} s^2 + (k_1^2 + \alpha k_2^2) & -(\alpha - 1)k_1 k_2 \\ -(\alpha - 1)k_1 k_2 & s^2 + (\alpha k_1^2 + k_2^2) \end{bmatrix} \tag{J.2.13}$$

and Eq.(2.9) can be written as

$$\bar{\bar{\mathbf{V}}} = \frac{Q^{ij}(s^2)}{D(s^2)}\bar{\bar{\mathbf{f}}} \tag{J.2.14}$$

where $Q^{ij}(s^2)$ and $D(s^2)$ are polynomials in s^2 and the degree of D is higher than that of Q^{ij}.

To carry out the inverse Laplace transform to Eq. (J.2.14), the method of partial decomposition is employed, which yields

$$\frac{Q^{ij}(s^2)}{D(s^2)} = \sum_{m=1}^{2} \frac{Q_m^{ij}}{D_m'} \frac{1}{(s^2 - s_m^2)} = \frac{Q_1^{ij}}{D_1'} \frac{1}{(s^2 + k^2)} + \frac{Q_2^{ij}}{D_2'} \frac{1}{(s^2 + \alpha k^2)} \tag{J.2.15}$$

where $s_m^2 = -W_m^2(\mathbf{k})$, $Q_m^{ij} = Q^{ij}(s_m^2)$

$$D_m' = D'(s_m^2) = \left.\frac{dD}{d(s^2)}\right|_{s^2 = s_m^2} = \prod_{n=1, n\neq m}^{2} (s_m^2 - s_n^2) = \prod_{n=1, n\neq m}^{2} (W_n^2 - W_m^2)$$

Substituting Eq. (J.2.13) into Eq. (J.2.15), the following equations can be obtained:

$$D_1' = (\alpha - 1)k^2, \quad D_2' = -(\alpha - 1)k^2$$
$$Q_1^{ij} = \begin{bmatrix} (\alpha - 1)k_2^2 & -(\alpha - 1)k_1 k_2 \\ -(\alpha - 1)k_1 k_2 & (\alpha - 1)k_1^2 \end{bmatrix}, \quad Q_1^{ij} = \begin{bmatrix} -(\alpha - 1)k_1^2 & -(\alpha - 1)k_1 k_2 \\ -(\alpha - 1)k_1 k_2 & -(\alpha - 1)k_2^2 \end{bmatrix} \tag{J.2.16}$$

With Eq. (J.2.15), Eq. (J.2.14) becomes

$$\bar{\bar{\mathbf{V}}} = \sum_{m=1}^{2} \left[\frac{Q_m^{ij}}{D_m'} \frac{1}{(s^2 - s_m^2)} \right]_{2\times 2} \bar{\bar{\mathbf{f}}} \tag{J.2.17}$$

Now the inverse Laplace transform is applied to the above equation via the convolution theorem, and

$$\tilde{\mathbf{V}}(\mathbf{k}, t) = \sum_{m=1}^{2} \frac{[Q_m^{ij}]_{2\times 2}}{D_m'} \frac{\sin(W_m t) * \tilde{\mathbf{f}}(\mathbf{k}, t)}{W_m} = \sum_{m=1}^{2} [\mathbf{Q}_m^1 \tilde{f}_1 + \mathbf{Q}_m^2 \tilde{f}_2] * \frac{\sin(W_m t)}{D_m' W_m} \tag{J.2.18}$$

where $*$ denotes convolution with respect to time,

$$\sin(W_m t) * \tilde{\mathbf{f}}(\mathbf{k}, t) = \int_0^t \tilde{\mathbf{f}}(\mathbf{k}, \xi) \sin W_m (t - \tau) d\tau \tag{J.2.19}$$

and $\mathbf{Q}_m^i(\mathbf{k})$ is 2×1 column vector, $\mathbf{Q}_m^i = [Q_m^{1i}, Q_m^{2i}]^T$, i = 1,2; that is

$$\mathbf{Q}_1^1 = \begin{bmatrix} (\alpha-1)k_2^2 \\ -(\alpha-1)k_1k_2 \end{bmatrix}, \quad \mathbf{Q}_1^2 = \begin{bmatrix} -(\alpha-1)k_1k_2 \\ (\alpha-1)k_1^2 \end{bmatrix}$$
$$\mathbf{Q}_2^1 = \begin{bmatrix} -(\alpha-1)k_1^2 \\ -(\alpha-1)k_1k_2 \end{bmatrix}, \quad \mathbf{Q}_2^2 = \begin{bmatrix} -(\alpha-1)k_1k_2 \\ -(\alpha-1)k_2^2 \end{bmatrix} \tag{J.2.20}$$

3. Transient stress wave solution

For the moment tensor at the origin, the Fourier transform of the dimensionless equivalent body-force, $\tilde{\mathbf{f}} = [\tilde{f}_1, \tilde{f}_2]^T$, can be expressed as

$$\tilde{f}_1 = -ik_1M_{11} - ik_2M_{12}$$
$$\tilde{f}_2 = -ik_1M_{21} - ik_2M_{22} \tag{J.3.1}$$

using the following identity:

$$\int_{-\infty}^{\infty} \exp(-ikx)\delta^{(n)}(x)dx = (ik)^n \tag{J.3.2}$$

With Eq. (J.3.1), the integral solution, Eq. (J.2.18) can be written in a compact form as

$$\tilde{\mathbf{V}} = -i\sum_{m=1}^{2}[F_1\mathbf{Q}_m^1 + F_2\mathbf{Q}_m^2]\frac{H_m}{D_m'} \tag{J.3.3}$$

where $F_i = k_1M_{i1}^0 + k_2M_{i2}^0$. (J.3.4)

The function $H_m(\mathbf{k},t)$ is defined as

$$H_m(\mathbf{k},t) = I(t) * \frac{\sin(W_mt)}{W_m} = W_m^{-1}\int_0^t I(\tau)\sin W_m(t-\tau)d\tau, \quad m = 1,2 \tag{J.3.5}$$

where $I(t)$ is the source time function for the AE source.

Finally, applying the inverse Fourier transform to Eq. (J.3.3), the solution is given by

$$\mathbf{V} = [u,v]^T = \frac{-i}{4\pi^2}\sum_{m=1}^{2}\int_{-\infty}^{\infty}[F_1\mathbf{Q}_m^1 + F_2\mathbf{Q}_m^2]\frac{H_m}{D_m'}\exp(i\mathbf{k}\cdot\mathbf{x})d\mathbf{k} \tag{J.3.6}$$

4. Solution in the polar coordinate system

The transient solutions, Eq. (J.3.6), are given by the two-dimensional inverse Fourier transform. For isotropic plates they may be expressed as a series involving inverse Hankel transforms. In terms of polar coordinates: $k_1 = k\cos\phi$, $k_2 = k\sin\phi$ and $x_1 = r\cos\theta$, $x_2 = r\sin\theta$, one has

$$\exp(i\mathbf{k}\cdot\mathbf{x}) = \exp[ikr\cos(\phi-\theta)], \quad d\mathbf{k} = dk_1dk_2 = kdkd\phi$$

Eq. (J.3.3) indicates that the Fourier transform of the displacement field, for example, $\tilde{u}$ can be written as

$$\tilde{u}(\mathbf{k},t) = -i\sum_{m=1}^{2}(F_1Q_m^{11} + F_2Q_m^{12})H_m / D_m' \tag{J.4.1}$$

$\tilde{u}$ can be further expressed in terms of trigonometric functions.

$$\begin{aligned}\tilde{u}(\mathbf{k},t) &= \frac{i(\alpha-1)k^3}{4}\sum_{m=1}^{2}\sum_{n=1}^{3}[C_{mn}\cos(n\phi) + S_{mn}\sin(n\phi)]H_m / D_m' \\ &= \frac{i(\alpha-1)k^3}{8}\sum_{m=1}^{2}\sum_{n=1}^{3}[(C_{mn} - iS_{mn})\exp(in\phi) + (C_{mn} + iS_{mn})\exp(-in\phi)]H_m / D_m'\end{aligned} \tag{J.4.2}$$

where the coefficients C_{mn} and S_{mn} are obtained by substituting Eq. (J.2.16) and Eq. (J.3.4) into Eq. (J.4.1). This process is tedious even for the two degree of freedom plane stress problem. For the **u** displacement for mode 1 this process is carried out in Appendix J.A . Once the coefficients have been determined, substituting Eq. (J.4.2) into the integrand of Eq. (J.3.6) and integrating with respect to ϕ first, the integration with respect to k leads to a series of inverse Hankel transforms. For example, the displacement u can be expressed as

$$u(r,\theta,t)=\frac{i(\alpha-1)}{16\pi^2}\sum_{m=1}^{2}\sum_{n=1}^{3}\left\{\int_0^\infty\frac{C_{mn}-iS_{mn}}{2}\frac{H_m}{D'_m}k^4dk\int_0^{2\pi}\exp[in\phi+ikr\cos(\phi-\theta)]d\phi\right.$$
$$\left.+\int_0^\infty\frac{C_{mn}+iS_{mn}}{2}\frac{H_m}{D'_m}k^4dk\int_0^{2\pi}\exp[-in\phi+ikr\cos(\phi-\theta)]d\phi\right\} \tag{J.4.3}$$

Making a change of variable $\phi-\theta=\beta+\pi/2$, and using the integral representation of the Bessel function of order n,

$$J_n(kr)=\frac{1}{2\pi}\int_{\beta_0}^{2\pi+\beta_0}\exp[i(n\beta-kr\sin\beta)]d\beta$$

and $J_{-n}(kr)=(-1)^nJ_n(kr)$ $(\beta_0=-(\theta+\pi/2))$, Eq. (J.4.3) is reduced to

$$u(r,\theta,t)=\frac{i(\alpha-1)}{16\pi^2}\sum_{m=1}^{2}\sum_{n=1}^{3}\left\{\int_0^\infty\frac{C_{mn}-iS_{mn}}{2}\frac{H_m}{D'_m}k^4dk\left(2\pi i^n\exp(in\theta)J_n(kr)\right)\right.$$
$$\left.+\int_0^\infty\frac{C_{mn}+iS_{mn}}{2}\frac{H_m}{D'_m}k^4dk\left(2\pi i^n\exp(-in\theta)J_n(kr)\right)\right\}$$
$$=\frac{i^{n+1}(\alpha-1)}{8\pi}\sum_{m=1}^{2}\sum_{n=1}^{3}\left\{\int_0^\infty\frac{H_m}{D'_m}\left[\frac{C_{mn}-iS_{mn}}{2}(\cos n\theta+i\sin n\theta)\right]\right.$$
$$\left.+\frac{C_{mn}+iS_{mn}}{2}\left(\cos n\theta-i\sin n\theta\right)\right]J_n(kr)k^4dk\right\}$$
$$=\frac{i^{n+1}(\alpha-1)}{8\pi}\sum_{m=1}^{2}\sum_{n=1}^{3}\int_0^\infty\frac{H_m}{D'_m}(C_{mn}\cos n\theta+S_{mn}\sin n\theta)J_n(kr)k^4dk$$

In summary,

$$\boxed{u=\frac{(\alpha-1)}{8\pi}\sum_{m=1}^{2}\sum_{n=1}^{3}\int_0^\infty\frac{H_m}{D'_m}U_{mn}(\theta)J_n(kr)k^4dk} \tag{J.4.4}$$

where $U_{mn}(\theta)=i^{n+1}(C_{mn}\cos n\theta+S_{mn}\sin n\theta)$ and each term of U_{mn} is

$$\begin{aligned}
&U_{12}(\theta)=U_{22}(\theta)=0\\
&U_{11}(\theta)=(M_{11}^0-M_{22}^0)\cos\theta+2M_{12}^0\sin\theta\\
&U_{13}(\theta)=(M_{11}^0-M_{22}^0)\cos3\theta+2M_{12}^0\sin3\theta\\
&U_{21}(\theta)=-(3M_{11}^0+M_{22}^0)\cos\theta-2M_{12}^0\sin\theta\\
&U_{23}(\theta)=U_{13}(\theta)
\end{aligned} \tag{J.4.5}$$

More detail of this derivation can be found in Appendix J.B. In a similar manner, the displacement $\tilde{v}$ can be obtained by

$$\tilde{v}(\mathbf{k},t) = -i\sum_{m=1}^{2}[F_1 Q_m^{21} + F_2 Q_m^{22}]H_m / D'_m \tag{J.4.6}$$

The more compact form can be expressed by

$$\begin{aligned}\tilde{v}(\mathbf{k},t) &= \frac{i(\alpha-1)k^3}{4}\sum_{m=1}^{2}\sum_{n=1}^{3}[c_{mn}\cos(n\phi) + s_{mn}\sin(n\phi)]H_m / D'_m \\ &= \frac{i(\alpha-1)k^3}{8}\sum_{m=1}^{2}\sum_{n=1}^{3}[(c_{mn} - is_{mn})\exp(in\phi) + (c_{mn} + is_{mn})\exp(-in\phi)]H_m / D'_m\end{aligned} \tag{J.4.7}$$

where coefficients c_{mn} and s_{mn} are obtained from Eq. (J.2.16) and Eq. (J.3.4) in a manner similar to that sown for u:

The inverse Fourier transform of $\tilde{v}$ gives

$$v = \frac{(\alpha-1)}{8\pi}\sum_{m=1}^{2}\sum_{n=1}^{3}\int_0^\infty \frac{H_m}{D'_m}V_{mn}(\theta)J_n(kr)k^4 dk \tag{J.4.8}$$

where $V_{mn}(\theta) = i^{n+1}(c_{mn}\cos n\theta + s_{mn}\sin n\theta)$ and each term of V_{mn} is

$$\begin{aligned}V_{12}(\theta) &= V_{22}(\theta) = 0 \\ V_{11}(\theta) &= 2M_{12}^0\cos\theta + (-M_{11}^0 + M_{22}^0)\sin\theta \\ V_{13}(\theta) &= -2M_{12}^0\cos 3\theta + (M_{11}^0 - M_{22}^0)\sin 3\theta \\ V_{21}(\theta) &= -2M_{12}^0\cos\theta - (M_{11}^0 + 3M_{22}^0)\sin\theta \\ V_{23}(\theta) &= V_{13}(\theta)\end{aligned} \tag{J.4.9}$$

In summary, for isotropic plates the transient wave solutions are reduced to a series of the inverse Hankel transforms. Performing similar manipulation, the displacements are

$$\begin{Bmatrix} u \\ v \end{Bmatrix} = \frac{\alpha-1}{8\pi}\sum_{m=1}^{2}\sum_{n=1}^{3}\int_0^\infty \frac{H_m}{D'_m}\begin{Bmatrix} U_{mn}(\theta) \\ V_{mn}(\theta) \end{Bmatrix} J_n(kr)k^4 dk \tag{J.4.10}$$

5. Closed Form Solution for Heavyside Loading

For the source time function described by Heaviside step function, Eq. (J.3.5) becomes $H_m(k,t) = (1-\cos W_m t)/W_m^2$. Then

$$H_1(k,t) = (1-\cos kt)/(k^2) \tag{J.5.1a}$$

$$H_2(k,t) = (1-\cos\sqrt{\alpha}kt)/(\sqrt{\alpha}k^2) \tag{J.5.1b}$$

and $H_1 / D'_1 = \dfrac{(1-\cos kt)}{(\alpha-1)k^4}$ and $H_2 / D'_2 = -\dfrac{(1-\cos\sqrt{\alpha}kt)}{(\alpha-1)\sqrt{\alpha}k^4}$ (J.5.2)

then Eq. (J.4.4) can be reduced to

$$
\begin{aligned}
u &= \frac{1}{8\pi}\int_0^\infty (1-\cos kt)[U_{11}J_1(kr)+U_{13}J_3(kr)]dk \\
&\quad -\frac{1}{8\sqrt{\alpha}\pi}\int_0^\infty (1-\cos\sqrt{\alpha}kt)[U_{21}J_1(kr)+U_{23}J_3(kr)]dk \\
&= \frac{1}{8\pi}\left[U_{11}\int_0^\infty (1-\cos kt)J_1(kr)dk + U_{13}\int_0^\infty (1-\cos kt)J_3(kr)dk\right] \\
&\quad -\frac{1}{8\sqrt{\alpha}\pi}\left[U_{21}\int_0^\infty (1-\cos\sqrt{\alpha}kt)J_1(kr)dk + U_{23}\int_0^\infty (1-\cos\sqrt{\alpha}kt)J_3(kr)dk\right]
\end{aligned}
\tag{J.5.3}
$$

The first term above represents the mode 1 solution and the second term the mode 2 contribution To u. Using the following formulas:

$$
\int_0^\infty J_n(kr)dk = \frac{1}{r}
$$

$$
\int_0^\infty J_n(kr)\cos ktdk = \begin{cases} \dfrac{\cos\left(n\arcsin\frac{t}{r}\right)}{\sqrt{r^2-t^2}}, & t<r \\ \infty \; or \; 0, & t=r \\ \dfrac{-r^n\sin\frac{n\pi}{2}}{\sqrt{t^2-r^2}\left(t+\sqrt{t^2-r^2}\right)^n}, & t>r \end{cases}
\tag{J.5.4}
$$

One has

$$
\int_0^\infty (1-\cos kt)J_1(kr)\,dk = \begin{cases} 0, & t<r \\ 0, & t=r \\ \dfrac{t}{r\sqrt{t^2-r^2}}, & t>r \end{cases}
\tag{J.5.5}
$$

Or

$$
\int_0^\infty (1-\cos kt)J_1(kr)\,dk = \frac{t}{r\sqrt{t^2-r^2}}
$$

$$
\int_0^\infty (1-\cos\sqrt{\alpha}kt)J_1(kr)\,dk = \begin{cases} 0, & t<r \\ 0, & t=r \\ \dfrac{\sqrt{\alpha}t}{r\sqrt{\alpha t^2-r^2}}, & t>r \end{cases}
\tag{J.5.6}
$$

$$\int_0^\infty (1-\cos kt) J_3(kr)\, dk = \begin{cases} 0, & t < r \\ 0, & t = r \\ \dfrac{(t-\sqrt{t^2-r^2})^3}{r^3\sqrt{t^2-r^2}}, & t > r \end{cases} \tag{J.5.7}$$

Putting it together for the **u** contribution for $t > r$ from mode 1 for example, is given by;

$$\begin{aligned} \mathbf{u_1}(\mathrm{r},\theta,\mathrm{t}) &= \frac{1}{8\pi}\left[U_{11}\frac{t}{r\sqrt{t^2-r^2}} + U_{13}\frac{\left(t-\sqrt{t^2-r^2}\right)^3}{r^3\sqrt{t^2-r^2}} \right] \\ &= \frac{1}{8\pi}\left[\begin{array}{l} \left[(M_{11}-M_{22})\cos\theta + (2M_{12})\sin\theta\right]\dfrac{t}{r\sqrt{t^2-r^2}} \\ +\left[M_{11}-M_{22})\cos 3\theta + (2M_{12})\sin 3\theta\right]\dfrac{\left(t-\sqrt{t^2-r^2}\right)^3}{r^3\sqrt{t^2-r^2}} \end{array} \right] \end{aligned} \tag{J.5.8}$$

Once the displacements are derived, applying spatial differentiation, strains are readily obtained. The piezoelectric sensor to measure the surface strains, $\varepsilon_{kk} = \varepsilon_{11} + \varepsilon_{22}$, generated by the source is often adopted in structural health monitoring. Therefore the surface strain is given as follows:

$$\varepsilon_{kk} = \frac{1}{4\pi^2}\sum_{m=1}^{2}\int_{-\infty}^{\infty}[(k_1 Q_m^{11} + k_2 Q_m^{21})F_1 + (k_1 Q_m^{12} + k_2 Q_m^{22})F_2]\frac{H_m}{D_m'}\exp(i\mathbf{k}\cdot\mathbf{x})d\mathbf{k} \tag{J.5.9}$$

The response of the surface strains to the point source can be obtained from Eq. (J.5.9) by performing similar manipulation and it follows that

$$\varepsilon_{kk} = \frac{\alpha-1}{2\pi}\sum_{m=1}^{2}\sum_{n=0}^{2}\int_0^\infty \frac{H_m}{D_m'}E_{mn}(k,\theta)J_n(kr)k^5 dk \tag{J.5.10}$$

where

$$E_{mn} = E_{mnc}(k)\cos n\theta + E_{mns}(k)\sin n\theta \tag{J.5.11}$$

$$\begin{aligned} &E_{10}(k) = E_{11}(k) = E_{12}(k) = E_{21}(k) = 0, \\ &E_{20}(k) = -(M_{11}^0 + M_{22}^0) \\ &E_{22}(k) = \tfrac{1}{2}[(M_{11}^0 - M_{22}^0)\cos 2\theta + (M_{12}^0 + M_{21}^0)\sin 2\theta] \end{aligned}$$

6. Dispersion relation

First, the relation between frequency and number can be obtained from Eq.(J.2.9), $\left|\mathbf{T}(\mathbf{k}) - \omega^2\mathbf{I}\right| = 0$, and it follows that

$$\omega^2 = W_1^2(\mathbf{k}) = k^2$$

$$\omega^2 = W_2^2(\mathbf{k}) = \alpha k^2$$

In the polar coordinates, the above relation becomes

$$\omega_1 = k, \quad \omega_2 = \sqrt{\alpha}k \tag{J.6.1}$$

where ω_1 and ω_2 are the analytical forms of the frequencies associated with the two stress wave modes. According to Eq.(6.1), the phase velocity associated with the **SH$_0$** and **S$_0$** modes can be obtained as

$$c_p = \omega / k = 1, \ \sqrt{\alpha} \tag{J.6.2}$$

As the frequency changes, the phase velocity doesn't change. Therefore, it could be seen that the phase velocity is not dispersive.

7. Results

The vertical tensile crack will be considered., In the case of plane stress the discontinuity extents through the thickness of the thin body, as opposed to the higher order theories, where the discontinuity can have a z location somewhere through the thickness. The closed form solution for mode 1 has been

Considering a vertical tensile crack loading in the x1 direction the only non zero terms in the moment tensor are the diagonal terms for which $M_{11}=\beta$ and $M_{22}=1$. For this case the mode one solution for **u** given in Eq. (5.8) can be simplified and expressed explicitly as

$$\mathbf{u_1}(\mathrm{r},\theta,\mathrm{t}) = \frac{1}{8\pi}\left[\left[(\beta-1)\cos\theta\right]\frac{t}{r\sqrt{t^2-r^2}} + \left[(\beta-1)\cos 3\theta\right]\frac{\left(t-\sqrt{t^2-r^2}\right)^3}{r^3\sqrt{t^2-r^2}}\right] \tag{J.7.1}$$

This result will be plotted directly and compared with the result using Eq. (J.4.10), shown again below, with numerical integration in MATHEMATICA.

$$\begin{Bmatrix} u \\ v \end{Bmatrix} = \frac{\alpha-1}{8\pi}\sum_{m=1}^{2}\sum_{n=1}^{3}\int_0^\infty \frac{H_m}{D'_m}\begin{Bmatrix} U_{mn}(\theta) \\ V_{mn}(\theta) \end{Bmatrix} J_n(kr)k^4\,dk \tag{J.4.10}$$

The result shown in Fig. J.1 is a plot showing the closed form solution (Eq. (J.7.1) in dashed lines and the numerical solution Eq. (J.10) from MATHEMATICA in the solid line. The closed form solution is singular at the arrival time and the mathematical solution has a maximum response of 0.0065 dimensionless displacement. Mode 1 is the shear horizontal mode **SH$_0$**. Mode 2, the **S$_0$** longitudinal extensional mode, is shown in Fig. J.2 and has a maximum response of 0.00575 dimensionless displacement and an earlier dimensionless arrival time.

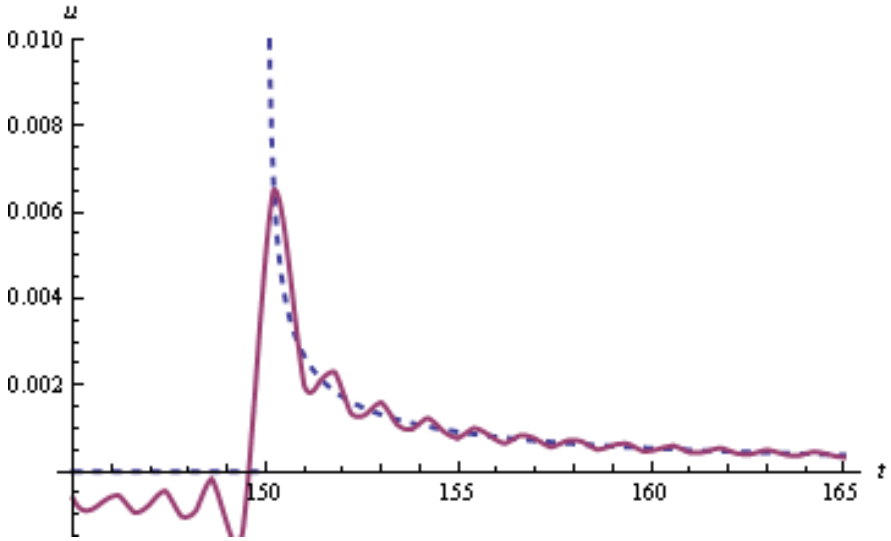

Figure J.1 Comparison of closed form and numerical solutions for the mode 1 **u** displacement for a vertical tensile crack. r=150, θ=45°

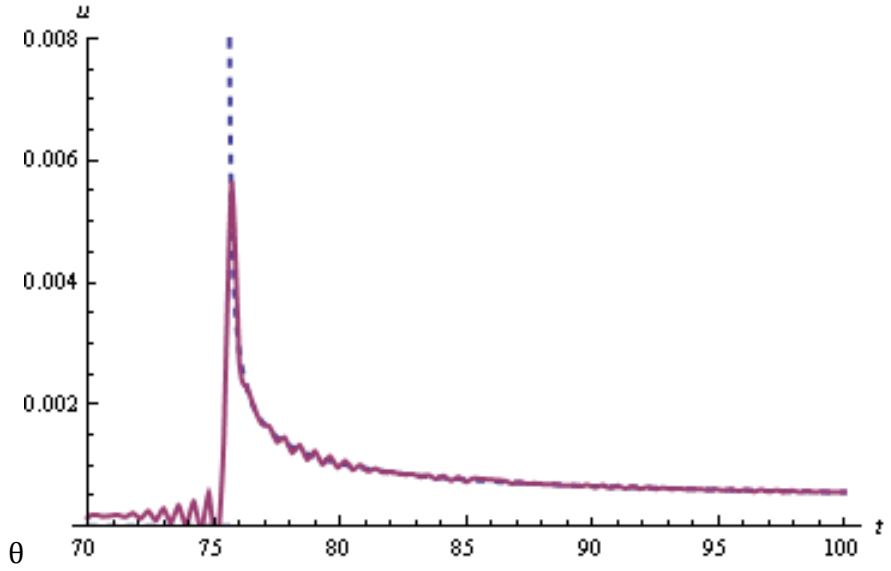

Figure J.2 Comparison of closed form and numerical solutions for the mode 2 **u** displacement for a vertical tensile crack. r=150, θ=45°

Figure J.3 provides four snapshots in increasing time and shows the **u** displacement as a function off **r** and **θ** for the shear horizontal mode near the origin. It is observed that

the response increases off axis as the θ=0 line is a symmetry axis for the **SH_0** mode with small **u** response.

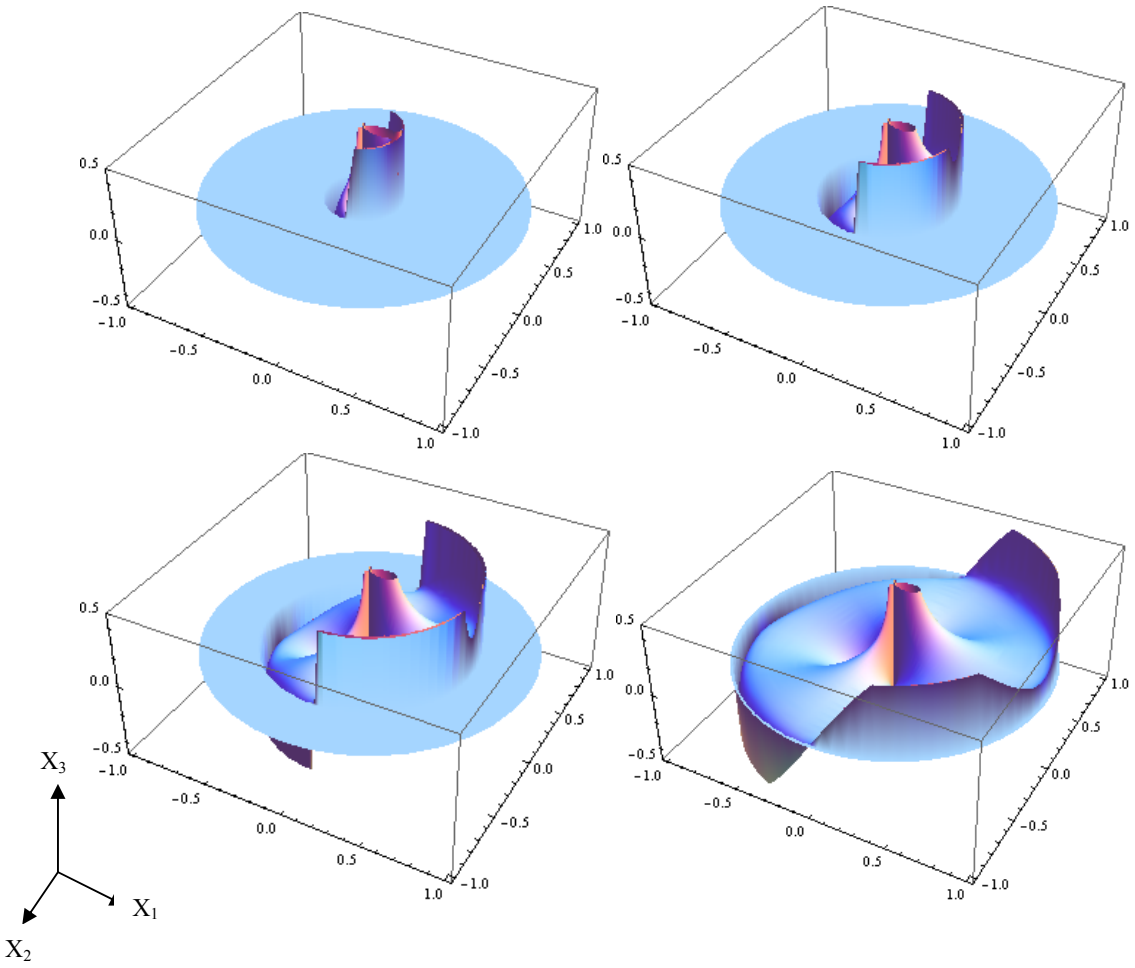

Figure J.3 – MATHEMATICA animation of **u** displacement for **SH_0** mode as a function of r, θ, at four snapshots in time

Figure J.4 provides four snapshots in increasing time and shows the **u** displacement as a function off **r** and **θ** for the longitudinal mode near the origin. It is observed that the response decreases off axis, as the θ=0 line is directly along the load direction for a vertical tensile crack and should experience the strongest response for the $\mathbf{S_0}$ mode.

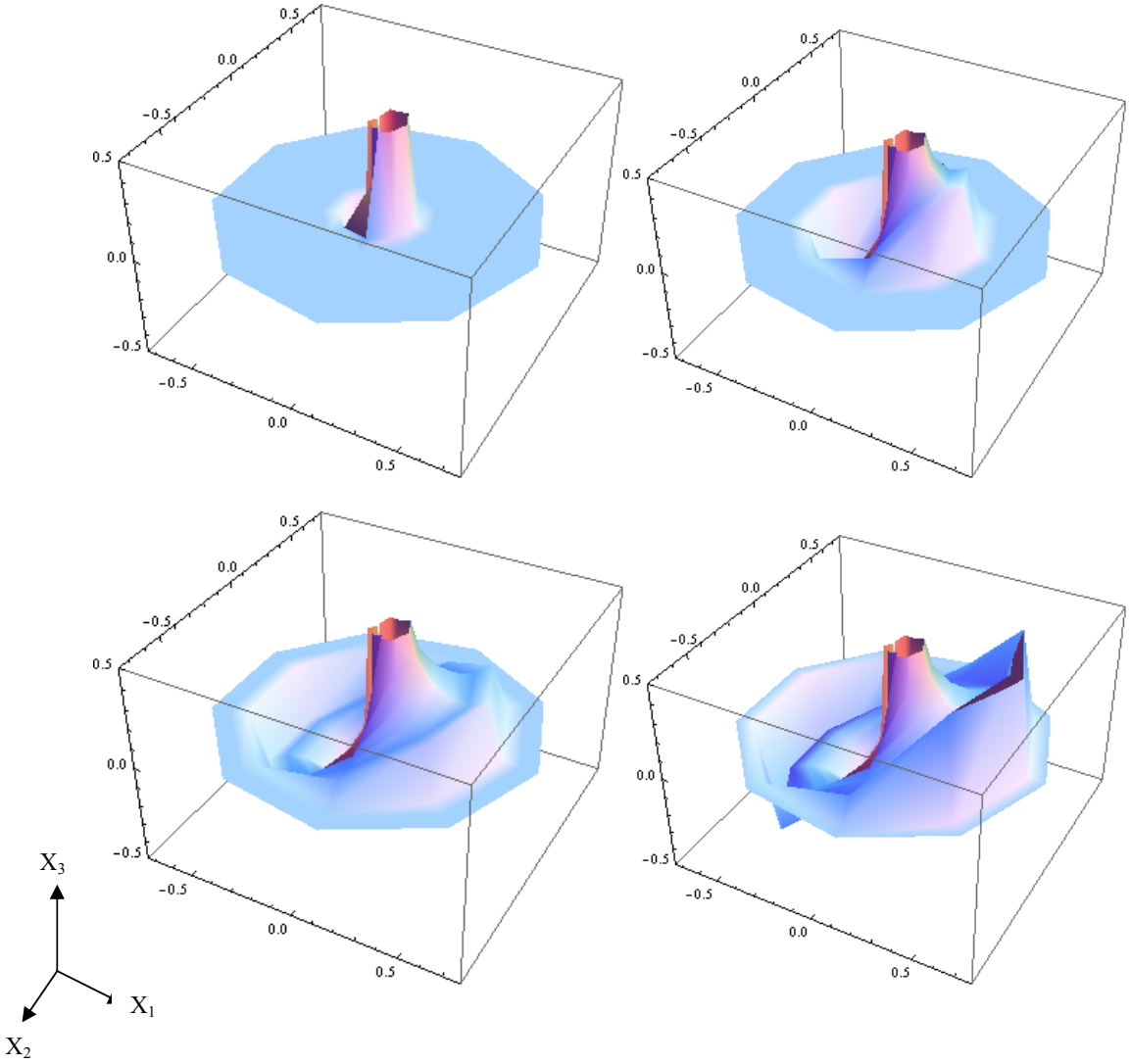

Figure J.4 – MATHEMATICA animation of **u** displacement for $\mathbf{S_0}$ mode as a function of r, θ, at four snapshots in time

Appendix J.A – Calculation of Coefficients U_{mn} for the u Displacement Mode 1 Contribution

To illustrate the algebraic and trigonometric manipulations involved consider the **u** displacement only or mode 1. Performing the operation indicated in the parentheses in Eq. (J.4.1),

$$F_1\mathbf{Q}_1^1 = [k_1M_{11} + k_2M_{12}]\begin{bmatrix}(\alpha-1)k_2^2\\ -(\alpha-1)k_1k_2\end{bmatrix} = \begin{bmatrix}k_1k_2{}^2M_{11}(\alpha-1)\\ -k_2{}^2k_1M_{12}(\alpha-1)\end{bmatrix}$$

Ignoring the summation over the modes by considering m=1 only, using the polar form of the wave number, $k_1=k\cos\varphi$ and $k_2=k\sin\varphi$ and using only the first row of the result above for the **u** component only, the parenthetical portion of the right side of Eq. (J.4.1) of interest becomes ;

$$\begin{aligned}
&-i\{[k\cos\phi M_{11} + k\sin\phi M_{12}](\alpha-1)k^2 - [k\cos\phi M_{21} + k\sin\phi M_{22}](\alpha-1)k^2\cos\phi\sin\phi\\
&= -i\{(\alpha-1)k^3[\cos\phi\sin^2\phi M_{11} + \sin^3\phi M_{12}] - (\alpha-1)k^3[\cos^2\phi M_{21} + \cos\phi\sin^2\phi M_{22}]\}\\
&= -i\{(\alpha-1)k^3\{\cos\phi\sin^2\phi M_{11} + \sin^3\phi M_{12} - \cos^2\phi\sin\phi M_{21} - \cos\phi\sin^2\phi M_{22}\}
\end{aligned}$$

Trigonometric reduction is facilitated with the following formulas,

$$\sin^2\phi = \frac{1}{2} - \frac{1}{2}\cos 2\phi \qquad \cos^2\phi = \frac{1}{2} + \frac{1}{2}\cos 2\phi$$

$$\sin^3\phi = \frac{3}{4}\sin\phi - \frac{1}{4}\sin 3\phi \qquad \cos^3\phi = \frac{3}{4}\cos\phi + \frac{1}{4}\cos 3\phi$$

These substitutions, after some manipulations, result in:

$$-i\{(-i\{(\alpha-1)k^3\begin{Bmatrix}\cos\phi\left(\frac{1}{2}(1-\cos 2\phi)\right)M_{11} + \frac{1}{4}(3\sin\phi - \sin 3\phi)M_{12}\\ -\frac{1}{2}(1+\cos 2\phi)\sin\phi M_{21} - \frac{1}{2}\cos\phi(1-\cos 2\phi)M_{22}\end{Bmatrix}$$

$$= -i\{(\alpha-1)k^3\begin{Bmatrix}\left[\frac{1}{2}\cos\phi - \frac{1}{2}\cos\phi\cos 2\phi\right]M_{11} + \left[\frac{3}{4}\sin\phi - \frac{1}{4}\sin 3\phi\right]M_{12}\\ -\frac{1}{2}[\sin\phi + (1-2\sin^2\phi)\sin\phi]M_{21} - \frac{1}{2}[\cos\phi - \cos\phi(2\cos^2\phi - 1)]M_{22}\end{Bmatrix}$$

Which, after further reduction of the remaining $\sin^2\emptyset$, $\cos^2\emptyset$ and $\sin^3\emptyset$ terms, yields;

$$i\{(\alpha-1)k^3\begin{Bmatrix}\left[\frac{1}{2}\cos\phi - (\frac{3}{4}\cos\phi + \frac{1}{4}\cos 3\phi) + \frac{\cos\phi}{2}\right]M_{11} + \left[\frac{3}{4}\sin\phi - \frac{1}{4}\sin 3\phi\right]M_{12}\\ +\left[-\sin\phi + (\frac{3}{4}\sin\phi - \frac{1}{4}\sin 3\phi)\right]M_{21} - \left[\frac{1}{2}\cos\phi - \left(\frac{3}{4}\cos\phi + \frac{1}{4}\cos 3\phi\right) + \frac{1}{2}\cos\phi\right]M_{22}\end{Bmatrix}$$

Adding like terms further simplifies the expression to

$$-i\{(\alpha-1)k^3\left\{\begin{array}{l} M_{11}\left[\frac{1}{2}\cos\phi-\frac{3}{4}\cos\phi-\frac{1}{4}\cos 3\phi+\cos\phi\right]+M_{12}\left[\frac{3}{4}\sin\phi-\frac{1}{4}\sin 3\phi\right]+ \\ M_{21}\left[-\sin\phi+\frac{3}{4}\sin\phi-\frac{1}{4}\sin 3\phi\right]+M_{22}\left[-\frac{1}{2}\cos\phi-\frac{3}{4}\cos\phi-\frac{1}{4}\cos 3\phi+\frac{1}{2}cos\phi\right] \end{array}\right\}$$

$$=-i\{(\alpha-1)k^3\left\{\begin{array}{l} M_{11}\left[\frac{3}{4}\cos\phi-\frac{1}{4}\cos 3\phi\right]+M_{12}\left[\frac{3}{4}\sin\phi-\frac{1}{4}\sin 3\phi\right] \\ +M_{21}\left[-\frac{1}{4}\sin\phi-\frac{1}{4}\sin 3\phi\right]+M_{22}\left[-\frac{3}{4}\cos\phi-\frac{1}{4}\cos 3\phi\right] \end{array}\right\}$$

Now assigning the coefficients of each trig term C_{mn} or S_{mn} where C_{mn} picks out the cosine terms and S_{mn} the sine terms for mode m with the second subscript n indicating with the factor multiplying ∅ in the trig function, for example, an n of 3 indicating a cos3∅, the above expressions can be inserted into the right side of Eq. (J.4.2) in the compact form shown.

$$C_{11}(k)=\frac{-i(\alpha-1)k^3}{4}\left[M_{11}-M_{22}\right] \qquad S_{11}(k)=\frac{-i(\alpha-1)k^3}{4}\left[3M_{12}-M_{22}\right]$$

$$C_{13}(k)=\frac{-i(\alpha-1)k^3}{4}\left[-M_{11}+M_{22}\right] \qquad S_{13}(k)=\frac{-i(\alpha-1)k^3}{4}\left[-M_{12}-M_{21}\right]$$

$$C_{21}(k)=\frac{-i(\alpha-1)k^3}{4}\left[-3M_{11}-M_{22}\right] \qquad S_{21}(k)=\frac{-i(\alpha-1)k^3}{4}\left[M_{12}-M_{21}\right]$$

$$C_{23}(k)=\frac{-i(\alpha-1)k^3}{4}\left[-M_{11}+M_{22}\right] \qquad S_{23}(k)=\frac{-i(\alpha-1)k^3}{4}\left[M_{12}+M_{21}\right]$$

Notice that a factor of ¼, and the leading multiplier, except for the minus sign, have been taken outside of the summations in Eq. (J.4.2) and are no longer book kept in the coefficients. A final step which yields the exponential form of Eq. (J.4.2) is to use Euler's rule, shown below, to convert the trigonometric terms to exponential terms.

$$\cos n\phi=\frac{1}{2}\left(\exp(in\phi)+\exp(-in\phi)\right)$$

$$\sin n\phi==\frac{1}{2i}\left(\exp(in\phi)-\exp(-in\phi)\right)$$

This will be very useful in the next step in which a polar conversion will reduce the order of integration by adding the powers of exponential terms and recognizing Bessel function forms.

Note that $M_{12}^0=M_{21}^0$ is imposed in the above derivation and C_{mn}, S_{mn}, H_m and D'_m are independent of ϕ.

Appendix J.B- Derivation of Eq. (J.4.4)

Making a change of variable $\phi - \theta = \beta + \pi/2$,

$$\int_0^{2\pi} \exp[in\phi + ikr\cos(\phi-\theta)]d\phi = \exp(in\theta + i\tfrac{\pi}{2}n) \int_{-\theta-\pi/2}^{-\theta+3\pi/2} \exp[i(n\beta - kr\sin\beta)]d\beta$$

Using the integral representation of the Bessel function of order *n*,

$$J_n(kr) = \frac{1}{2\pi}\int_{\beta_0}^{2\pi+\beta_0} \exp[i(n\beta - kr\sin\beta)]d\beta$$

$$\int_0^{2\pi} \exp[in\phi + ikr\cos(\phi-\theta)]d\phi = i^n \exp(in\theta) \int_{-\theta-\pi/2}^{-\theta+3\pi/2} \exp[i(n\beta - kr\sin\beta)]d\beta \qquad (*)$$

$$= 2\pi i^n \exp(in\theta) J_n(kr)$$

$$\boxed{\int_0^{2\pi} \exp[in\phi + ikr\cos(\phi-\theta)]d\phi = 2\pi i^n \exp(in\theta) J_n(kr)}$$

Similarly,

$$\int_0^{2\pi} \exp[-in\phi + ikr\cos(\phi-\theta)]d\phi = \exp(in\theta - i\tfrac{\pi}{2}n) \int_{-\theta-\pi/2}^{-\theta+3\pi/2} \exp[i(n\beta - kr\sin\beta)]d\beta$$

Using $J_{-n}(kr) = (-1)^n J_n(kr)$ $(\beta_0 = -(\theta + \pi/2))$,

$$\int_0^{2\pi} \exp[-in\phi + ikr\cos(\phi-\theta)]d\phi = (-i)^n \exp(-in\theta) \int_{-\theta-\pi/2}^{-\theta+3\pi/2} \exp[i(n\beta - kr\sin\beta)]d\beta \qquad (**)$$

$$= 2\pi(-i)^n(-1)^n \exp(-in\theta) J_n(kr) = 2\pi(i)^n \exp(-in\theta) J_n(kr)$$

$$\boxed{\int_0^{2\pi} \exp[-in\phi + ikr\cos(\phi-\theta)]d\phi = 2\pi(i)^n \exp(-in\theta) J_n(kr)}$$

Substituting (*) and (**) into Eq. (J.4.3)

$$u(r,\theta,t) = \frac{1}{4\pi^2}\sum_{m=1}^{2}\sum_{n=0}^{2}\{\int_0^\infty \frac{C_{mn} - iS_{mn}}{2}\frac{H_m}{D_m'} kdk[2\pi i^n \exp(in\theta)J_n(kr)]$$

$$+\int_0^\infty \frac{C_{mn} + iS_{mn}}{2}\frac{H_m}{D_m'} kdk[2\pi(i)^n \exp(-in\theta)J_n(kr)]$$

$$= \frac{1}{2\pi}\sum_{m=1}^{2}\sum_{n=0}^{2} i^n\{\int_0^\infty \frac{C_{mn} - iS_{mn}}{2}\frac{H_m}{D_m'} kdk[\exp(in\theta)J_n(kr)]$$

$$+\int_0^\infty \frac{C_{mn} + iS_{mn}}{2}\frac{H_m}{D_m'} kdk[\exp(-in\theta)J_n(kr)]$$

$$= \frac{1}{2\pi}\sum_{m=1}^{2}\sum_{n=0}^{2}\{\int_0^\infty \frac{H_m}{D_m'}\left\{i^n[\frac{C_{mn} - iS_{mn}}{2}\exp(in\theta) + \frac{C_{mn} + iS_{mn}}{2}\exp(-in\theta)]\right\}J_n(kr)kdk$$

$$= \frac{1}{2\pi}\sum_{m=1}^{2}\sum_{n=0}^{2}\{\int_0^\infty \frac{H_m}{D_m'}\left\{i^n[\frac{C_{mn} - iS_{mn}}{2}[\cos(n\theta) + i\sin(n\theta)] + \frac{C_{mn} + iS_{mn}}{2}[\cos(n\theta) + i\sin(n\theta)]]\right\}J_n(kr)kdk$$

$$= \frac{1}{2\pi}\sum_{m=1}^{2}\sum_{n=0}^{2}\{\int_0^\infty \frac{H_m}{D_m'} U_{mn}(k,\theta)J_n(kr)kdk\}$$